Terms and Conditions of Use of Digitised Theses from Trinity College Library Dublin

Copyright statement

All material supplied by Trinity College Library is protected by copyright (under the Copyright and Related Rights Act, 2000 as amended) and other relevant Intellectual Property Rights. By accessing and using a Digitised Thesis from Trinity College Library you acknowledge that all Intellectual Property Rights in any Works supplied are the sole and exclusive property of the copyright and/or other IPR holder. Specific copyright holders may not be explicitly identified. Use of materials from other sources within a thesis should not be construed as a claim over them.

A non-exclusive, non-transferable licence is hereby granted to those using or reproducing, in whole or in part, the material for valid purposes, providing the copyright owners are acknowledged using the normal conventions. Where specific permission to use material is required, this is identified and such permission must be sought from the copyright holder or agency cited.

Liability statement

By using a Digitised Thesis, I accept that Trinity College Dublin bears no legal responsibility for the accuracy, legality or comprehensiveness of materials contained within the thesis, and that Trinity College Dublin accepts no liability for indirect, consequential, or incidental, damages or losses arising from use of the thesis for whatever reason. Information located in a thesis may be subject to specific use constraints, details of which may not be explicitly described. It is the responsibility of potential and actual users to be aware of such constraints and to abide by them. By making use of material from a digitised thesis, you accept these copyright and disclaimer provisions. Where it is brought to the attention of Trinity College Library that there may be a breach of copyright or other restraint, it is the policy to withdraw or take down access to a thesis while the issue is being resolved.

Access Agreement

By using a Digitised Thesis from Trinity College Library you are bound by the following Terms & Conditions. Please read them carefully.

I have read and I understand the following statement: All material supplied via a Digitised Thesis from Trinity College Library is protected by copyright and other intellectual property rights, and duplication or sale of all or part of any of a thesis is not permitted, except that material may be duplicated by you for your research use or for educational purposes in electronic or print form providing the copyright owners are acknowledged using the normal conventions. You must obtain permission for any other use. Electronic or print copies may not be offered, whether for sale or otherwise to anyone. This copy has been supplied on the understanding that it is copyright material and that no quotation from the thesis may be published without proper acknowledgement.

Mechanoregulation Algorithms Predicting Peri-Prosthetic Bone Adaptations

Paul Timothy Scannell, B.A., B.A.I.

A thesis submitted to the University of Dublin in partial fulfilment of the requirements for the degree of

Doctor in Philosophy

Trinity College Dublin

Supervisor

Prof. P.J. Prendergast

External examiner

Prof. M. Taylor

Internal examiner

Prof. D. Taylor

Declaration

I declare that I am the sole author of this thesis and that all the work presented in it, unless otherwise referenced, is my own. I also declare that this work has not been submitted, in whole or in part, to any other university or college for any degree or other qualification.

I authorise the library of Trinity College Dublin to lend and copy this thesis.

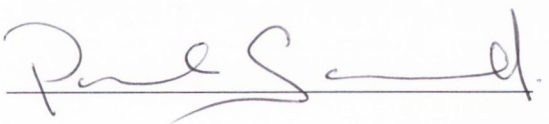

Paul Scannell

October 31st, 2006

Acknowledgements

First I would like to thank my supervisor Prof. Patrick Prendergast not only for providing me with the opportunity to carry out this research degree, but also for affording me the opportunity to take time out to travel, without which my work up to that point might have been submitted for a Masters. Thank you Paddy for your support and guidance throughout the last four years.

Before I thank everyone there are a few individuals who need to be singled out for special thanks. First I'd like to thank my "babysitters" in the office, Dr. Alex Lennon and Dr. John Britton. If it wasn't for Alex and his unnatural knowledge of the finite element method I would probably still be messing about with a two-dimensional "brick" model. Thank you Alex. Thanks to John Britton for all the help provided when using the Borelli cluster and subsequently the Aristotle high performance computer. With regard to the tissue differentiation aspect of this thesis I would like to extend a special thanks to Dr. Danny Kelly on the computational side and Louise McMahon on the biological side. I would like to thank all postgrads and postdocs past and present, and so to mention a few: Adriele, Brian, Bríanne, Conor, Damien, Emma, Eric, Geraldine, James, Jennifer, John G, Karen, Kevin, Louise, Mélanie, Michael, Niamh, Oran, Paula, Pavel, Ruth, and Tadhg.

Many thanks to Sheena Brown for everything from arranging meetings with Paddy to organising flights and accommodation for conferences. Thanks to Joan Gillen and Nicole Byrne for their assistance throughout the last four years. Thanks to John Gaynor for all the I.T. help provided. I would like to acknowledge Materials Ireland for the use of their 3D laser scanner.

I would like to say a special thanks to my parents, Ted and Paula, for their encouragement and support from day one, and also for "lending" me a couple of

euro from time to time. I would like to thank my sister Maria, who was there when I needed to take my frustration out on someone when simulations didn't run.

Finally, I would like to thank Máire for her support and for being there for me over the past four years. I would like to say I couldn't have done it without her, but her knowledge of FE is limited.

This work was supported by the Programme for Research in Third Level Institutions (PRTLI) Cycle 2 programme "MediLink" and by PRTLI Cycle 3 funding to the Trinity Centre for Bioengineering. The PRTLI is administered by the Higher Education Authority.

Publications and presentations resulting from this study

P. T. Scannell and P. J. Prendergast, 2003. Development of a bone remodelling algorithm based on strain and damage stimuli. Presented at the 7^{th} Conference of the European Society of Engineering and Medicine, 18^{th}-21^{st} September 2003, Halle (Salle), Germany.

P. T. Scannell and P. J. Prendergast, 2004. Bone adaptation based on a combined strain-damage mechanoregulation rule. Presented at Bioengineering in Ireland 10, 30^{th}-31^{st} January 2004, Castle Oaks House Hotel, Castleconnell, Co. Limerick.

P. T. Scannell and P. J. Prendergast, 2004. The combination of both strain and damage as a stimulus for bone adaptation. Presented at the 14^{th} European Society of Biomechanics Conference, 4^{th}-7^{th} July 2004 's-Hertogenbosch, The Netherlands.

P. T. Scannell and P. J. Prendergast, 2005. Bone remodelling (including remodelling at the bone/implant interface) with a non-cemented hip prosthesis. Presented at Bioengineering in Ireland 11, 28^{th}-29^{th} January 2005, Fitzpatrick Castle Hotel, Killiney, Co. Dublin.

P. T. Scannell and P. J. Prendergast, 2005. Simulation of changes in bone around hip replacement implants, *Engineers Journal* 59: 372-377.

P. T. Scannell and P. J. Prendergast, 2006. Influence of stem stiffness on bone adaptation around cementless hip replacements using a strain-damage stimulus. Presented at Bioengineering in Ireland 12, 27^{th}-28^{th} January 2006, Clybaun Hotel, Knocknacarra, Co. Galway.

P. J. Prendergast, P. T. Scannell, J. R. Britton, and A. B. Lennon, 2006. The role of computation in identifying failure of biomaterials in implant fixation. Proceedings of the 16th European Congress on Fracture. Alexandroupolis, Greece. [CD-Rom].

P. T. Scannell and P. J. Prendergast, 2006. Simulations predicting bone remodelling and interfacial tissue formation in uncemented hip replacements. Presented at the 5^{th} World Congress of Biomechanics, 29^{th} July - 4^{th} August, Munich, Germany.

P. T. Scannell and P. J. Prendergast, 2006. Peri-prosthetic bone adaptations around a non-cemented hip implant: predictions based on a combined strain-damage remodelling algorithm. Transactions of the American Society of Mechanical Engineers, *Journal of Biomechanical Engineering*, (accepted).

Contents

Abstract

Numerous mechanobiological algorithms have been developed in recent years to simulate biological processes such as bone remodelling and tissue differentiation. However, the implementation of such algorithms for the design and testing of orthopaedic devices has yet to be fully realised. In this thesis a mechanoregulation algorithm based on a combined strain-damage remodelling rule together with the integration of a tissue differentiation algorithm is proposed. Such a mechanoregulation approach was tested using a finite element model of a uncemented femoral hip prosthesis under idealized bonding characteristics. Three stem materials (iso-elastic, titanium, and CoCrMo) were investigated and compared to previous numerical and clinical observations to corroborate the predictive power of the algorithms.

Results of the bone remodelling algorithm predicted similar remodelling trends to those observed clinically. Namely, that while the use of an iso-elastic stem reduces proximal bone loss because stress shielding is prevented; proximal interface resorption is increased due to damage stimulated resorption. On the other hand, a stiff cobalt chrome stem increases both proximal strain-stimulated resorption and damage stimulated interfacial resorption at the distal tip. Simulations for the titanium stem were predicted to minimise both strain and damage related remodelling. The inclusion of the tissue differentiation simulation predicted bone regeneration for all resorbed interfacial bone through either intramembranous or endochondral ossification, which can be corroborated by clinical observations of implant stabilisation through osseointegration. However, it was predicted that some soft-tissue formation persisted at the proximal medial interface of the iso-elastic stem, following the trend of what is observed clinically; early failure of iso-elastic stems due to excessive proximal soft tissue formation.

In conclusion, by integrating different mechanoregulation algorithms simultaneous predictions of remodelling and differentiation can be achieved. This opens new avenues for computational pre-clinical testing of orthopaedic implants.

List of Figures

List of Tables

Nomenclature

Roman letters

k	Permeability [m^4/Ns]
C_d	Damage remodelling rate constant
C_s	Strain remodelling rate constant
S_{ref}	Reference remodelling Stimulus [Jg^{-1}]
$A(\rho)$	Free surface area [mm^2]
$a(\rho)$	Free surface area per unit volume [mm^2/mm^3]
d	Damage lazy zone
E	Young's modulus [MPa]
N	Number of cycles per month
N_f	Number of cycles to failure
S	Strain remodelling stimulus [Jg^{-1}]
S_d	Tissue differentiation stimulus
t_{diff}	Differentiation time
U	Strain energy density [MPa]
V	Volume [mm^3]
s	Half width of the '*lazy zone*'

Greek letters

$\Delta\omega$	Damage stimulus
Δt_d	Damage time step
Δt_s	Strain time step
Δt	Time step
$\dot{\omega}$	Damage formation rate
$\dot{\omega}_{\mathrm{RE}}$	Damage repair rate
γ	Octahedral shear strain
ν	Fluid velocity
ω	Damage
ω_{CRIT}	Critical amount of damage
ω_{RE}	Homeostatic damage
ρ	Apparent density [g/cm^3]
σ	Stress [MPa]
τ_{d}	Damage time constant
τ_{s}	Strain time constant

Chapter 1

Introduction

Contents

1.1 General introduction

Total joint replacement (TJR) is one of the most successful surgical procedures to treat patients suffering from degenerative joint disease and injury of the articular cartilage. Hip replacement has been a particular success: some 4,793 total and partial hip replacements were carried out in public hospitals in the Republic of Ireland in 2005 (ESRI, 2006). The primary challenge facing the surgeon during a total hip replacement is to achieve a stable long-term fixation between the orthopaedic implant and the host bone. This fixation may be achieved by either a cemented or uncemented fixation technique. Cemented prostheses are secured in the bone with the use of an acrylic bone cement consisting of PMMA (polymethylmethacrylate) with antibiotic and other additives. Uncemented fixation may be achieved by either using a press-fit stem, where the stem is wedged into the bone, or by using

a biological fixation, where the implant is secured by the process of osseointegration. Osseointegration occurs by bony ingrowth onto the surface of the prosthesis, which can either have a porous coating (Engh et al., 1987) or a hydroxyapatite coating (D'Antonio et al., 1996).

The primary function of a joint replacement is to provide stable pain-free articulation; however it is the stress patterns generated by the load transfer that often determines the success or failure of the prosthesis. Regardless of the method of fixation the leading causes of implant failure are aseptic loosening (see Fig. 1.1a), exacerbated by peri-prosthetic bone changes e.g. osteolysis (see Fig. 1.1b), and stress shielding (see Fig. 1.1c,d).

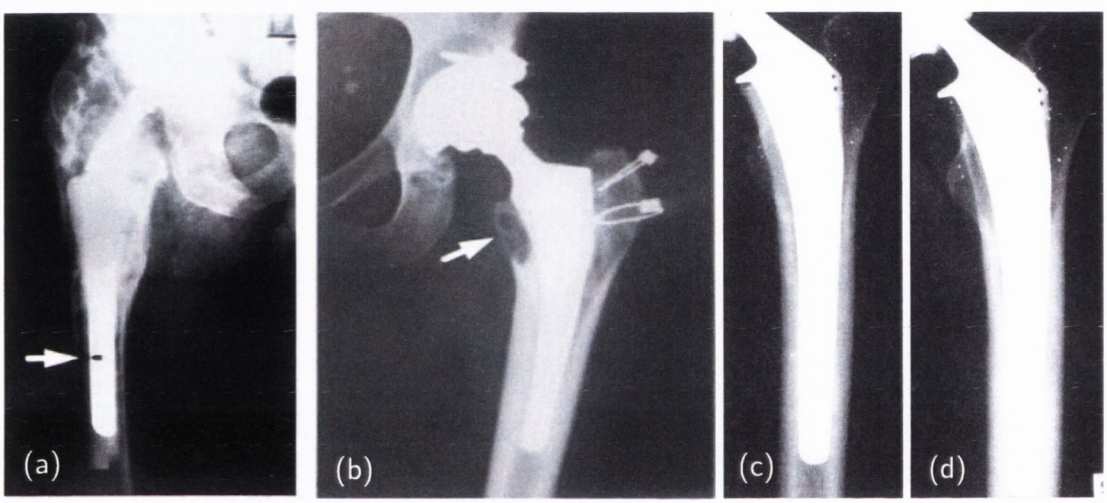

Figure 1.1. Aseptic loosening, osteolysis, and stress shielding surrounding femoral stems. (a) Aseptic loosening at the cement bone interface (*arrow*). Adapted from Sinha et al. (2004). (b) Osteolysis in the calcar region (*arrow*). Adapted from Learmonth et al. (1995). (c) postoperative titanium alloy hydroxyapatite coated cementless stem, and (d) two years after operation showing proximal bone loss due to stress shielding. Adapted from Kärrholm et al. (1994).

Aseptic loosening in cemented stems is generally associated with cement fatigue and failure of the stem-cement and/or cement-bone interfaces leading to bone resorption and formation of a soft tissue interface. Uncemented stems can produce excessive interfacial stresses and micro-motions at the stem-bone interface causing failure of the interfacial bond, damage accumulation, and possible bone resorption and soft tissue interposition. Osteolysis occurs as a result of wear particles from the articulating surfaces migrating to cement-bone interface (or stem-bone interface

in the case of uncemented fixation) leading to bone death and loosening. Atrophy in the form of proximal bone resorption, induced by stress shielding, is more commonly seen in uncemented stems as they are generally larger and more rigid. Stress shielding is caused by the altered load transfer from prosthesis to bone leading to adaptive bone remodelling. Therefore it can be appreciated that peri-prosthetic bone adaptations are complex and contribute in a variety of ways to THA failure.

By combining the finite element method with mechano-biological algorithms, such as bone remodelling and tissue differentiation algorithms, the peri-prosthetic bone response, and hence, the likely long-term success of the arthroplasty may be predicted.

1.2 Bone remodelling and tissue differentiation

1.2.1 Bone remodelling

Bone is a dynamic living material which is continually being renewed, resorbed, or formed by the processes of bone modelling and remodelling. Bone *modelling* is characterised by the formation of new bone by osteoblasts or the resorption of existing bone by osteoclasts. Bone *remodelling* is the process of bone renewal with both the osteoclasts and osteoblasts working together, resorbing and forming bone respectively, with osteocytes mediating the resorption/formation signal to the relevant cells in units called Bone Multicellular Units (BMU), see Fig. 1.2.

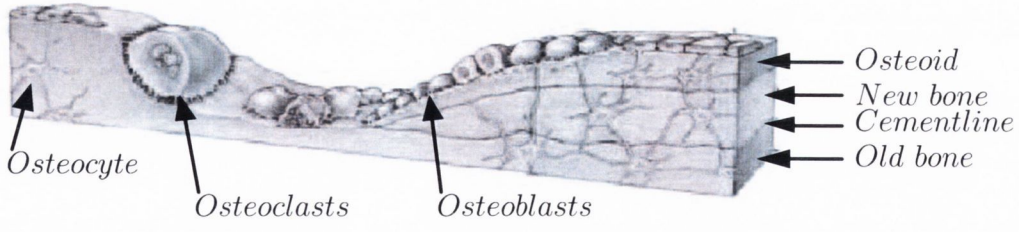

Figure 1.2. Schematic of Bone Multicellular Unit (BMU). Adapted from McNamara (2004).

In the 19^{th} century Julius Wolff first proposed the concept that the architecture of bone adapts to the mechanical stresses and strains acting upon it. In recent times mathematical models have been developed to model bone adaptation. These

models assume that bone contains sensors, or mechanoreceptors, which can detect changes in the mechanical stimulus and relate this signal to a biological response in order to meet the new functional demand. During normal loading conditions bone resorption by osteoclasts is balanced by bone formation by osteoblasts and a dynamic equilibrium exists such that there is no net increases or decrease in bone mass. However, if the mechanical stimulus were to deviate from normal levels the bone responds with either a net increase or decrease in mass. Despite many years of investigation the governing mechanical stimulus is still not agreed among researchers, with different researchers proposing different stimuli; some have proposed a strain related stimulus (Cowin and Hegedus, 1976; Fyhrie and Carter, 1986; Huiskes et al., 1987), others propose a damage-based stimulus (Carter et al., 1987; Martin, 1992; Prendergast and Taylor, 1992, 1994). Recently McNamara and Prendergast (2005, 2006) have proposed a combined strain and microdamage remodelling algorithm based on the earlier work of Prendergast and Huiskes (1995, 1996b).

Numerous studies have been carried out on the influence of femoral hip prostheses on adaptive bone remodelling using both strain-adaptive (Huiskes et al., 1987, 1989; Weinans et al., 1992, 1993; van Rietbergen et al., 1993) and damage-adaptive (Prendergast and Taylor, 1992; McNamara et al., 1997) remodelling theories. These models have realistically predicted proximal bone resorption as of a result of stress shielding around the prosthesis. However, no simulation of interfacial bone adaptations has yet been performed; it has only been assumed from these models that high interface stresses promote a failed ingrowth scenario (Weinans et al., 1992; Huiskes et al., 1992). Being able to model simultaneously both the influence of stress shielding and interfacial damage on bone remodelling patterns would allow for a better prediction of implant performance.

1.2.2 Tissue differentiation

If the gap between the implant and bone is too large osseointegration may be prevented and the formation of a fibrous tissue interface leading to eventual implant loosening and failure is promoted. These gaps may be present post-operatively due

to a poor fit between the prosthesis and the underlying bone, or may be caused by in interfacial bone adaptations. The differentiation of the granulation tissue in these gaps determines whether fibrous tissue, cartilage or bone is formed. Several mechanical stimuli have been proposed as regulators of tissue differentiation: octahedral shear stress and hydrostatic stress (Carter et al., 1988), hydrostatic pressure and strain (Claes and Heigele, 1999), tissue shear strain and fluid velocity (Prendergast et al., 1997). The approach of Prendergast et al. (1997) has been successfully applied to several types of models: tissue differentiation at implant interfaces (Prendergast et al., 1997; Huiskes et al., 1997; Geris et al., 2003), fracture healing (Lacroix and Prendergast, 2002a,b; Lacroix et al., 2002; Isaksson et al., 2006), and osteochondral defect repair (Kelly and Prendergast, 2005, 2006).

Surgical implantation of an endoprosthesis gives rise to tissue reactions that are analogous to fracture healing (Willert and Buchhorn, 1999). The repair of resorbed bone tissue surrounding a femoral prosthesis can determine the success or failure of the prosthesis. Following a study by Søballe et al. (1992a) which showed that micromovements between bone and implant inhibit bone ingrowth and promote a fibrous tissue membrane formation around implants, Søballe et al. (1993) showed that a HA coating on an initially unstable implant helps promote eventual implant stability. Combining algorithms for mechanoregulation of tissue differentiation with bone remodelling algorithms could provide a significant step forward in computational modelling of the performance of uncemented hip replacements.

1.3 Objectives of this thesis

From the foregoing, it is clear that the long term success of a femoral hip prosthesis is dependant on numerous factors, and predominant among them is the peri-prosthetic bone reactions. Numerous investigations have been successful at predicting these adaptations; however, the limitations of these investigations is that they are based on either a strain or damage stimulus whereas bone tissue seems to react to both. Furthermore, tissue differentiation mechanoregulation algorithms have yet to be applied to real prosthesis geometries. These limitations to previous approaches can

be overcome by integrating and further developing existing algorithms.

It is first proposed in this thesis that a combined strain-damage remodelling algorithm can predict, simultaneously, both bulk bone remodelling due to stress shielding *and* interface bone adaptations at bone/implant interfaces. Secondly, the inclusion of a simplified tissue differentiation rule, based on that of Prendergast et al. (1997), could allow for either the repair of the gap by new bone formation (i.e. osseointegration) or persistence of the interfacial fibrous gap tissue (i.e. failed ingrowth). Incorporating both a strain-damage stimulated remodelling algorithm with a tissue differentiation algorithm would be a significant step forward in the development of pre-clinical and patient-specific testing tools in orthopaedics.

Chapter 2

Literature Review

Contents

2.1 Physiology of bone remodelling and tissue differentiation

It is widely accepted that mechanical loads generate a biophysical stimulus within tissue that leads to a biochemical signal which causes cells within the bone to mod-

ulate their production of extracellular matrix, causing both bone remodelling and tissue differentiation. Numerous investigations have been carried out into possible candidates for both the stimulus and mechanosensory cells for both remodelling and differentiation.

2.1.1 Bone remodelling

Bone consists of an extracellular matrix with four primary cell types: (i) osteoclasts, (ii) osteoblasts, (iii) bone lining cells, and (iv) osteocytes. Osteoclasts are giant cells with can have more than 50 nuclei. Their role is to dissolve the bony matrix by secreting acids. Osteoblasts form bone by expressing collagen and other proteins which later mineralize. Bone lining cells are flattened and elongated in-active or resting osteoblasts covering quiescent bone surfaces (Jee, 2001). They are capable of becoming active osteoblasts in order to form bone. Osteocytes are the most abundant cell in mature bone. They are formed when some osteoblasts become encased in the newly formed bone matrix. These remaining osteoblasts differentiate into osteocytes forming a long cell processes called canaliculi, to allow for contact with other bone cells (Jee, 2001). Osteocytes have been proposed as the likely candidates for mechanosensor cells (Cowin, 1991; Lanyon, 1993; Burger and Klein-Neulend, 1999; Noble and Reeve, 2000; Burger, 2001) because of their favorable distribution throughout the bone and interconnections with bone the bone effector cells (bone lining cells, osteoblasts, and osteoclasts). Structures resembling trabecular architectures have been generated in computer simulations by using osteocytes as mechansensors to sense mechanical signals and mediate local bone remodelling (Mullender et al., 1994; Mullender and Huiskes, 1995, 1997).

Bone remodelling is carried out by a group of bone cells in what is known as a basic multicellular unit (BMU). A BMU consists of osteoclasts and osteoblasts working simultaneously to resorb and deposit bone respectively. There are five stages in the bone remodelling process: (i) *resting*, where bone lining cells cover the inactive bone surfaces (80-95% of bone surface is inactive at any given time) (ii) *activation*, some stimulus converts a resting bone surface into a remodelling surface and osteo-

clast precursor cells are recruited (iii) *resorption*, newly formed osteoclasts begin to resorb bone forming cutting cones in cortical bone, see Fig. 2.1a and Howship's lacunae in cancellous bone see Fig. 2.1b (iv) *reversal*, is the transition between bone resorption and bone formation, cutting cones and Howship's lacunae lack osteoclasts but contain osteoblast proprogenitors (v) *formation*, first osteoblasts deposit bone matrix (osteoid) in discrete layers known as lamallae, secondly mineralization of the organic matrix occurs with full mineralization taking 3 to 6 months. A net loss in bone, and hence a decrease in bone mass is observed when the amount of bone resorbed exceeds that which is subsequently formed.

So if osteocytes are the mechanosensors which transduce a mechanical stimulus into a biological signal, what exactly is the driving stimulus? There have been a number of experimental investigations proposing different stimuli.

First it is considered that strain is a stimulus for remodelling. It is widely accepted that bone is able to alter its bone mass and shape in response to mechanical loading, namely that under conditions of reduced loading bone atrophy is observed, while over loading promotes hypertrophy. Numerous animal experiments have shown the adaptive response of bone to a altered mechanical loading. Uhthoff and Jaworski (1978) immobilised the right forelimb in beagle dogs and observed a reduction in bone mass of between 30% and 50%, see Fig. 2.2. O'Connor et al. (1982) demonstrated that the ratio between the maximum artificial strain state during experimental loading and the maximum strain state during normal loading, in the radii and ulnae of sheep, correlates to the degree of bone hypertrophy. The experiments of Lanyon et al. (1982), showed the removal of the ulna in mature sheep increased the

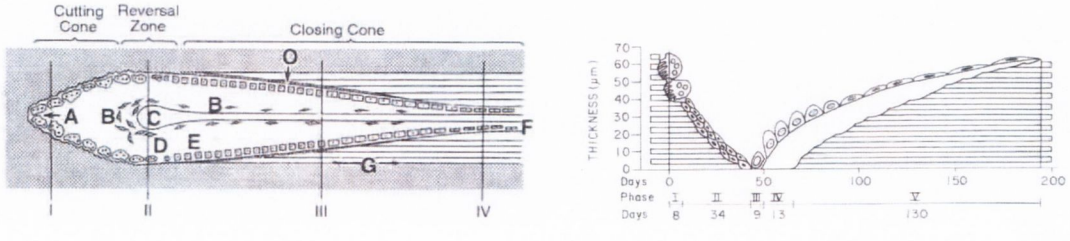

(a) (b)

Figure 2.1. Basic multicellular unit in (a) cortical bone and (b) cancellous bone. Adapted from Jee (2001).

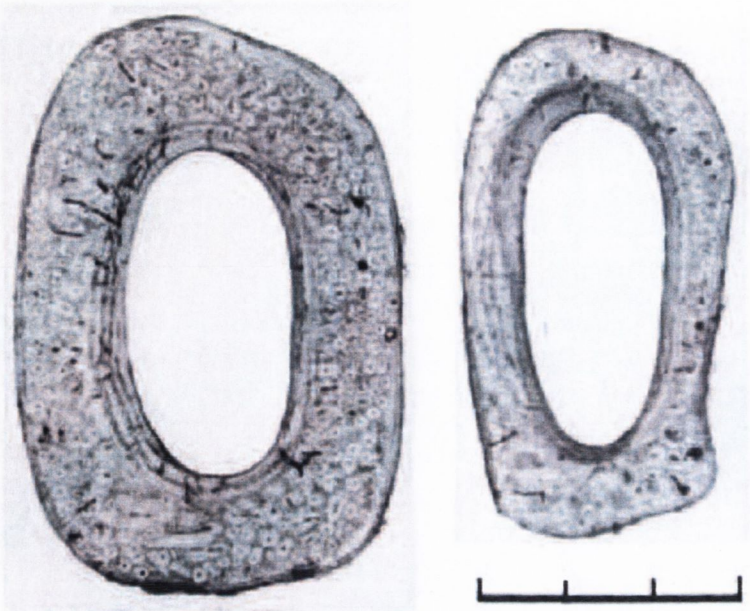

(a) (b)

Figure 2.2. Cross-section of metacarpal at forty weeks for (a) control and (b) experimental sides. Taken from Uhthoff and Jaworski (1978).

loading of the radius thus inducing new bone deposition, equilibrating the strains in the osteotomised and non-osteomised limbs. Similar results on the influence of strain on remodelling and bone formation were found in the four point bending of rat tibiae (Turner et al., 1991), and dynamic axial loading of rat ulnae (Mosley and Lanyon, 1998). It is thought that stresses and strains placed upon the bone cause fluid flow within the the lacunar-canalicular network stimulating osteocytes, which in turn emit signals to cells on the bone surface to regulate bone formation and resorption (Klein-Nulend et al., 1995; Turner et al., 1994).

Microdamage has also been proposed as a stimulus for bone remodelling. Microdamage accumulates over time as of a result of cyclic loading (Schaffler et al., 1995). Experimental evidence suggests that microdamage induces bone remodelling (Burr et al., 1985; Burr, 1993; Mori and Burr, 1993; Bentolila et al., 1998; Verborgt et al., 2000). Burr et al. (1985) found that a load producing 1500 microstrain for 10,000 cycles on the radii of dogs produced significant microdamage and that there were 44 times as many microcracks in areas associated with resorption spaces. Following this Mori and Burr (1993) considered the possibility that microcracks accumulated at preexisting resorption spaces, and consequently were caused by remodelling

rather than initiating it. They applied three-point bending load at 10,000 cycles with 2500 microstrain to the left limb of 13 dogs. Eight days later the right limb was loaded in the same manner and the dogs sacrificed immediately after. The results showed an increase in new remodelling events subsequent to microdamage formation, demonstrating that bone remodelling occurs in response to microdamage and not that microdamage accumulates at preexisting resorption spaces. A similar finding was found by Bentolila et al. (1998) in the ulnae of rats using an end-load bending system. Lee et al. (2002) observed that the location of and timing of microcracks, resorption cavities, and secondary osteons in overloaded sheep's radaii were consistent with the activation-resorption-formation of the remodelling cycle. Possible causes of the observed bone remodelling found in locations of damage accumulation include: osteocyte apoptosis induced by microdamage (Verborgt et al., 2000; Noble, 2003), unloading of osteocyte lacuna by microdamage (Prendergast and Huiskes, 1996a), and fracture of the osteocyte processes spanning the crack due to the shearing motion between crack faces (Taylor et al., 2003).

2.1.2 Tissue differentiation

Mesenchymal stem cells (MSCs) are cells that exist as unspecialised cells which lack tissue-specific characteristics until they are exposed to some appropriate signal (Barry, 2003). Tissue differentiation is a process by which MSCs can be directed to change into specific cell phenotypes which then produce extracellular matrices, forming specific tissue types of the skeletal system. When MSCs are exposed to specific growth factors they have the capacity to differentiate into several tissue types, including bone, cartilage, muscle, marrow, tendon and ligament, and other connective tissues, see Fig. 2.3.

It is believed that after injury mesenchymal stem cells migrate to the site of injury in an effort to repair the damaged tissue. Shapiro et al. (1993) observed, using a rabbit model, that the first step in the tissue repair/regeneration of an osteochondral defect is the proliferation and differentiation of the mesenchymal stem cells into tissue specific cells in the defect. Fibroblasts and chondrocytes were observed to form

fibrous connective tissue and cartilaginous tissues respectively, while bone matrix is laid down by osteoblasts.

It is well documented that mechanical stimulation is required to maintain the integrity of skeletal tissues. Although mechanoregulation theories have postulated for many years that mechanical stimulation can influence tissue differentiation (Pauwels, 1980; Perren, 1979; Carter et al., 1988; Claes and Heigele, 1999; Prendergast et al., 1997), it has only been in recent years that in vitro experiments have been carried out to demonstrate that mechanical loading can direct MSC differentiation (Matsuda et al., 1998; Altman et al., 2002; Angele et al., 2003; Knippenberg et al., 2005; Miyanishi et al., 2006; McMahon et al., 2006).

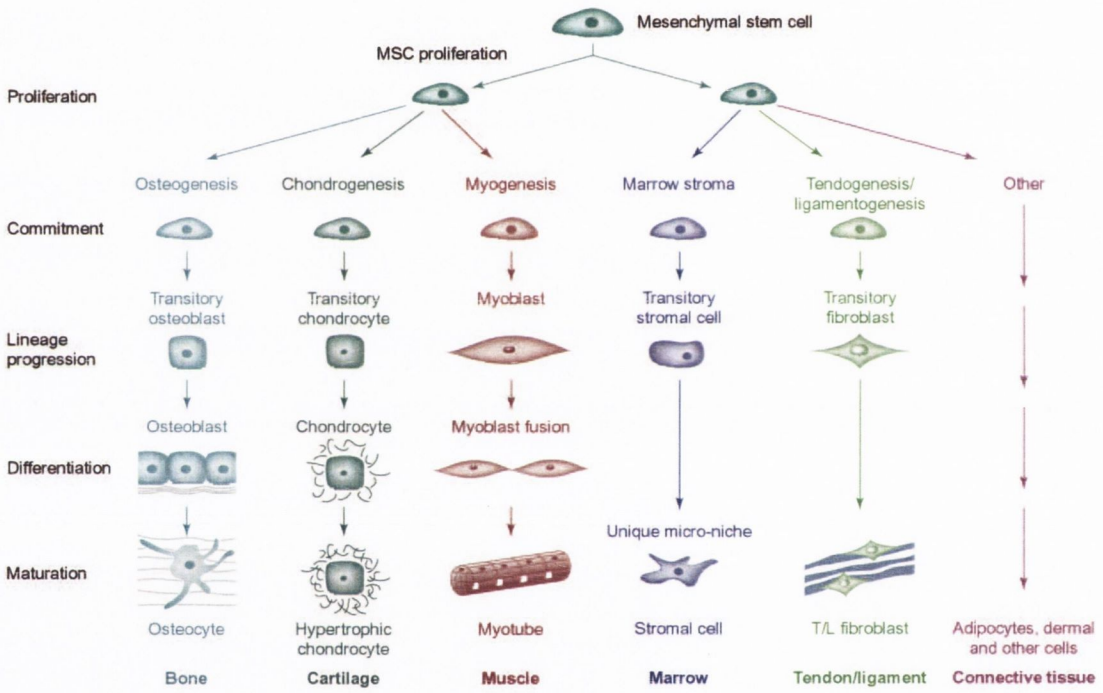

Figure 2.3. Mesenchymal stem cell differentiation pathways. Taken from Caplan and Bruder (2001).

2.2 Mechanoregulation models

Mechanobiology is the study of how mechanical forces influence biological processes. Numerous researchers have proposed different theoretical mechanoregulation models for both bone remodelling and tissue differentiation. These mechanoregulation

models have been combined with finite element methods to simulate the density distribution in the proximal femur (Carter et al., 1989; Fyhrie and Carter, 1990; Beaupré et al., 1990a), the morphological changes around prostheses (Huiskes et al., 1987; Weinans et al., 1992), tissue differentiation at implant interfaces (Prendergast et al., 1997; Huiskes et al., 1997; Geris et al., 2003), fracture healing (Lacroix and Prendergast, 2002a,b; Lacroix et al., 2002; Isaksson et al., 2006), and osteochondral defect repair (Kelly and Prendergast, 2005, 2006).

2.2.1 Strain stimulated remodelling

The theory of adaptive elasticity developed by Cowin and Hegedus (1976) proposes that bone has the capacity to adapt both its density and shape to attain a remodelling equilibrium strain state. Remodelling equilibrium is characterised by the homeostatic equilibrium strain state, which is based on physiological loading, material properties and boundary conditions. This method can be considered 'site specific', as the remodelling equilibrium strain state is site dependent, i.e. different from one position to another in the bone. Any deviation from the equilibrium strain state, caused by a change in load, produces a local strain difference. Consequently, the bone strives to re-establish the remodelling equilibrium strain state by adapting the density and shape of the bone. Equation 2.1 was proposed by Cowin and Buskirk (1979) to predict surface remodelling based on the theory of adaptive elasticity

$$S(Q) = [\mathrm{B}]\{\varepsilon - \varepsilon^0\} \tag{2.1}$$

where S represents the rate of change in position of point Q on the external bone surface, ε and ε^0 are the strain and remodelling equilibrium strain vector at that point, and [B] is the row matrix of remodelling rate constants.

Huiskes et al. (1987) proposed a development of Cowin's adaptive elasticity theory whereby the remodelling signal used was the, scalar, local strain-energy density (SED) as opposed to the local strain tensor. In addition the concept of a 'lazy zone', suggested by Carter (1984), was introduced. This assumes that bone must be either over or under-loaded before bone adaptation occurs, giving a non-linear rate

equation expressed as

$$\frac{\mathrm{d}E}{\mathrm{d}t} = \begin{bmatrix} C_e(U-(1+s)U_n), & U > (1+s)U_n \\ 0, & (1-s)U_n \leq U \leq (1+s)U_n \\ C_e(U-(1-s)U_n), & U < (1-s)U_n \end{bmatrix} \tag{2.2}$$

where s is half the width of the lazy zone, E is the elastic modulus, C_e is the remodelling rate coefficient, U_n and U is the homeostatic and measured strain-energy density respectively. This method was applied to investigate the influence of intramedullary prosthesis design characteristics on bone remodelling patterns, with the stiffer stems exhibiting an increased amount of proximal bone loss due to stress shielding.

The two theories explained above are 'site-specific', or 'site-dependent', as the homeostatic strain levels vary depending on the location in the bone. Fyhrie and Carter (1986) proposed an alternative 'site-independent' theory to predict the adaptation of both the apparent bone density and trabecular orientation to a change in applied stress. It was assumed that cancellous bone is a self-optimizing material which simultaneously minimizes the amount of bone while maximizing its structural integrity for a given stress. An objective function, $Q(\rho, \theta, \sigma)$, where ρ is the apparent density, θ is the orientation, and σ is the stress tensor, is used to find the minimum acceptable apparent density and optimal trabecular orientation. Two approaches were investigated: one on optimizing the strain energy density (stiffness), and another on optimizing the strength. Both of the methods predict that, at remodelling equilibrium, the relationship between the applied stress and the apparent density of cancellous bone is given by

$$\rho \propto \sigma_{eff}^{C} \tag{2.3}$$

where σ_{eff} is an effective stress and the value of C depends on whether stiffness or strength optimization is assumed. This method was investigated by Fyhrie and Carter (1990) using a finite element model to predict the bone density distribution in the femoral head and neck during the single-limb-stance phase of gait. The

apparent density was predicted using: (i) the von Mises, (ii) the energy stress and (iii) a spherical stress. They showed that the von Mises stress was not accurate in predicting the apparent density of the femoral head, while both the energy and effective stress predicted a dense column of trabecula bone through the head as seen physiologically. This difference was attributed to the exclusion of the influence of dilatational, or hydrostatic, stress on bone remodelling in the von Mises model, and areas experiencing purely dilatational stress would experience zero von Mises stress and hence resorbtion is experienced. The theory proposed by Fyhrie and Carter (1986) was further expanded by Carter et al. (1987) to include the multiple loading conditions experienced by the bone and subsequently applied to a two-dimensional finite element model of the proximal femur to predict the distribution of trabecular bone density (see Fig. 2.4) using Equation 2.4 (Carter et al., 1989)

$$\rho = K \left(\sum_{i=1}^{c} n_i \sigma_i^M \right)^{(1/2M)} \tag{2.4}$$

where c is the number of discrete loading conditions, K and M are constants, n is the number of loading cycles, σ is the 'energy stress' $\sigma_{energy} = \sqrt{2EU}$, and ρ is the bone apparent density. The results showed multiple loading conditions are required to predict a realistic trabecular density distribution, and the orientation of the trabeculae are not necessarily perpendicular, as proposed by Wolff. However, the model did not converge to an equilibrium with excessive density predicted for

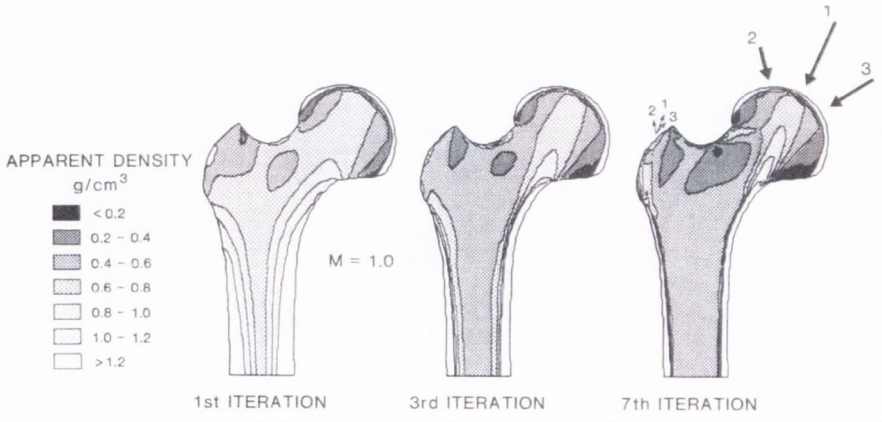

Figure 2.4. Predicted density distribution using multiple loads. Adapted from Carter et al. (1989).

the seventh iteration. The progressive increase in bone density after the seventh iteration was attributed to four causative factors: (1) the constitutive relation in Equation 2.4 whereby the advantage of increasing the bone density is diminished as the the effective stress is related to the square of the apparent density while the modulus increases as a cube of the density thus increasing the magnitude of the stress in the following iteration, (2) more subtle density changes when a greater variation in loading conditions is used, (3) the use of a continuum model to represent cancellous bone whereby no limit was imposed on remodelling resulting in densities incompatible with practical limits of the continuum model, and (4) the assumption that remodelling proceeds to a unique equilibrium solution i.e. no 'lazy zone' was used.

Beaupré et al. (1990b) developed this concept further by making the theory into a time-dependent one. The daily tissue level stress stimulus ψ_b is defined as

$$\psi_b = \left(\sum_{day} n_i \bar{\sigma}_{b_i}^m \right)^{(1/2m)} \tag{2.5}$$

where n_i is the number of loading cycles of load type i, $\bar{\sigma_{b_i}}$ is the tissue level effective stress, and the stress exponent m is an empirical constant. The relationship between the stress stimulus and rate of bone resorption/formation, denoted $\dot{r}$, was expressed as

$$\dot{r} = \begin{bmatrix} c_1(\psi_b - \psi_{b_{AS}}) + (c_1 - c_2)w_1, & (\psi_b \psi_{b_{AS}} < -w_1) \\ c_2(\psi_b - \psi_{b_{AS}}), & (-w_1 \leq \psi_b - \psi_{b_{AS}} < 0) \\ c_3(\psi_b - \psi_{b_{AS}}), & (0 \leq \psi_b - \psi_{b_{AS}} < -w_2) \\ c_4(\psi_b - \psi_{b_{AS}}) + (c_3 - c_4)w_2, & (\psi_b \psi_{b_{AS}} > +w_2) \end{bmatrix} \tag{2.6}$$

where $\psi_{b_{AS}}$ is the attractor, remodelling, equilibrium stress stimulus, ψ_b is the daily tissue stress stimulus, c_1, c_2, c_3, and c_4 are empirical rate constants, and w_1 and w_2 is the width of the central, normal activity region (Beaupré et al., 1990b). Equation 2.6 can be used to predict the rate of bone deposition or resorption on external bone surfaces. However, to model the rate of internal remodelling the relationship between bone surface area and apparent density, developed by Martin (1984), was included

to derive an equation for the rate of change of apparent density

$$\dot{\rho} = \dot{r} S_v \rho_t \tag{2.7}$$

where $\dot{\rho}$ is the time rate of change in apparent density, $\dot{r}$ is the rate of bone apposition or resorption, S_v is the bone surface area density (see Fig. 2.5), and ρ_t is the true density of bone tissue. This method was used to determine the distribution of bone density in a two-dimensional model of the proximal femur (see Fig. 2.6) using a simplified version of Equation 2.6 where no bone remodelling occurs within the lazy zone i.e. $c_2 = c_3 = 0$. As with Carter et al. (1989) satisfactory distribution of bone density was predicted. However, convergence was achieved this time, even after a period of reduced loading and subsequent reinstatement of the original load.

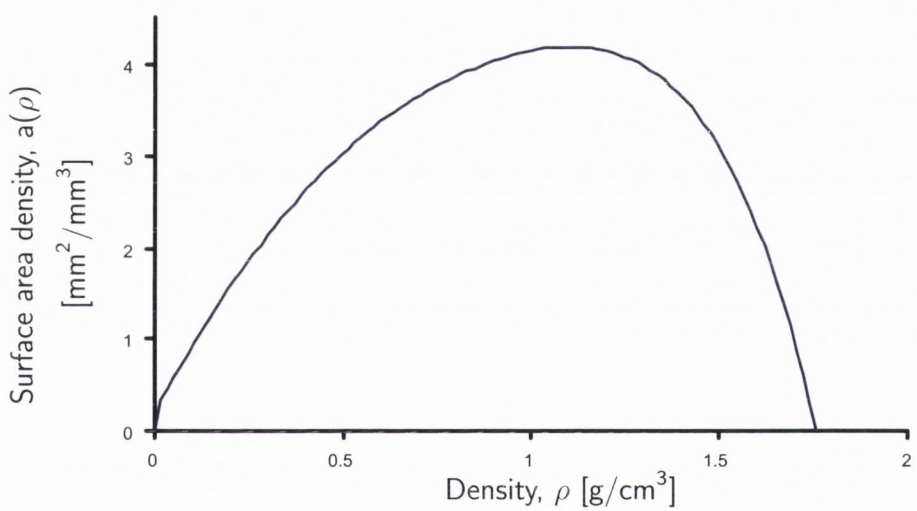

Figure 2.5. Density (ρ) versus free surface area per unit volume (a(ρ)).

2.2.2 Damage stimulated remodelling

An alternative approach to the simulation of bone remodelling is based on microdamage. Carter et al. (1987) proposed fatigue damage accumulation as a bone maintenance stimulus whereby the local apparent density is altered to ensure an efficient factor of safety. Prendergast and Taylor (1994) expanded this concept by accounting for damage accumulation with a continuous damage rate. It was hypothesised that, even at remodelling equilibrium, damage exists in the form of microcracks in

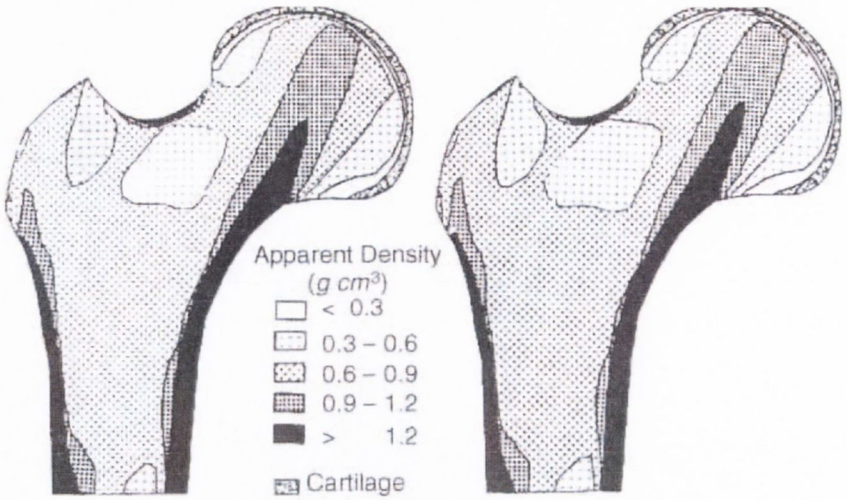

Figure 2.6. Predicted density distribution using multiple loads after (a) 40 (330 days) and (b) 50 (412.5 days) time increments. Adapted from Beaupré et al. (1990a).

the bone; this remodelling equilibrium damage was denoted ω_{RE}. A second hypothesis was that the homeostatic stress determines the rate of damage repair, and at remodelling equilibrium the rate of damage formation equals that of damage repair, i.e. $\dot{\omega} = \dot{\omega}_{\mathrm{RE}}$. Deviation of the damage formation rate from the remodelling repair rate results in an accumulation of damage and a remodelling stimulus

$$\Delta\omega = \dot{\omega} - \dot{\omega}_{\mathrm{RE}} \neq 0 \tag{2.8}$$

where $\dot{\omega}$ and $\dot{\omega}_{\mathrm{RE}}$ are the rate of damage formation and repair respectively, and $\Delta\omega$ is the difference between the actual damage and the equilibrium amount, i.e. it is the change in accumulated damage and can be calculated as

$$\Delta\omega = \int_{t_o}^{t} (\dot{\omega} - \dot{\omega}_{\mathrm{RE}}) dt \tag{2.9}$$

The rate of remodelling at a time t can be expressed as

$$\frac{\mathrm{d}X}{\mathrm{d}t} = C \int_{t_o}^{t} (\Delta\omega) \mathrm{d}t \tag{2.10}$$

where C is a rate constant and X represents the periosteal bone diameter. This approach was applied to a bone diaphysis under a reduced torsional load giving physically reasonable results. However, convergence to a homeostatic strain was not achieved. Instead an overshoot was predicted. This is attributed to the accumulative nature of the model whereby even when $\dot{\omega} = \dot{\omega}_{RE}$ and the rate of increase of $\Delta\omega$ is zero, $\Delta\omega$ itself will not be zero. Hence, a backlog of accumulated damage remains to be repaired and bone adaptation will continue until the damage is fully repaired. A similar approach was applied to a simplified axi-symmetric finite element model of an intramedullary prosthesis (Prendergast and Taylor, 1992). This theory was further developed by (McNamara et al., 1997) who modeled damage as a function of crack length, and was applied to a finite element model of a noncemented femoral prosthesis. The results of the damage stimulated remodelling were shown to be equivalent to those based on strain energy density and successfully predicted the adaptive remodelling of bone in response to an altered load once damage was assumed as nonlinear.

2.2.3 Strain and damage stimulated remodelling

Prendergast and Huiskes (1996b) investigated the influence of microdamage on the local strain sensed by osteocytes, assuming that osteocytes exists as strain sensors. It was predicted that accumulation of microdamage continually alters the local deformation of the osteocyte-containing lacunae. They proposed that both strain-adaptive and damage-adaptive remodelling work simultaneously, whereby high loads induce damage accumulation causing local stress reductions and subsequent bone resorption. This was corroborated by Burr et al. (1985) and Mori and Burr (1993). Prendergast (2002) carried on from this and developed a combined strain and damage stimulated remodelling "mechanoregulation rule". It was proposed that below a certain critical damage level, remodelling is governed by strain, and above it a stimulus due to damage also acts. This is shown graphically in

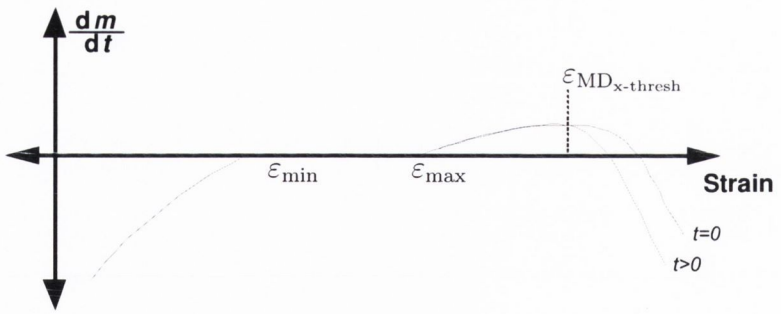

Figure 2.7. Bone remodelling in response to strain and damage simultaneously. Adapted from Prendergast (2002).

Fig. 2.7, and the rate of change of mass can be expressed mathematically by

$$\frac{\mathrm{d}m}{\mathrm{d}t} = C(\epsilon - \epsilon_{ref}) + xC_1(\Delta\omega) \tag{2.11}$$

where $x = 1$ if $\Delta\omega$ is positive else $x = 0$, C and C_1 are remodelling rate constants, and $\Delta\omega$ is the change in damage from equilibrium, see Equation 2.8.

The influence of strain and/or damage on a two-dimensional model of BMU remodelling on the surface of a trabecula was investigated by McNamara and Prendergast (2006). Four mechanoregulation rules were studied: (i) strain only, (ii) damage only, (iii) strain and damage combined and (iv) strain or damage where damage-adaptive remodelling is prioritised over strain-adaptive remodelling when damage exceeds a critical level. The only algorithm which gave physiologically reasonable results, where both damage removal and refilling of existing cavities was predicted, was the algorithm which prioritised damage remodelling once a critical level was reached i.e. (iv), this can be described by

$$\begin{aligned} \omega < \omega_{CRIT} \quad & \frac{\mathrm{d}\rho_j}{\mathrm{d}t} = C_1 S^j_{strain} \\ \omega > \omega_{CRIT} \quad & \frac{\mathrm{d}\rho_j}{\mathrm{d}t} = C_2 S^j_{damage} \end{aligned} \tag{2.12}$$

where C_1 and C_2 are strain and damage rate constants respectively, ω_{CRIT} is the critical damage, and S denotes the stimulus (either strain or damage).

2.2.4 Tissue differentiation

Pauwels (1980) proposed that the differentiation of the mesenchymal cells is a function of both the change in shape, due to shear (deviatoric) stresses, and volume, due to hydrostatic (dilatational) stresses, of the cells, see Fig. 2.8. A schematic of Pauwels' theory is shown in Fig. 2.9. It proposes that under a shear stimulus mesenchymal cells differentiate into fibroblasts and fibrous connective tissue is formed, and under hydrostatic compression chondrocytes proliferate and cartilage is formed. For a combination of both stimuli differentiation into fibrocartilage is assumed. The arrows on Fig. 2.9 show that, once the soft tissue is formed a stabilised mechanical environment can lead to ossification.

Perren (1979) introduced the theory of interfragmentary strain (IFS) which proposes that the tissue which fills the fracture gap must be able to sustain the IFS without failure. High IFS promotes formation of granulation tissue, which in turn reduces the IFS. Due to the reduced IFS chondrocytes can proliferate allowing for endochondral ossification. However, this may only be regarded as a theoretical relationship between tissue formation and IFS as many other mechanical and structural

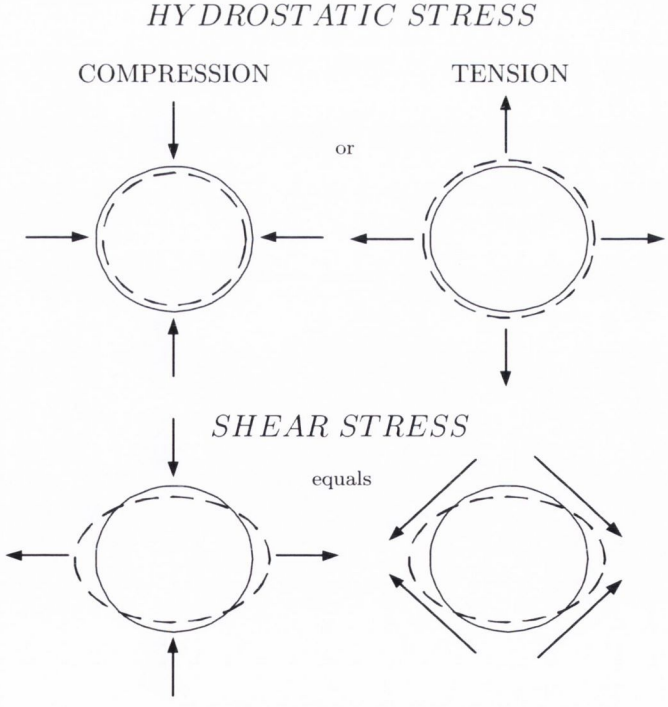

Figure 2.8. Schematics of hydrostatic (dilatational) stresses and shear (deviatoric) stresses. From Carter et al. (1988).

factors may influence the IFS.

Carter et al. (1988) proposed that both the vascularity and intermittent or cyclic stress play an important role in tissue differentiation. Two stress invariants were proposed to regulate bone formation: octahedral shear stress S defined as

$$S = \frac{1}{3}\sqrt{(\sigma_1 - \sigma_2)^2 + (\sigma_2 - \sigma_3)^2 + (\sigma_3 - \sigma_1)^2} \tag{2.13}$$

and hydrostatic stress D defined as

$$D = \frac{1}{3}(\sigma_1 + \sigma_2 + \sigma_3) \tag{2.14}$$

where σ_1, σ_2, and σ_3 are the peak cyclic principal stresses. It is hypothesised that high shear and/or hydrostatic tensile stress would promote fibrous tissue formation, and at low hydrostatic and shear stress, with a good vascular supply, bone formation is permitted, see Fig. 2.10. A linear combination of the stress invariants expresses

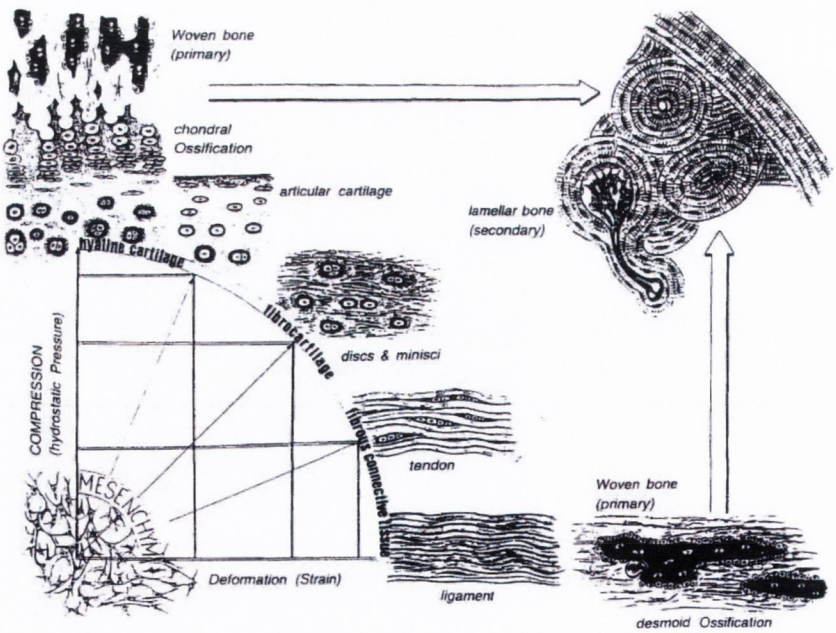

Figure 2.9. Pauwels' theory of tissue differentiation. From Weinans and Prendergast (1996).

the net stimulus, the osteogenic index (I) for ossification, given by

$$I = \sum_{i=1}^{c} n_i(S_i + kD_i), \tag{2.15}$$

where i indicates a specific loading case, n_i is the number of loading cycles, and k is an empirical constant. High shear and/or tensile dilatational stresses and hence, high levels of I, will promote fibrous tissue formation, while high compressive dilatational stresses encourage chondrogensis. Subsequently if a chondroid-like tissue forms, high shear stresses or tensile dilatational stresses promote endochondral ossification, with compressive dilatational stresses inhibiting it (Carter and Wong, 1988). This method was applied to two-dimensional finite element models of (i) healing of fracture callus' (Carter et al., 1988; Blenman et al., 1989; Gardner et al., 2004) (ii) chondroosseous development in diarthrodial joints (Carter and Wong, 1988), and (iii) tissue differentiation at implant interfaces (Prendergast and Huiskes, 1996a), see Fig. 2.11. Carter et al. (1988) found that the ossification patterns were consistent with experimental observations, and that high compressive hydrostatic stresses inhibit ossification. In a follow on study of ossification of the callus during the later stages of healing, Blenman et al. (1989) found that ossification can occur in the presence of intermediate hydrostatic compressive stresses. This was also observed by Gardner et al. (2004) who suggested that the hypothesis was not totally successful at predicting the healing pattern.

Claes and Heigele (1999) compared the local strains and stresses of their finite element model with the histological findings from a fracture callus of an animal

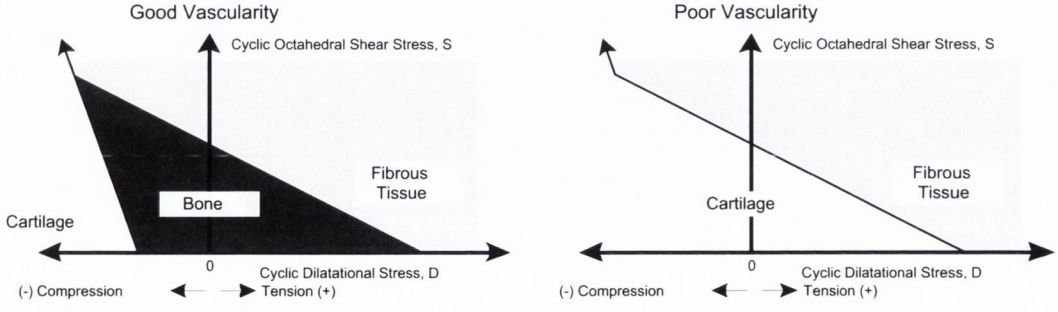

Figure 2.10. Schematic of influence of hydrostatic stress, octahedral shear stress, and vascularity on differentiation. Adapted from Carter et al. (1988).

model. They found that strains less than 5% and hydrostatic stresses smaller than ± 0.15 MPa promote intramembranous ossification, while strains less than $\pm 15\%$ and compressive hydrostatic stresses greater than -0.15 MPa favor endochondral ossification, everything else predicts connective or fibrous tissue formation, see Fig. 2.12.

The previously mentioned models assumed the tissue had elastic material properties whereas Prendergast and Huiskes (1996a) considered the tissue as a bi-phasic

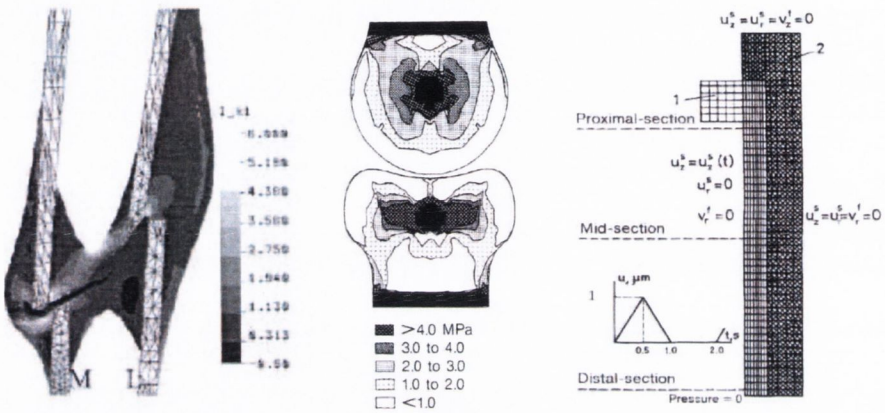

Figure 2.11. Two-dimensional models of (i) fracture callus (Gardner et al., 2004), (ii) diarthrodial joint (Carter and Wong, 1988), and (iii) bone/implant interface (Prendergast and Huiskes, 1996a).

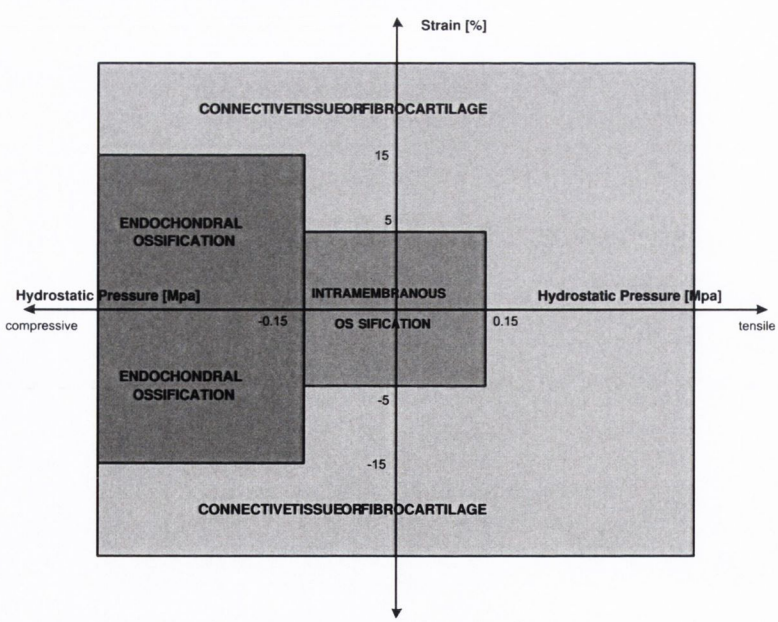

Figure 2.12. Relationship between mechanical stimuli and tissue types in the fracture callus. Adapted from Claes and Heigele (1999).

material accounting for both the solid and fluid constituents. This approach was further developed by Prendergast et al. (1997) who proposed a mechanoregulation rule where tissue differentiation depends on two biophysical stimuli: shear strain in the solid phase and fluid velocity in the fluid phase, see Fig. 2.13. It was shown that the biophysical stimulus felt by the cells changes significantly as the tissue type changes, and that these changes may regulate tissue differentiation.

High levels of shear strain and fluid velocity promote fibrous tissue formation, intermediate levels promote cartilageous tissue, and bone formation is assumed at low levels. Huiskes et al. (1997) quantified the limits of the mechanical stimulus for each of the tissue phenotypes, given by

$$S = \frac{\gamma}{a} + \frac{\nu}{b}, \tag{2.16}$$

where γ is the peak shear strain and ν is the peak fluid velocity, and a and b are empirical constants. If $S > 3$ differentiation of mesenchymal stem cells to fibroblasts leading to fibrous tissue formation is assumed, when $1 \leq S \leq 3$ cartilage is formed, and when $S < 1$ bone formation occurs. This was further extended by Lacroix et al. (2002) to include mesenchymal cell migration using a diffusion analysis and applied to a two-dimensional axi-symmetric finite element model of fracture healing. The results compared favorably to observed tissue formation patterns, however the origin of the progenitor cells (from either the medullary cavity, the periosteum, or the muscle) were found to influence the healing pattern. This approach has also been applied to a three-dimensional model of a tibia with a fracture callus (Lacroix

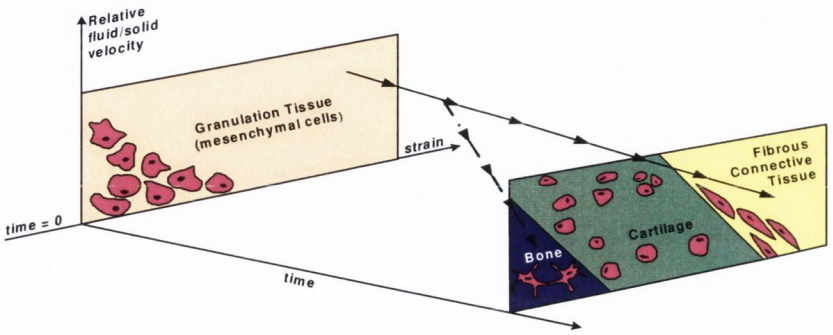

Figure 2.13. Mechanoregulation diagram of tissue differentiation based on shear strain and fluid flow. Adapted from Prendergast et al. (1997).

and Prendergast, 2002b). Kelly and Prendergast (2005) further expanded the work of Lacroix et al. (2002) to included the influence of the mechanical stimuli on cell mitosis and death, and the influence of tissue phenotype on cell dispersal in a two-dimensional model of an osteochondral defect. This approach was later applied to the same model to predict optimal scaffold material properties in osteochondral defect repair (Kelly and Prendergast, 2006).

Pérez and Prendergast (2006) proposed a model whereby cells disperse using a random walk model rather than a diffusion model. A cell in the random walk model is assumed to be surrounded by four possible locations that a daughter cell can occupy, providing that position is not already occupied, see Fig. 2.14. Cell migration was also modeled based on the random walk approach, whereby five random jumps are performed for each cell with the final position being that at the end of the iteration, again, providing that space is free. Using the same biophysical stimuli as Prendergast et al. (1997) (octahedral shear strain and fluid velocity) a simulation of gap tissue differentiation in a two dimensional model of an implant/bone interface was performed. The predicted stiffness of the gap tissue was similar to that predicted by the diffusion model; however the pattern of of tissue differentiation differed. While the diffusion model predicted continuous patterns (Fig. 2.15a), the random walk model predicted discontinuous patterns (Fig. 2.15b).

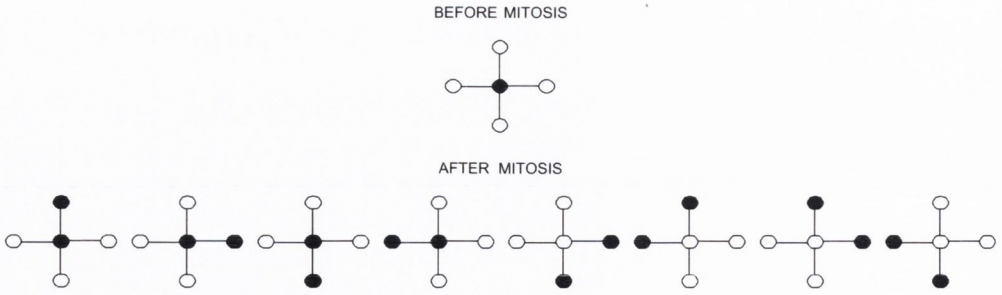

Figure 2.14. Possible states that a daughter cells can occupy after mitosis using the random walk model. Taken from Pérez and Prendergast (2006).

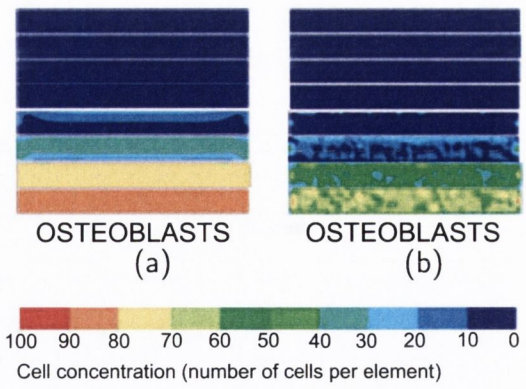

Figure 2.15. Predicted osteoblast cell distribution at implant/bone interface with (a) diffusion and (b) random walk analysis. Adapted from Pérez and Prendergast (2006).

2.3 Total hip arthroplasties

Hip prostheses can generally be classified according to their method of fixation to the underlying bone, namely cemented or cementless fixation. In the case of a cemented prosthesis, fixation is achieved using a bone cement, with polymethylmethacrylate (PMMA) the most commonly used. This contains: (i) particles of barium sulphate ($BaSO_4$) or zirconia (ZrO_2) which act as radiopacificiers which make the cement visible in radiographs, (ii) an inhibitor (hydroquinone) to prevent spontaneous polymerization and an initiator to initiate polymerization at room temperature, and (iii) antibiotics to prevent infection (Prendergast, 2006). Charnely (1960) was the first to fixate a hip arthroplasty using an acrylic bone cement, see Fig. 2.16a. The bone cement acts as a filler adapting the irregular surface of the femoral canal to the smooth surface of the prosthesis, distributing the load over a larger bone area, thus avoiding any localised over-loading. Primary fixation is achieved by pressurising the bone cement so it penetrates the cancellous bone structure to achieve mechanical interdigitation, with the strength of the cement/bone interface having a positive correlation to the degree of interdigitation (Mann et al., 2001).

Cementless fixation may be achieved through either a biological or a press-fit means. Biological fixation is achieved through a process know as osseointegration, where a stable bone/implant interface is achieved by bone ingrowth onto the surface of the prosthesis, which can have a porous or hydroxyapatite (HA) coating,

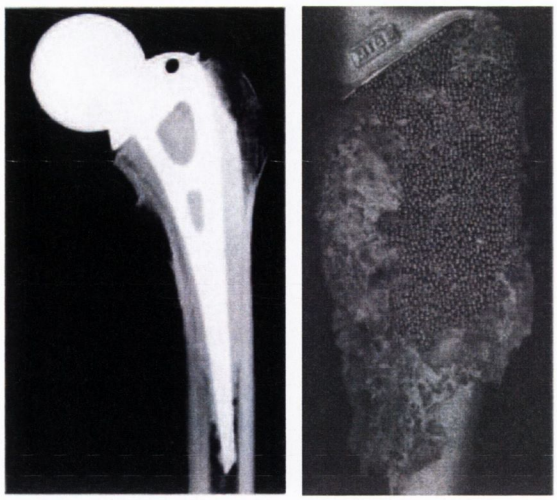

(a) (b)

Figure 2.16. Methods of fixation (a) radiograph of prosthesis fixed by bone cement (Charnely, 1960) (b) prosthesis fixation by bone ingrowth (Eldridge and Learmonth, 1999).

see Fig. 2.16b. Successful fixation does not require osseointegration over the full surface of the coating; Sychterz et al. (2002) found osseointegration to occur over approximately 35% of the porous coating. This osteoconductive surface tends to be located on the proximal part of the prosthesis to facilitate proximal load transfer in an attempt to reduce the degree of stress shielding. Press-fit fixation depends on a very tight fit, or interference fit, of the device into the bone. This may be achieved by implanting a larger stem into a somewhat smaller medullary cavity.

However, failures of the both cemented and cementless do occur, and is generally observed as aseptic loosening and pain for the patient. Loosening of cemented prostheses commonly occurs by fatigue failure of the bone cement, which may be caused by: crack growth from pores within the cement or stress concentrations at the implant/cement interface, or bone resorption causing an increase in stress in the cement (Prendergast, 2006). For cementless prostheses, relative micro-motions between the bone and implant inhibits bone ingrowth leading to failed ingrowth and eventual loosening. Huiskes (1993) proposed six *failure scenarios* to describe the nature of aseptic loosening:

1. *Accumulated Damage:* Accumulation of damage in the prosthesis during cyclic loading and/or gradual cracking of the bone cement.

2. *Particulate Reaction:* Particles migrating to interfaces causing osteolysis and fibrous tissue formation. Particles may come from: wear of articulating surfaces, abrasion of PMMA/prosthesis/bone interfaces, fretting between metal parts.

3. *Failed Ingrowth:* Large gaps between prosthesis and bone or excessive micromotion prevent bone ingrowth in noncemented implants.

4. *Stress Shielding:* The load formerly carried by the bone alone is now shared with the rigid prosthesis resulting in some areas of the bone being shielded from the stresses. This may lead to bone resorption.

5. *Stress Bypass:* Localised osseointegration and stress transfer causing some bone to be bypassed reducing the stress, causing local bone atrophy.

6. *Destructive Wear:* Wear of bearing surfaces leading to eventual disintegration of component.

2.4 Peri-prosthetic bone adaptations

It is widely believed that these changes in bone around a prosthesis are related to the changes in bone stress/strain patterns that inevitably result from the introduction of the prosthesis. It is the aim of finite element models incorporating mechanobiological algorithms to predict these changes so as to gain a better understanding of the intimate relationship between prosthesis design factors, such as material choice and geometry, and the host bone response. An ultimate objective would be to use such algorithms for pre-clinical testing (Prendergast et al., 2006).

2.4.1 Clinical observations

The extent of bone remodelling subsequent to the introduction of a cementless femoral hip replacement depends critically on the design of the prosthesis. Cementless prostheses need to have larger cross-sections in order to fill the medullary canal in order to increases the initial stability and the potential for osseointegration.

Hence, they tend to be larger and stiffer than cemented stems are more susceptible to stress shielding, see Fig. 2.17.

In an attempt to better understand the causative factors of stress shielding, and possible steps which could be taken to avoid it, numerous clinical studies have been performed investigating prosthesis design factors, such as stem stiffness, stem size, and area of coating, on adaptive bone remodelling.

Engh et al. (1987) evaluated 307 patients after two years and 89 patients after five years with a porous-coated cobalt-chrome femoral implant. It was found that 88% of the cases examined at two years showed little or no stress shielding, while only first (slight rounding off of the proximal medial bone edge) or second degree stress shielding (rounding off of proximal medial femoral neck with loss of medial cortical density in the proximal femur, level 1) was observed in all of the cases studied after five years. This was attributed to the fact that most of the implants used had a small stem width. Twenty-four of the thirty-six cases which showed increased stress shielding had been implanted with larger, and hence stiffer, implants with a stem diameter of 15.0 mm or more. In a similar study Engh and Bobyn (1988)

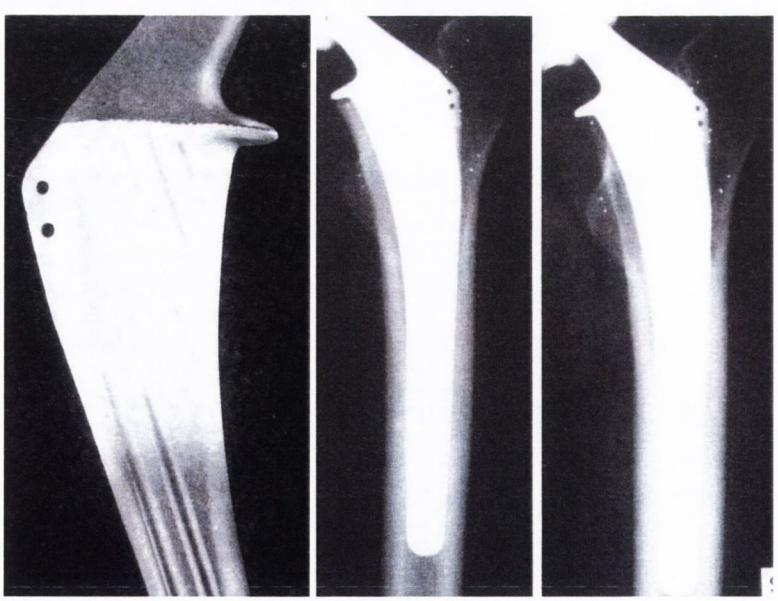

(a) (b) (c)

Figure 2.17. (a)Tifit (Smith and Nephew Richards) titanium alloy hydroxyapatite coated cementless stem (b) postoperatively and (c) two years after operation showing proximal bone loss due to stress shielding. Adapted from Kärrholm et al. (1994).

observed the influence the stem size and also the extent of porous coating on femoral bone resorption in 411 cases (380 patients) implanted with the same porous-coated cobalt-chrome femoral prosthesis as mentioned above over a two year period. One-third proximal coating was used in 110 cases, 166 cases of two-thirds coated, and 135 cases of fully coated stems. The influence of stem size was first considered and showed, similar to Engh et al. (1987), that the incidence of second and third degree (more extensive cortical resorption) stress shielding increased five fold in the larger stem group, 13.5 mm diameter and above. The influence of porous coating was investigated for both large and small stem groups. For stem with a diameter $\leq$ 12.0 mm the amount of porous coating had little influence, while stems porous coating had a significant effect on larger stems with a diameter $\geq$ 13.5 mm where second and third degree bone resorption increased twofold to fourfold in cases with two-thirds and fully coated stems. As regards bone ingrowth both Engh et al. (1987) and Engh and Bobyn (1988) observed a higher percentage of bone ingrowth in the thicker canal filling stems, thus presenting two competing objectives: bone ingrowth fixation and reduction proximal stress shielding.

In an effort to improve osseointegration and reduce stress shielding hydroxyapatite-coated titanium stems have been introduced (D'Antonio et al., 1992, 1996; Jaffe and Scott, 1996; Capello et al., 1997). Scott and Jaffe (1996) studied the host bone response to both hydroxyapatite-coated titanium and porous-coated cobalt-chrome stems in three paired bilateral cases. Proximal bone mineral density (BMD), obtained from DXA analysis, showed the HA-coated titanium stem was, on average, 7.9% and 12% higher in Gruen zones 1 and 7 respectively. A higher BMD was also found adjacent to the coated regions of the titanium stems suggesting greater osseointegration and improved fixation.

Cementless prostheses with lower stem stiffness has been subject to a number of clinical studies (Jakim et al., 1998; Buma et al., 1997; Harvey et al., 1999). Jakim et al. (1998) found a 32% rate of aseptic loosening of low modulus "iso-elastic" femoral stems. Radiologically, radiopaque lines within radiolucent zones indicated loosening. In the study of Buma et al. (1997), three HA-coated load bearing prosthe-

ses of varying stiffness were inserted into the tibia of the goat with a finite element model used to quantify the interfacial stresses and relative motions. The interface conditions for the stiff implants (stainless steel) provided favorable conditions initially for osseointegration. However, evidence of loosening was observed after 24 weeks where by delamination at the HA-metal interface and fibrous tissue formation at the distal tip, which coincides with the location of the highest interface stresses predicted by the FE model, promotes micromotions and further soft tissue interposition. The intermediate (hollow titanium) and flexible (polyacetal) stems exhibited unfavorable initial interface conditions with high interface motions (unbonded) and stresses (bonded) and consequently a higher incidence of early initial loosening and interfacial fibrous tissue formation. In an animal study in dogs, Søballe et al. (1992a) showed that this lack of initial stability inhibits bone ingrowth and promotes fibrous tissue formation surrounding an implant. In a bilateral arthroplasty study by Harvey et al. (1999) a titanium alloy and a more flexible composite stem were implanted in dogs. The composite stems showed less bone ingrowth and a high incidence of radiopaque line formation indicative of fibrous tissue formation. The tissue reactions at the interface, which may result in the formation of fibrous tissue, have been shown to be analogous to fracture healing (Willert and Buchhorn, 1999), where mesenchymal stem cells invade the gaps between the stem and bone,which can then differentiate to form bone, fibrous tissue, or fibrocartilage.

2.4.2 Computational analyses

Some of the remodelling and tissue differentiation theories, discussed in chapter 2.2, have been incorporated with either two or three-dimensional finite element models to predict the influence of peri-prosthetic stresses and strains, on bone adaptations. The first of these studies was carried out by Huiskes et al. (1987) who applied a site-specific approach to predict the stress-related adaptive bone remodelling around a simplified two-dimensional FE model, with sideplate, of an intramedullary prosthesis. The strain energy density (SED) was used as the remodelling stimulus, and deviations from the homeostatic SED determined the rate of bone remodelling, see

Equation 2.2. The stem diameter, and contact conditions were varied to study there influence on bone adaptation. The influence of stem rigidity on stress shielding induced bone loss is shown in Fig. 2.18, with the stiffer stem experiencing more severe bone loss. In a later study Huiskes et al. (1989) used more physiologically shaped two-dimensional models to investigate the relationship between stem designs and stress patterns. Three stem models were investigated: an axisymmetric model of a Lord femoral prosthesis, side plate models of two types of Zweymüller stems (the traditional and SL model) and an Osteonics stem. In the first analysis the Young's modulus of all prostheses was varied from a cobalt-chrome-molybdenum, CoCrMo, stem (E = 200 GPa) to a titanium alloy stem (E = 110 GPa) and a hypothetical iso-elastic material (E = 17 GPa). Stress shielding was found to be directly related to the Young's moduli of the prostheses. The lower stiffness stems, such as the hypothetical iso-elastic stem, reduced the degree of stress shielding. However, using a lower modulus stem shifts the load transfer proximally inducing high proximal interface shear stresses. In an analysis of bone resorption induced by stress shielding only a fully bonded Osteonics stem was analysed. Results showed high interface stresses

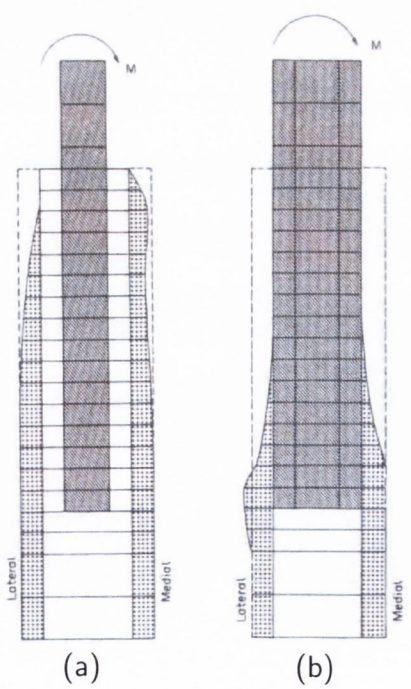

Figure 2.18. External remodelling showing stress shielding around (a) the most flexible stem and (b) the stiffest stem. Adapted from Huiskes et al. (1987).

in the bone surrounding the distal tip and stress bypass of the proximal bone leading to severe bone resorption. In the last analysis a bonded fixation was compared to a press-fit fixation for all three stems. In all cases the loose press-fit stem produced higher cortical bone stresses reducing the degree of stress shielding. However, it was proposed that press-fit stems may generate elevated interface stresses, which may bring about interface necrosis, resorption, and subsidence - but this hypothesis was not tested. Hence, it was proposed that a noncemented stem should be neither too stiff nor too flexible, and should be partly coated and slightly tapered.

Weinans et al. (1992) investigated the effects of different stem materials, both cemented and uncemented, on post-operative femoral bone remodelling. As with Huiskes et al. (1989), a two-dimensional side plate model was used. A non site-specific remodelling theory was used whereby a constant value reference stimulus, S_{ref}, was assigned to each location in the model. The stimulus S, calculated as

$$S = \frac{1}{n} \sum_{i=1}^{n} \left(\frac{U_i}{\rho} \right) \tag{2.17}$$

where U is the strain-energy density, ρ is the apparent density, and n is the load case, strives to attain the value of the reference stimulus by adaptive remodelling. The relationship between the change in density and the stimulus was expressed as

$$\begin{aligned} \Delta\rho &= A\Delta t\{S - k(1 \pm s)\}^{\alpha} \\ \text{if} \quad S &\geq k(1+s) \quad \text{or} \quad S \leq k(1-s) \end{aligned} \tag{2.18}$$

where A is a time constant, Δt is the time step in the analysis, k is the reference stimulus, and $s = 0.35$ is half the width of the lazy zone. The exponent, α, was set at 2 for bone formation, and 3 for resorption to allow for faster bone resorption than formation; note that previous formulations had $\alpha = 1$.

Two stems were analysed in the cemented model, a CoCrMo (E = 210,00 GPa) and titanium stem (E = 110 GPa). A third, iso-elastic stem (E = 20 GPa), was included in the simulations of uncemented stems. The resulting density distribution is shown in Fig. 2.19. Mild proximal bone resorption was predicted in the both of the cemented models, with the stiffer CoCrMo stem having a maximum loss

of 38% versus 23% for the titanium stem in the same region. The uncemented stems of the same materials predicted far greater bone loss, 76% and 54% for the CoCrMo and titanium stems respectively. Little proximal bone loss was predicted in the iso-elastic model; the value was 7% bone loss, suggesting that a more flexible stem is the preferable material choice. However, a study of the interfacial stresses suggested otherwise; while the stiffer stems generate higher distal interface stresses, it was found that the proximal medial interface stresses become quite large in the iso-elastic stem suggesting a failed ingrowth scenario. The titanium stem was suggested as the optimal material choice for the uncemented stem as it reduced both the degree of stress shielding, in comparison to the CoCrMo stem, and interfacial stresses, in comparison to the iso-elastic stem.

Weinans et al. (1994) applied the method developed above (Weinans et al., 1992) to investigate the effects of fit and bonding characteristics on bone morphology changes due to stress shielding in a two-dimensional model. Seven models were simulated with varied contact conditions and fit between the implant and bone. It was predicted that partial coating of the stem reduces the atrophy in comparison to fully coated stems, but only when the coating is applied to a small portion of the proximal stem. Press-fit stems reduced the amount of bone loss in comparison

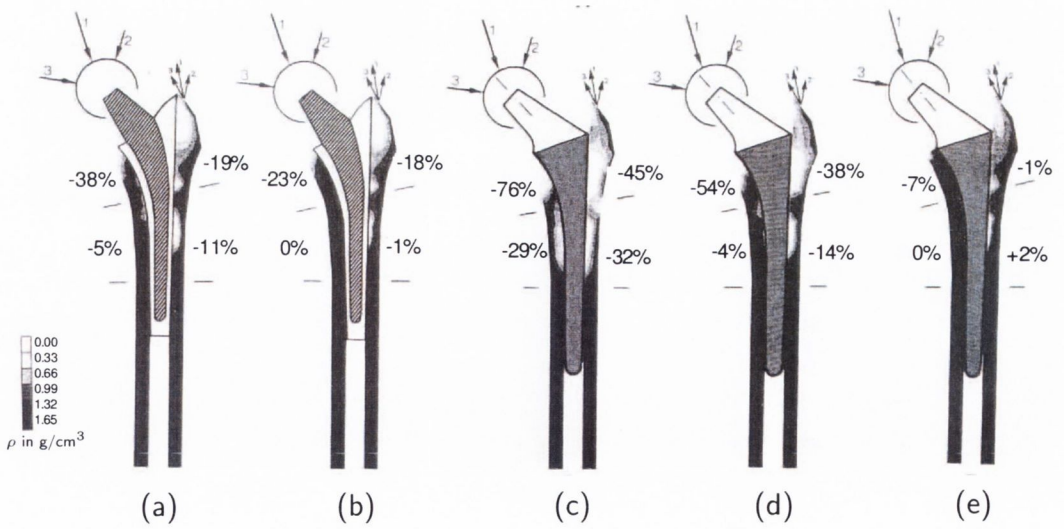

Figure 2.19. Remodelled density distribution in proximal for (a) cemented CoCrMo stem (b) cemented titanium stem (c) uncemented CoCrMo stem (d) uncemented titanium stem (e) uncemented iso-elastic stem. Adapted from Weinans et al. (1992).

to both the fully and one-third partially coated stems. Overrreaming of the distal bone reduced further the proximal atrophy. However, overreaming of the proximal bone drastically increased the amount of proximal bone loss.

A similar study to Weinans et al. (1992) by Huiskes et al. (1992) also considered the influence of stem stiffness on adaptive bone remodelling, this time using a three-dimensional model of a noncemented stem. The remodelling algorithm contained several differences to the one used by Weinans et al. (1992): a site-specific approach was used, whereby the reference stimulus is dependent on location and was derived from a reference intact model, the exponent α was set at 1, and the remodelling rate was determined by the amount of free surface area available $a(\rho)$, hence the change in density was expressed as

$$\begin{aligned} \frac{\Delta\rho}{\Delta t} &= a(\rho)\{S - (1 \pm s)S_{ref}\} \\ \text{if} \quad S &\geq (1+s)S_{ref} \quad \text{or} \quad S \leq (1-s)S_{ref}. \end{aligned} \tag{2.19}$$

The influence of stem stiffness on bone remodelling was studied for two stem materials, an iso-elastic and titanium stem, while a further two stem materials were included in a study of material choice on stress shielding and interfacial stresses, E = 50 GPa and 80 GPa. The bone stiffness and the width of the lazy zone were also varied. As with Weinans et al. (1992), it was predicted that the use of an iso-elastic stem reduces the amount of bone loss while increasing the proximal interface stress, see Fig. 2.20. In reducing the width of the lazy zone from s=0.75 to 0.35, the net amount of bone loss increased from 23% to 41%. They suggested that if the width of the lazy zone is subject to patient-specific variations it may explain patient specific differences in bone resorption patterns. Increasing the bone stiffness had a similar effect to that of reducing the stem stiffness i.e. the degree of bone loss is reduced, suggesting that implant stiffness relative to bone stiffness is an important causative factor for bone remodelling rather than solely implant stiffness.

This method was subsequently applied to investigate the influence of coating placement on bone resorption and interface failure probability for a three-dimensional noncemented stem by Huiskes and van Rietbergen (1995). Four stem

coatings were analysed: a fully coated, a partial proximal coating, a five stripe proximal coating, and no coating (press-fit). The probability of interface failure and amount of bone loss were similar for both the fully coated stem and partly coated stem. The uncoated stem was predicted to reduce the amount of proximal bone loss due to the proximal press-fit stressing the bone interface in compression, producing tensile hoop stresses in the bone. There was no net loss in bone mass because the initial high proximal interface stresses increased trabecular bone density which was subsequently followed by a reduction in cortical density which develops slower than trabecular densification. The stripe-coated stem reduced the amount of bone loss, which was attributed to an increase in trabecular bone density due to spot-welds. However, the maximal Hoffman number, which relates the interfaces stresses to the probability of failure, was almost twice that of the other coatings. This decreased after long-term remodelling but was still slightly higher than what was found with the other coatings. This suggested that although the likelihood of long-term failure was higher for the striped coating the likelihood of early loosening due to failed ingrowth, compromising initial stability, was much higher.

Weinans et al. (1993) compared the results of an animal experiment with those of a computer simulation of a three-dimensional fully bonded noncemented hip prosthesis. Once more a site-specific rule was used with the strain energy density per

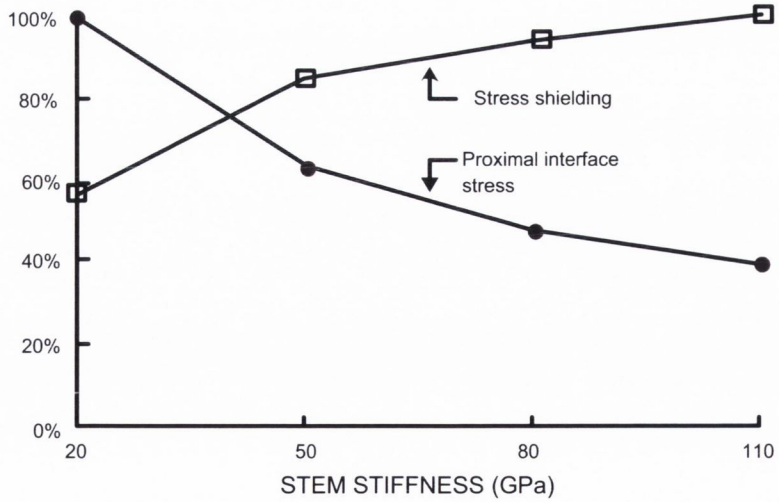

Figure 2.20. The relationship between stress shielding (relative to the titanium stem) and and proximal interface stress (relative to the iso-elastic stem) with stem stiffness. Adapted from Huiskes et al. (1992).

unit mass as the remodelling stimulus. Both internal and external remodelling were considered in the simulations, with the nodal point displacements given by

$$\begin{aligned} \Delta x &= \tfrac{\tau}{\rho}(S - [1 \pm s]S_{ref})\Delta t \\ \text{if} \quad S &\geq (1+s)S_{ref} \quad \text{or} \quad S \leq (1-s)S_{ref} \end{aligned} \tag{2.20}$$

and the change in apparent density given by

$$\begin{aligned} \Delta \rho &= \tau a(\rho)(S - [1 \pm s]S_{ref})\Delta t \\ \text{if} \quad S &\geq (1+s)S_{ref} \quad \text{or} \quad S \leq (1-s)S_{ref} \end{aligned} \tag{2.21}$$

where τ is a time constant, which was calculated by comparing cross sectional density distributions of the simulation with the animal model after 2 years. A time constant of $\tau = 129.6$ g/[mm^2(J/g)months] gave the best fit with the animal experiment with a lazy zone width of $s = 0.35$.

van Rietbergen et al. (1993) followed on from this study by applying the same equations as Weinans et al. (1993) to an unbonded press-fit implant to investigate why similar amounts of bone resorption were found around press-fitted and bonded implants in a 2 year animal experiment. Namely, after 6 months cortical resorption in the press-fit stems was less compared to that of the bonded stems. However, after 2 years the amount of cortical bone resorption increased to levels similar to those of the bonded stems. Two models were tested: a model with perfect fit betweeen the stem and bone, and a model with a proximal fibrous tissue interface. Initially high stresses were found in the peri-prosthetic proximal bone, particularly for the perfect fit model due to the wedging effect. The resulting density distribution contradicted the expected densification of bone in areas of high stress. Instead, bone resorption was predicted for both models, with the interface gap model predicting more proximal bone loss. This was explained by the distal bone gradually increasing in density taking over the load transfer form the initially highly stressed proximal part, and hence inducing stress shielding. In comparison to the animal model both models compared favorably, particulary the proximal gap model as proximal interface gaps were found in all experimental animals.

Prendergast and Taylor (1992), using a damage stimulated remodelling algorithm (see Equation 2.10), investigated the influence of prosthesis Young's modulus and the presence of a prosthesis collar on bone adaptations in an axisymmetric model of a cemented femoral implant. Two Young's moduli were investigated: a metal alloy (E = 200 GPa) and polymer composite (E = 25 GPa). Greater bone loss was predicted with the stiffer metal alloy stem than with the polymer composite stem. The inclusion of a prosthesis collar was found to have little influence on remodelling as it does not increase the stresses high enough to prevent calcar bone resorption. Another study by McNamara et al. (1997) further investigated the validity of the damage based remodelling algorithm, and compared it to an algorithm based on strain energy using a three-dimensional finite element model to compute, rather than simulate, bone adaptation patterns around a femoral prosthesis. The damage stimulated remodelling algorithm of Prendergast and Taylor (1994) was further developed to define damage as the cumulative crack length with the evolution of damage based on fatigue crack growth. A non-linear site-independent damage rule was found to give the more physically reasonable results. It should be noted that, although Prendergast and Taylor (1992) did a simulation albeit with a simplified geometry, McNamara et al. (1997) did not do a simulation but rather presented a post-op analysis. A simulation, using a damage-based algorithm, has not yet been performed on a realistic geometry.

Huiskes et al. (1997) applied the tissue differentiation theory of Prendergast et al. (1997) to an axisymmetric biphasic finite element model of the piston micromotion experiment of Søballe et al. (1993). The elastic modulus and permeability were changed depending on the distortional strain, γ and the fluid velocity, ν, see Equation 2.16. A 300 N force was applied to the model which gave a maximal piston displacement of $160\mu m$ (see Fig. 2.21a) and the fluid velocity and strain were calculated for each element and the corresponding tissue types were determined, see Fig. 2.21b. As the tissue became stiffer the displacement of the piston, fluid velocity and tissue strains reduce until all elements have turned to bone, see Fig. 2.21c. The predictions of the tissue adaptations resemble those found in the animal experiment

of Søballe et al. (1993). Although this study did show the potential of tissue differentiation algorithms to predict peri-prosthetic tissue formation, they were not applied to realistic prosthesis geometries.

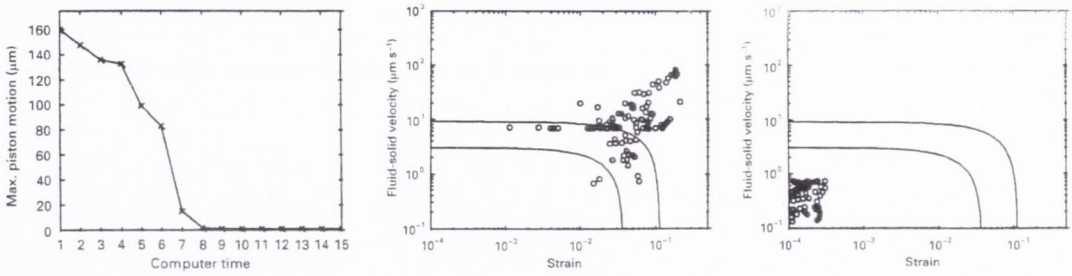

(a) (b) (c)

Figure 2.21. Influence peri-prosthetic tissue adaptations on (a) piston displacement over time, and resulting phase diagrams for (b) the 1st iteration, and (c) 15th iteration. Adapted from Huiskes et al. (1997).

2.5 Conclusion

Total hip replacement has proven to be a successful method of relieving pain and restoring joint function for patient suffering from degenerative joint diseases. However, the success of a noncemented THA is critically dependant on favourable peri-prosthetic bone adaptations, in particular minimal bulk bone loss and interfacial bone ingrowth.

From the literature it can be seen that no approach has yet been presented that can predict the time-course of tissue reactions around a load-bearing implant. Many bone remodelling theories have been developed, some based on strain while others are based on damage. These theories have been applied to finite element models to predict peri-prosthetic bone adaptations in response to the introduction of a prosthesis.

However, it is only by applying an algorithm incorporating both stimuli that the possibility of predicting both bulk-bone and interfacial-bone adaptations exists. The ability to predict interfacial bone adaptations due to excessive interfacial stresses and damage accumulation in conjunction with bulk bone remodelling would provided a significant improvement in the prediction of the likelihood of peri-prosthetic

bone adaptations in the long-term, such an approach should be complimented by predictions of the tissue differentiation that repairs interfacial tissue to cause in-growth and stabilization. In this thesis the author takes up the challenge of applying strain/damage algorithms, integrated with tissue differentiation algorithms, to peri-prosthetic bone adaptations. Furthermore the aim is to show this can be done in 3D realistic geometries.

Chapter 3

Methods

Contents

3.1 Introduction

This chapter presents the methods used to investigate bone remodelling and tissue differentiation around an uncemented femoral prosthesis. Solid models of both the

femur and prosthesis were generated and meshed to create a finite element model of the implanted femur.

A proposed theoretical model of bone remodelling, which combines both strain and damage as a stimulus is used to investigate the influence of stem stiffness on bulk bone and interfacial bone remodelling. Additionally, a tissue differentiation algorithm is incorporated into the remodelling algorithm to simulate interfacial tissue generation following bone resorption.

3.2 Solid Modelling

This section describes the process of reverse engineering and subsequent positioning of the prosthesis in the femur to generate a virtual solid model of the implanted proximal femur.

3.2.1 Reverse engineering of prosthesis

The chosen prosthesis is an uncemented Osteonics ® Omnifit ® hydroxyapatite coated femoral implant, shown in Fig. 3.1. The stem is made from a titanium alloy (Ti_6Al_4V) with a hydroxyapatite coating on the proximal one-third of the stem.

A Roland PICZA 3D laser scanner was used to scan the implant and produce the data in point cloud format. To avoid reflection of the laser off the metallic prosthesis surface, a white coat of paint was applied to the implant before scanning. Due to the irregular shape of the implant numerous scans were required in order to get a complete scan of the geometry , see Fig. 3.2. The tip, stem shaft, and head were scanned individually. Data was collected at a circumferential pitch of 2mm for each section, and at a hight pitch of 0.8mm (tip), 1mm (shaft), and 1mm (head). Pixform, A 3D editing software package, was used to align and merge the individual scans together in order to get a complete point cloud of the prosthesis. The was then be converted to NURB surfaces, see Fig. 3.3.

Figure 3.1. Osteonics® Omnifit® titanium alloy prosthesis with one-third proximal hydroxyapatite coating. Taken from Lee et al. (2005)

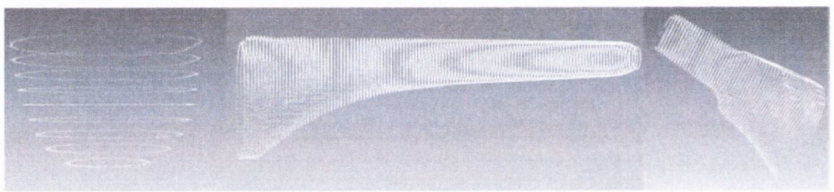

(a) (b) (c)

Figure 3.2. Individual scans of stem (a) tip, (b) shaft, and (c)head.

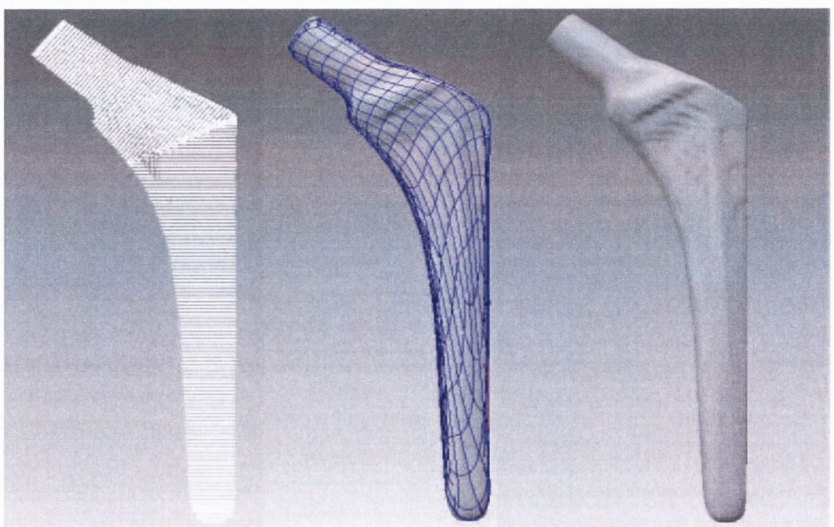

(a) (b) (c)

Figure 3.3. Point cloud data to NURB surfaces using Pixform (a) point cloud, (b) NURB surfaces, and (c) rendered surface.

3.2.2 Solid Model Generation

Solid models of both the femur and prosthesis were created using the Rhinoceros3D solid modelling software (Robert McNeel & Associates, Seattle, USA). The prosthesis was positioned within the femur model and the head of the femur was resected to give a solid model of the implanted femur.

3.2.2.1 Solid Model: Prosthesis

The NURB surfaces generated in Pixform were imported into Rhino in IGES format and used to generate cross sectional splines, through which a surface could be lofted and a solid volume rendered, see Fig. 3.4a-d.

3.2.2.2 Solid Model: Femur

The solid model of the femur was created in the same way as the prosthesis, cross sectional splines were created through which a surface could be lofted and a solid volume rendered, see Fig. 3.5. The "Standardized Femur" was used to generate the femur model (Viceconti et al., 1996).

3.2.2.3 Solid Model: Implanted Femur

Using the surgical protocol (Osteonics, 1995) and comparison to clinical xrays (D'Antonio et al., 1992, 1996) the prosthesis was positioned within the femur such that the shaft filled the medullary canal and the head center of the prosthesis matched that of the femur, see Fig. 3.6. A boolean division was used to subtract the stem volume from the bone volume, mimicking the reaming preformed clinically prior to insertion of the implant, and the appropriate resection level was introduced to produce a solid model of the implanted femur.

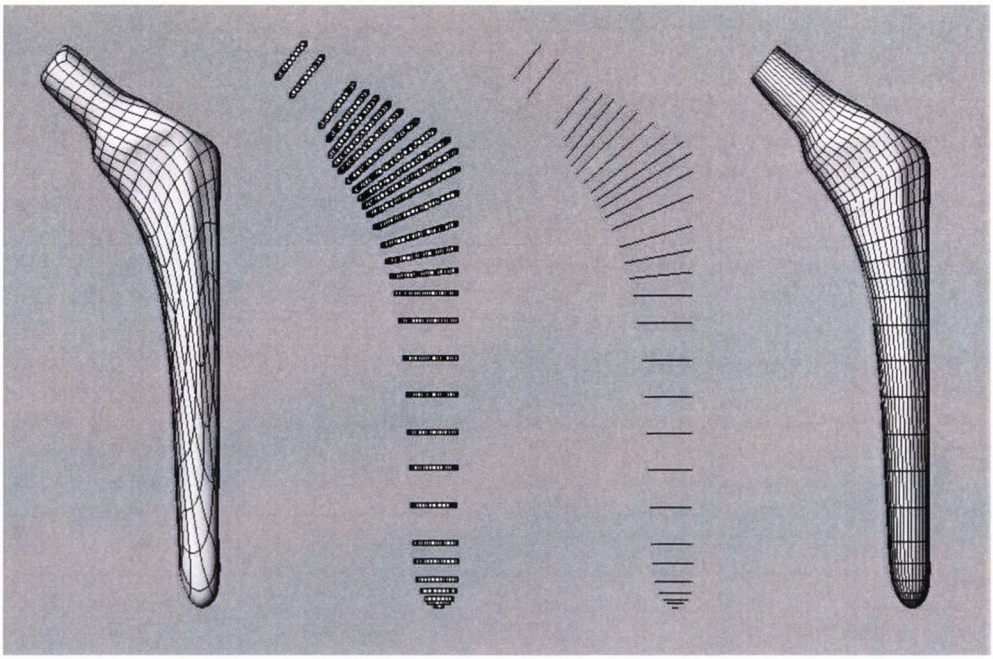

Figure 3.4. Stem solid model generation (a) NURB surfaces, (b) point extraction, (c) spline generation, and (d) solid model.

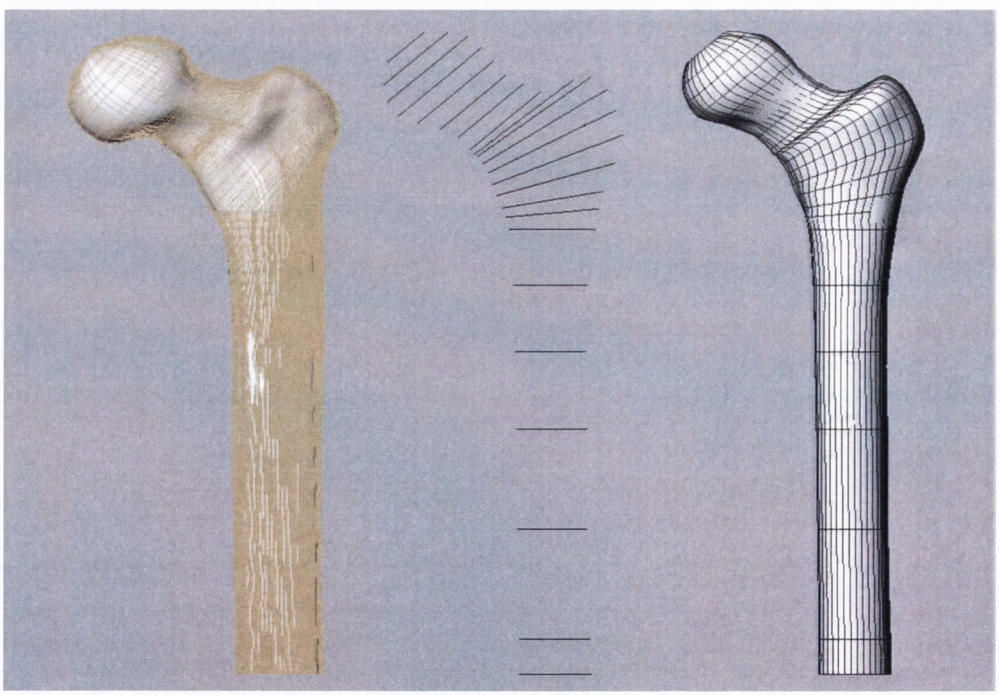

Figure 3.5. Femur solid model generation (a) standardized Femur, (b) spline generation, and (c) solid model.

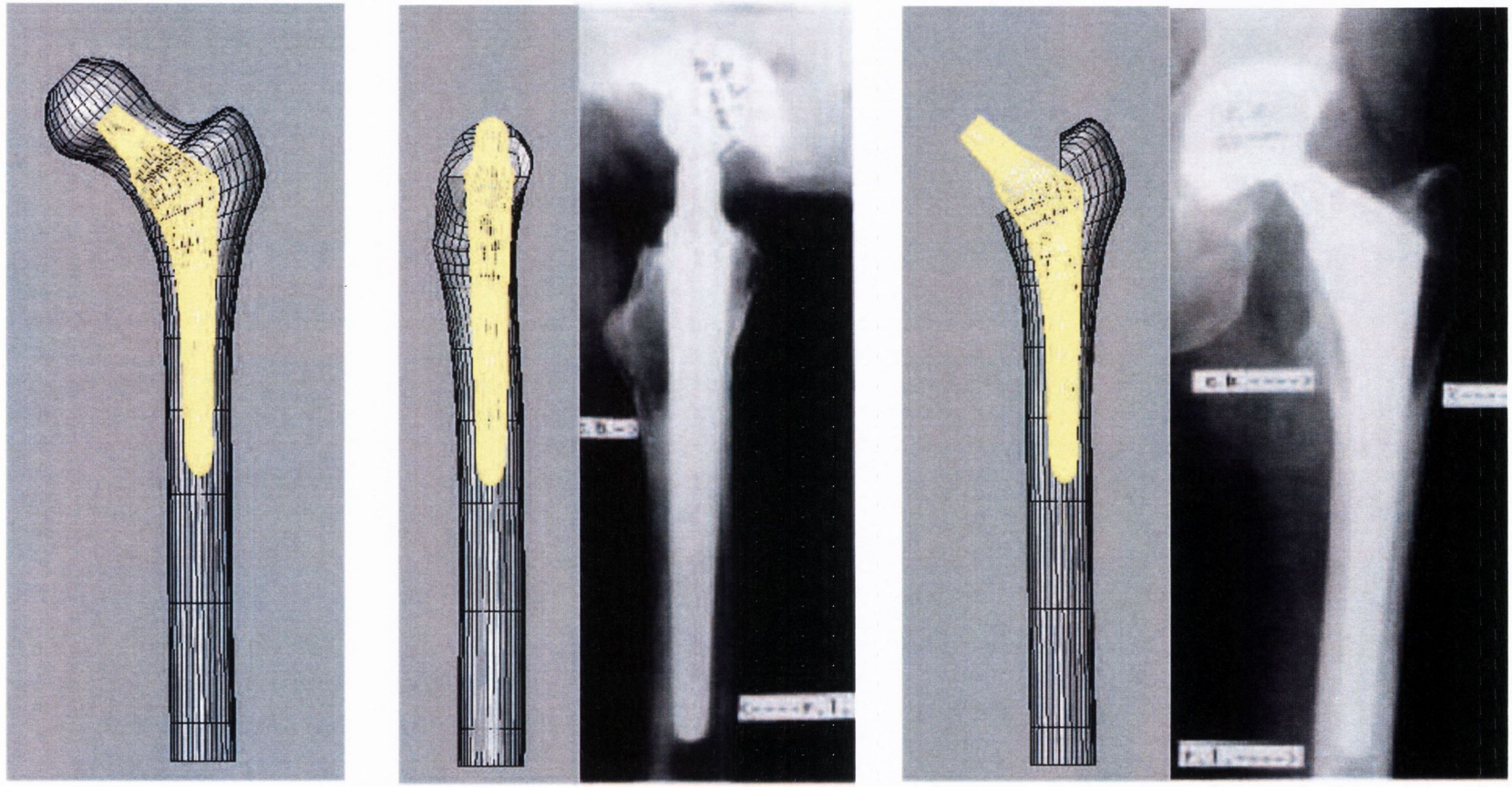

(a) (b) (c) (d) (e)

Figure 3.6. Stem resection and positioning (a) positioning of stem in the intact femur, (b) medial view of stem position with head resected, (c) medial radiograph (taken from D'Antonio et al. (1992)), (d) anterior view of stem position with head resected, and (d) anterior radiograph (taken from D'Antonio et al. (1992)).

3.3 Finite Element Model

In this section the conversion of the solid model into a finite element model is described, including material properties and boundary conditions assigned.

3.3.1 Mesh Generation

Cross sectional splines of the solid model of the implanted femur were created in Rhino and exported into Ansys 7.1 (Ansys Inc., USA). New volumes were created for each component of the model (cortical bone, cancellous bone, and stem) which were then meshed using eight-node hexahedral elements. The meshes were then imported into Mentat^{TM} release 2005 beta2 (MSC Software Corp.,USA) using a FORTRAN program, courtesy of Dr. Alex Lennon, to convert the Ansys text file into a suitable format for Marc (*.dat), and assembled to create the implanted and intact models, see Fig. 3.7. The femoral head of the intact model was modeled with beam elements linking the surface nodes of the resected surface to the femoral head center (Fig. 3.7c).

The model was divided into 7 Gruen zones (Gruen et al., 1979) for both the bulk bone mass and the interfacial bone to allow for comparison with clinical data. Gruen zones 1, 2, 3, 5, 6, and 7 were further divided into an anterior and posterior zone, see Fig. 3.8. By summing the density at each integration point per Gruen zone and comparing to that which was summed for the same Gruen zone in the reference model a percentage change in density can be calculated. This method of density calculation is similar to that used in DEXA scans whereby the bone mineral density (BMD) is calculated by the amount of X-rays absorbed by bone, less those absorbed by soft tissue, over an area.

A biphasic analysis was required to allow for the simulation of combined remodelling and tissue differentiation. Hence, a second model was generated using twenty-node hexahedral biphasic elements.

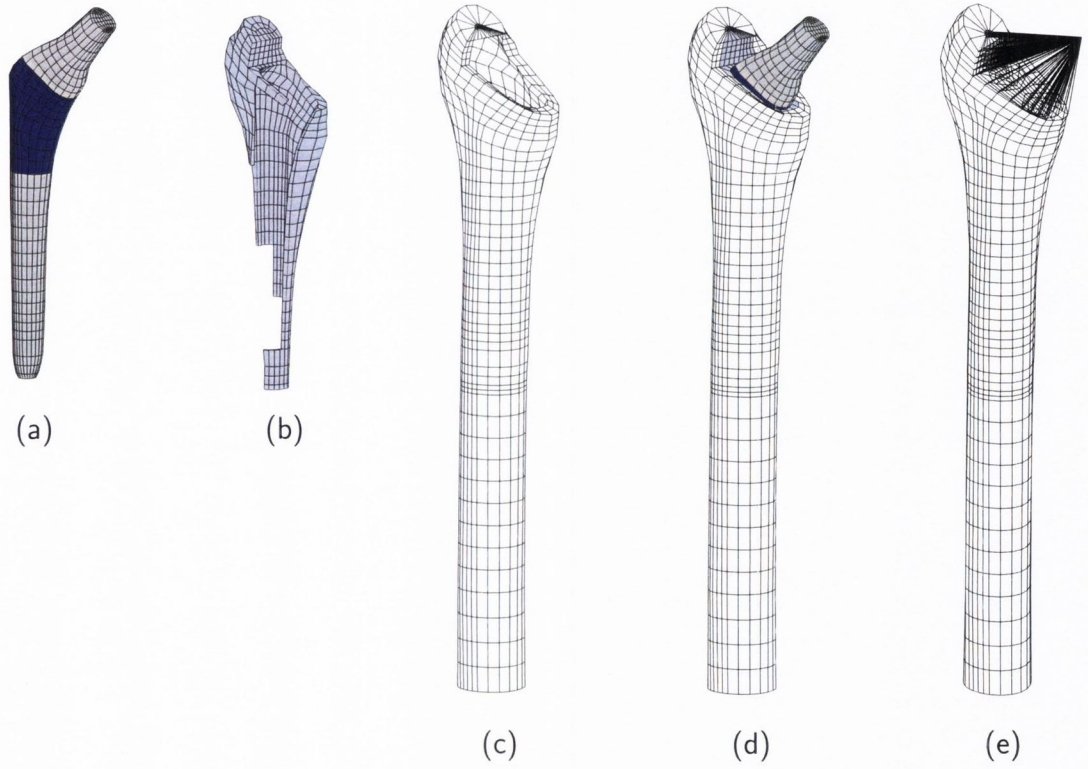

Figure 3.7. Finite element meshes of (a) stem with HA coating high-lighted in blue, (b) cancellous bone, (c) cortical bone, (d) implanted femur, and (e) assumed intact femur.

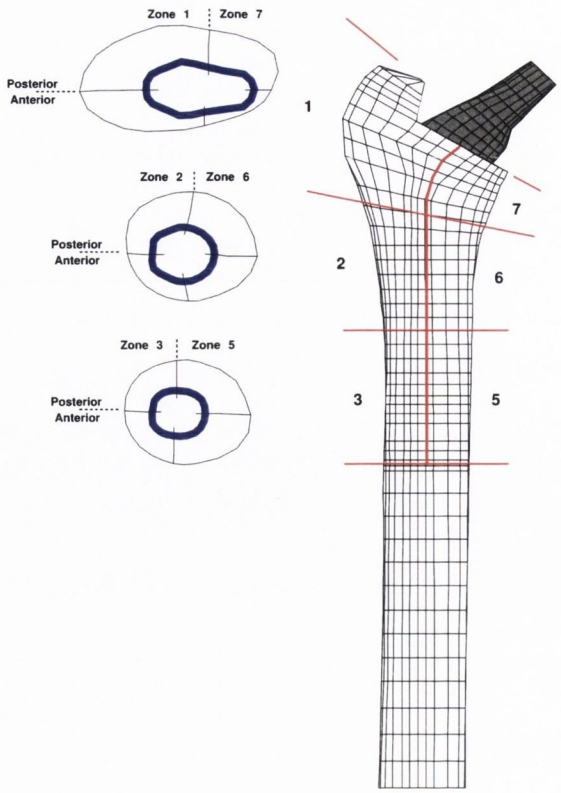

Figure 3.8. Division of model into anterior, posterior, bulk, and interfacial (blue line) Gruen zones.

3.3.2 Boundary Conditions

The loading applied to the model was taken from the work of Heller et al. (2005). As only the proximal femur is modeled the loads were applied using a comparable coordinate system of the femur, derived by Lennon and Prendergast (2001), to that of Bergmann et al. (1993). The single instant of maximum in vivo hip contact force during walking was assumed to derive the load profile (Heller et al., 2005), during which a simplified set of muscles exert a force on the proximal femur. The body mass was taken as 75 kg giving the joint and muscle loading magnitudes shown in Table 3.1.

Distally, all nodes were fully restrained. The muscle loads were applied to the muscle insertion points P1 and P2 and evenly distributed over areas equivalent to those in the muscle standardized femur (Viceconti et al., 2003), see Fig. 3.9.

The same loading conditions were applied to the intact and implanted femur for both the linear elastic and biphasic models. In the case of the biphasic model,

Table 3.1. Hip joint and muscle load magnitudes applied to the finite element model.

Force	x [N]	y [N]	z [N]	Acts at point
Hip joint reaction	-405	246	-1719	P0
Abductor	435	-32.25	648.75	P1
Tensor fascia latae, proximal part	54	-87	99	P1
Tensor fascia latae, distal part	-3.75	5.25	-142.5	P1
Vastus lateralis	-6.75	-138.75	-696.75	P2

only the elements at the stem bone interface were considered biphasic with the surrounding bone cortex modeled as impermeable to fluid fluid. At the free surfaces of the interface elements, those at the resection level and distal tip, free fluid flow was modeled by applying a zero pressure boundary condition, see Fig. 3.10.

The proximal hydroxyapatite coating on the prosthesis was assumed to be fully bonded to the surrounding bone, while the uncoated stem surface was assumed to have a friction coefficient of 0.42 (Ando et al., 1999).

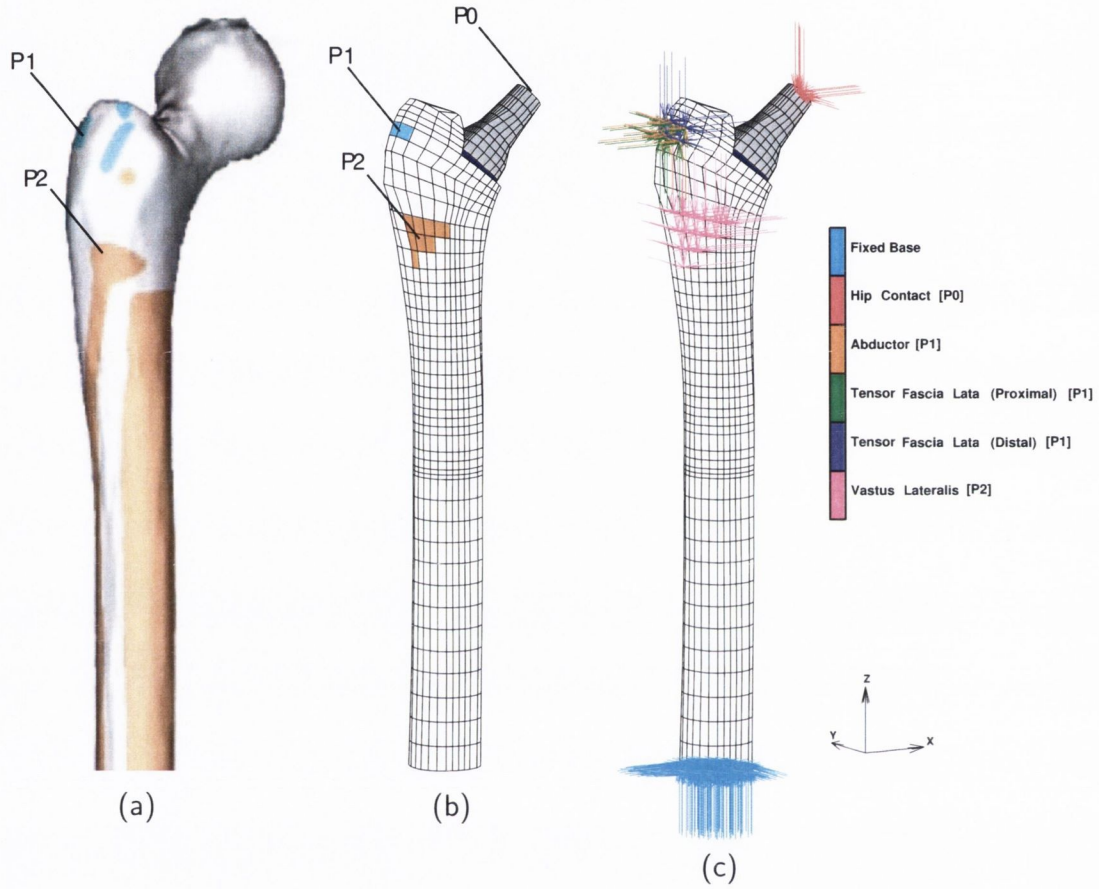

Figure 3.9. Application of loads to finite element model (a) muscle standardized femur showing muscle insertion areas P1 and P2 (adapted from Viceconti et al. (2003), (b) finite element model showing equivalent muscle insertion areas P1 and P2, and the hip contact point P0, (c) finite element model showing loads applied to muscle insertion areas and prosthesis head.

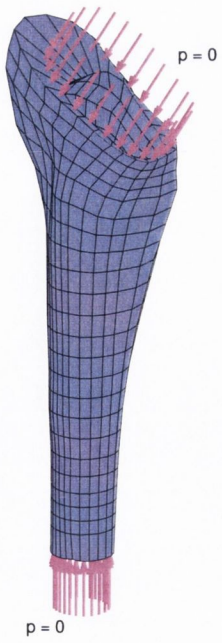

Figure 3.10. Zero pore pressure applied to the free surfaces of the interface elements.

3.3.3 Material Properties

Two kinds of material behaviour were used in the simulations: an isotropic linear elastic material was assumed in the bone remodelling only model, while both a linear elastic and biphasic material was used in the combined remodelling and tissue differentiation model. As tissue differentiation was only allowed at the interface of the prosthesis and bone, only those bone elements at the interface were modeled as biphasic, see Fig. 3.10.

The initial material properties were considered homogeneous throughout both models and are shown in Table 3.2, where the bone's Young's modulus is determined by the apparent density using the cubic relationship of Carter and Hayes (1977)

$$E = c\rho^3 \tag{3.1}$$

where $c = 3790$ MPa $\mathrm{g}^{-3}\mathrm{cm}^9$

Table 3.2. Material properties of the finite element models.

	Cortical bone	Cancellous bone
Young's modulus [MPa]†	17,000	1,500
Density [g/cm^3]	1.65	0.73
Poisson's ratio†	0.33	0.33
Permeability [m^4/Ns $\times$ 10^{-14}]‡	0.001	0.37
Fluid compression modulus [MPa]‡	2300	2300

† Lennon and Prendergast (2001)

‡ Kelly and Prendergast (2006)

3.4 Mechanoregulation algorithms

In this section, the combined strain-damage remodelling algorithm, and also the combined remodelling-differentiation algorithm are formulated. The incorporation of these algorithms into the finite element method is also explained.

3.4.1 Bone remodelling algorithm

3.4.1.1 Strain component of remodelling stimulus

Following Huiskes et al. (1987), the strain component of the remodelling stimulus, S, is calculated as the strain energy density per unit mass. This can be calculated in a continuum model from the strain energy density, U, expressed in MPa and apparent density, ρ, measured in g/cm^3 from

$$S = \frac{U}{\rho}. \tag{3.2}$$

A site-specific approach is used whereby bone mass is adapted in an attempt to return the local remodelling stimulus, S, back to the equilibrium stimulus levels, S_{ref}, as calculated in model of the unimplanted femur. The minimal inhibitory signal proposed by Frost (1964), and as used by Huiskes et al. (1987), Weinans et al. (1992) and van Rietbergen et al. (1993) among others, is included in the model as a '*lazy zone*', the width of which is denoted by the constant 2s. This assumes that no remodelling will occur in response to deviations from the reference remodelling stimulus unless the stimulus lies outside of the values S_{ref}(1-s) and S_{ref}(1+s). The half width of the lazy zone, s, is set to 0.75 following a parametric variation study of

three values of s: 0.35, 0.5, and 0.75, see Appendix A. This value (s=0.75) was also found to predict realistic results in human simulations by Weinans (1991), Huiskes et al. (1992), Huiskes and van Rietbergen (1995), Kerner et al. (1999), and Gupta et al. (2006). The rate of change of bone mass can be seen in Fig. 3.11, and can be expressed as

$$\frac{dm}{dt} = \begin{bmatrix} C_s(S - (1-s)S_{ref}) & \text{if} & S < (1-s)S_{ref} \\ 0 & \text{if} & (1-s)S_{ref} \leq S \leq (1+s)S_{ref} \\ C_s(S - (1+s)S_{ref}) & \text{if} & S > (1+s)S_{ref} \end{bmatrix} \tag{3.3}$$

where C_s is a remodelling rate constant in response to the strain stimulus.

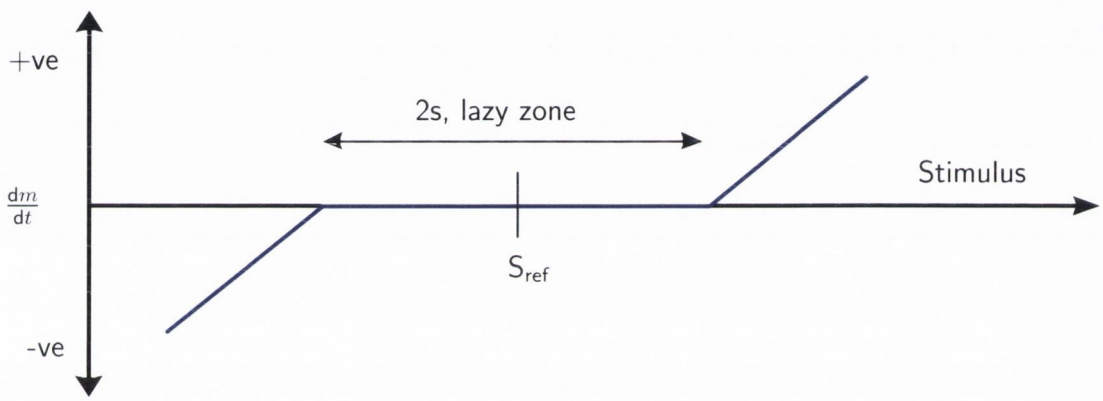

Figure 3.11. Schematic of strain stimulated remodelling.

3.4.1.2 Damage component of remodelling stimulus

Damage, denoted ω is calculated using the remaining life approach and ranges from the undamaged state, $\omega = 0$, to the fractured state, $\omega = 1$ (Prendergast and Taylor, 1994). It is assumed that there exists a certain amount of site-specific microdamage within the bone at remodelling equilibrium, which accumulates at a rate denoted $\dot{\omega}_{RE}$ which is calculated using the unimplanted femur model. Accumulation of damage gives rise to the damage remodelling stimulus, $\Delta\omega$, which can be found by integrating the difference between the damage formation rate, $\dot{\omega}$, and the damage repair rate, $\dot{\omega}_{RE}$, (the damage formation rate at remodelling equilibrium equals the damage

repair rate) giving

$$\Delta\omega = \int_0^t (\dot{\omega} - \dot{\omega}_{\mathrm{RE}})\mathrm{d}t. \tag{3.4}$$

Assuming a linear rate of damage accumulation, the damage formation rate can be calculated using Miner's rule

$$\dot{\omega} = \left(\frac{1}{N_f}\right) \tag{3.5}$$

where N_f is the number of cycles to failure at a given stress, which can be found from the empirical relationship of Carter et al. (1976)

$$\log(N_f) = \mathrm{H}\log(\sigma) + \mathrm{JT} + \mathrm{K}\rho + \mathrm{M} \tag{3.6}$$

where σ is the stress (MPa), T is the temperature (37°C), and H, J, K, and M are empirical constants with values of -7.789, -0.0206, 2.364, and 15.470 respectively.

A critical amount of accumulated damage, ω_{CRIT}, is the value limiting strain-adaptive remodelling. McNamara and Prendergast (2006) calculated ω_{CRIT} at a strain of $3500\mu\varepsilon$, $2000\mu\varepsilon$ above the centre of their lazy zone ($1500\mu\varepsilon$), or approximately 1.3 times the strain at the centre of the lazy zone. As the approach presented here is a site-specific model for both strain and damage influenced remodelling (whereas McNamara and Prendergast (2006) was not), a 'damage lazy zone', denoted d, is proposed, allowing for damage accumulation, without initiating bone resorption, up until the critical damage level ω_{CRIT} is reached, see Fig. 3.12. The critical damage rate, $\dot{\omega}_{\mathrm{CRIT}}$, is calculated at a stress 1.3 times that at S_{ref} using Equations 3.5 and 3.6.

Damage accumulation was predicted using forward Euler intergration

$$\Delta\omega_{i+1} = \Delta\omega_i + (\dot{\omega} - \dot{\omega}_{\mathrm{RE}})\mathrm{N}\Delta t \tag{3.7}$$

where Δt is the time step in the integration process and N, the number of cycles per month, is set at 125,000 cycles/month (Goldsmith et al., 2001). The rate of change

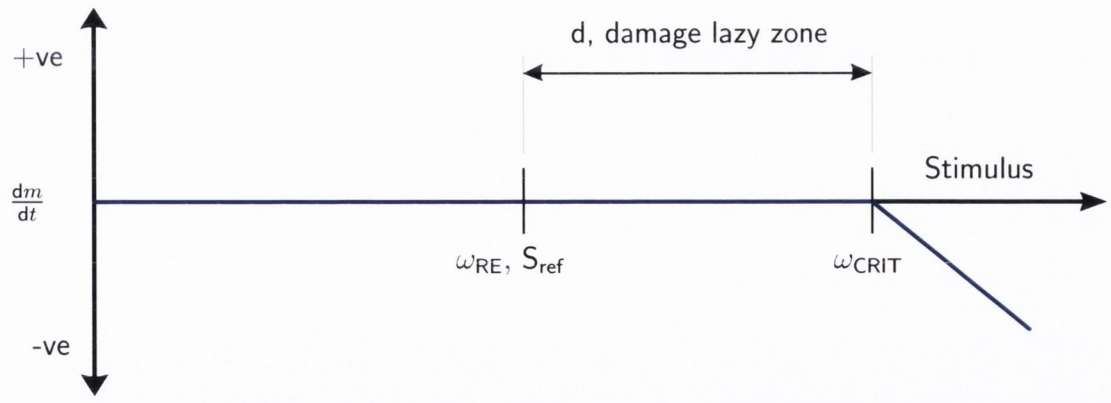

Figure 3.12. Schematic of damage stimulated remodelling.

of bone mass due to damage accumulation can now be expressed as

$$\frac{\mathrm{d}m}{\mathrm{d}t} = \mathrm{C_d}(\Delta\omega)\mathrm{N} \tag{3.8}$$

where $\mathrm{C_d}$ is a rate constant governing the rate of remodelling in response to damage.

3.4.1.3 Combined strain and damage remodelling mechanoregulation algorithm

Internal bone remodelling is simulated using the same method as used by Huiskes et al. (1992), van Rietbergen et al. (1993) and Weinans et al. (1993). This assumes that remodelling can occur only at free bone surfaces. In the case of internal remodelling, this occurs at the pore surfaces. Martin (1972) proposed a method to calculate the amount of internal free surface area as a function of the apparent density, $A(\rho)$. The internal free surface area per unit volume, $a(\rho)$, is shown in Fig. 3.13 and can be calculated as

$$a(\rho) = \frac{A(\rho)}{V}. \tag{3.9}$$

For $\rho = \rho_{max} = 1.73$ g/cm^3 it is assumed that no remodelling occurs as $a(\rho) = 0$, and a minimum density of $\rho = 0.01$ g/cm^3 represents complete resorption (van Rietbergen et al., 1993). It is assumed that the rate of internal remodelling in response to both strain and damage is dependent on the amount of free surface area. Hence, both the strain rate constant, $\mathrm{C_s}$, and the damage rate constant, $\mathrm{C_d}$, are a function of the free surface density. The strain remodelling rate constant can

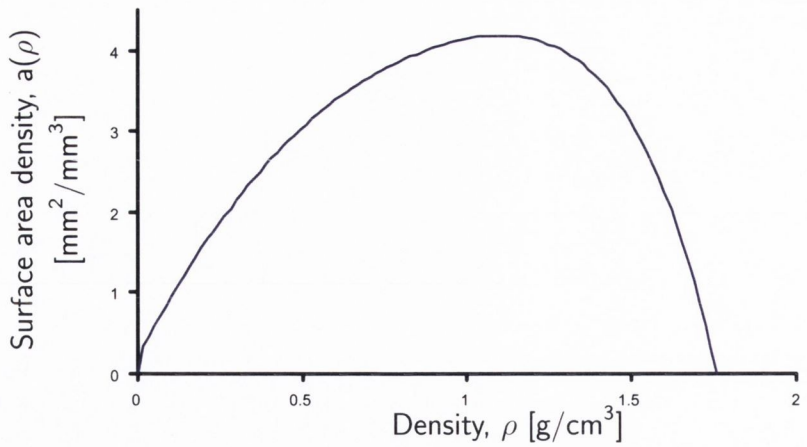

Figure 3.13. Density (ρ) versus free surface area per unit volume (a(ρ)).

now be determined by

$$C_s = a(\rho)\tau_s \tag{3.10}$$

where τ_s is a strain time constant with a value of 130 $g^2mm^{-2}J^{-1}$ per month (Weinans et al., 1993). The damage rate constant can similarly be expressed as

$$C_d = a(\rho)\tau_d \tag{3.11}$$

where τ_d is a damage time constant which was subject to a parametric study with a value of $\tau_d = 1 \times 10^7$ yielding the most realistic results, see Appendix B.

By combining Equations 3.3 and 3.8 and the rate equations, Equations 3.10 and 3.11, the rate of change in density can be expressed as

$$\frac{d\rho}{dt} = \begin{bmatrix} a(\rho)\tau_s(S-(1-s)S_{ref}) & \text{if} & S < (1-s)S_{ref} & \text{and} & \omega < \omega_{CRIT} \\ 0 & \text{if} & (1-s)S_{ref} \leq S \leq (1+s)S_{ref} & \text{and} & \omega < \omega_{CRIT} \\ a(\rho)\tau_s(S-(1+s)S_{ref}) & \text{if} & S > (1+s)S_{ref} & \text{and} & \omega < \omega_{CRIT} \\ a(\rho)\tau_d(\Delta\omega)N & \text{if} & S > (1+s)S_{ref} & \text{and} & \omega > \omega_{CRIT} \end{bmatrix}. \tag{3.12}$$

where the upper and lower limits of bone density are 0.01g/cm^3 and 1.75g/cm^3 respectively. Equation 3.12 assumes that bone remodelling can occur in response to either a strain or damage stimulus. While the damage is below a critical limit, strain initiated remodelling persists. However, once this limit has been reached or exceeded, damage stimulated remodelling is prioritised. The change in density over

time due to a strain (blue line) and damage (red line) stimulus is illustrated in Fig. 3.14.

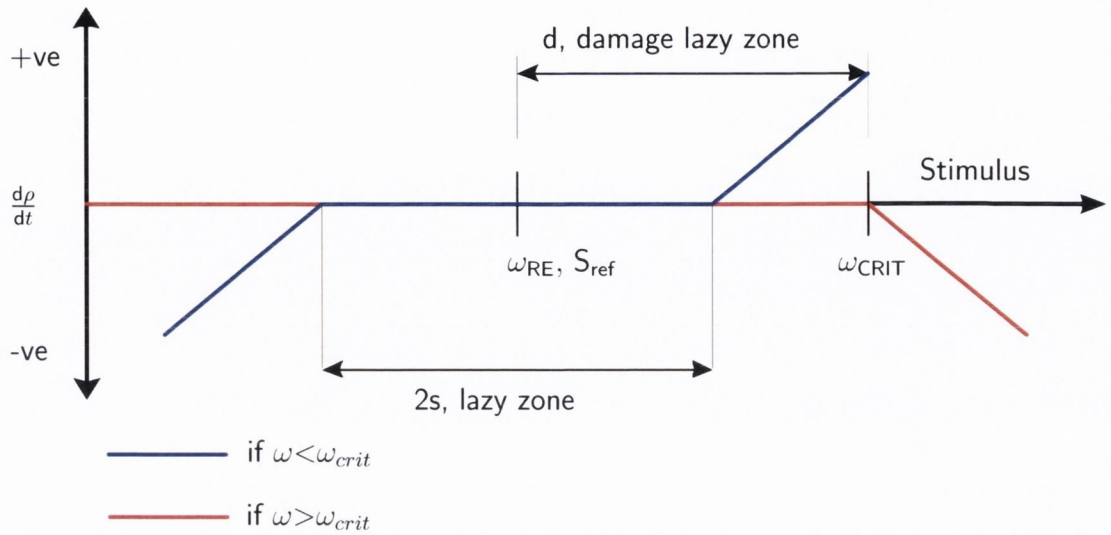

Figure 3.14. Schematic of combined strain-damage stimulated remodelling.

3.4.1.3.1 Determining the time step

For every integration point a strain time step, Δt_s, and a damage time step, Δt_d, is calculated such that the maximum change in density does not exceed 10% of the maximum allowable density. This is achieved by calculating Δt_s and Δt_d using the maximum values for the expressions $\{\tau_s a(\rho)[S-(1\pm \mathrm{s})\mathrm{S_{ref}}]\}$ and $\{\tau_d a(\rho)\Delta\omega \mathrm{N}\}$ from all integration points (van Rietbergen et al., 1993)

$$\Delta t_s = \frac{0.175}{\{\tau_s a(\rho)[S-(1\pm \mathrm{s})\mathrm{S_{ref}}]\}_{\max}} \tag{3.13}$$

$$\Delta t_d = \frac{0.175}{\{\tau_d a(\rho)\Delta\omega \mathrm{N}\}_{\max}} \tag{3.14}$$

The optimal time step, Δt, is then taken as the lower value of either Δt_s and Δt_d (Stolk et al., 2004)

$$\Delta t = min|\Delta t_s, \Delta t_d| \tag{3.15}$$

The time step in the integration process can now be expressed in terms of months.

3.4.1.3.2 Updating bone material properties

Using the calculated optimal time step a new density can be found for every integration point in the model by forward Euler integration

$$\rho_{i+1} = \rho_i + \frac{\mathrm{d}\rho_i}{\mathrm{d}t}\Delta t \tag{3.16}$$

which can then be related to the local elastic properties (E) according to the relationship of Carter and Hayes (1977)

$$E_{i+1} = 3790\rho_{i+1}^3 \tag{3.17}$$

where the elastic modulus is measured in MPa and the density in g/cm^3. The predicted elastic modulus is assumed to be isotropic.

3.4.1.4 Application to finite element model

The bone remodelling algorithm shown in Fig. 3.15 was written in the FORTRAN programming language and incorporated into the MARC$^{\text{TM}}$ release 2005 beta2 (MSC Software Corp.,USA) finite element code. The eight-node hexahedral element models of the intact and implanted femur were used in the simulation of bone remodelling where the unimplanted femur model was used to generate the reference levels of the strain stimulus, S_{ref}, equilibrium damage, ω_{RE}, and critical damage, ω_{CRIT}, for each integration point. The implanted femur model undergoes the same loading conditions, and the measured strain stimulus, S, and damage, ω, are calculated using the ELEVAR user subroutine. The optimum time step is calculated using Equations 3.13 - 3.15. If the accumulated damage exceeds the critical amount, damage stimulated remodelling is prioritised over strain stimulated remodelling. Based on the magnitude of the appropriate stimulus, the rate of change of density (Equation 3.12) and subsequent new density (Equation 3.16) is calculated. Using the HYPELA user subroutine the stiffness of the element is updated based on the predicted change in density (Equation 3.17). After each iteration the time step is updated until 10 years worth of remodelling has been simulated.

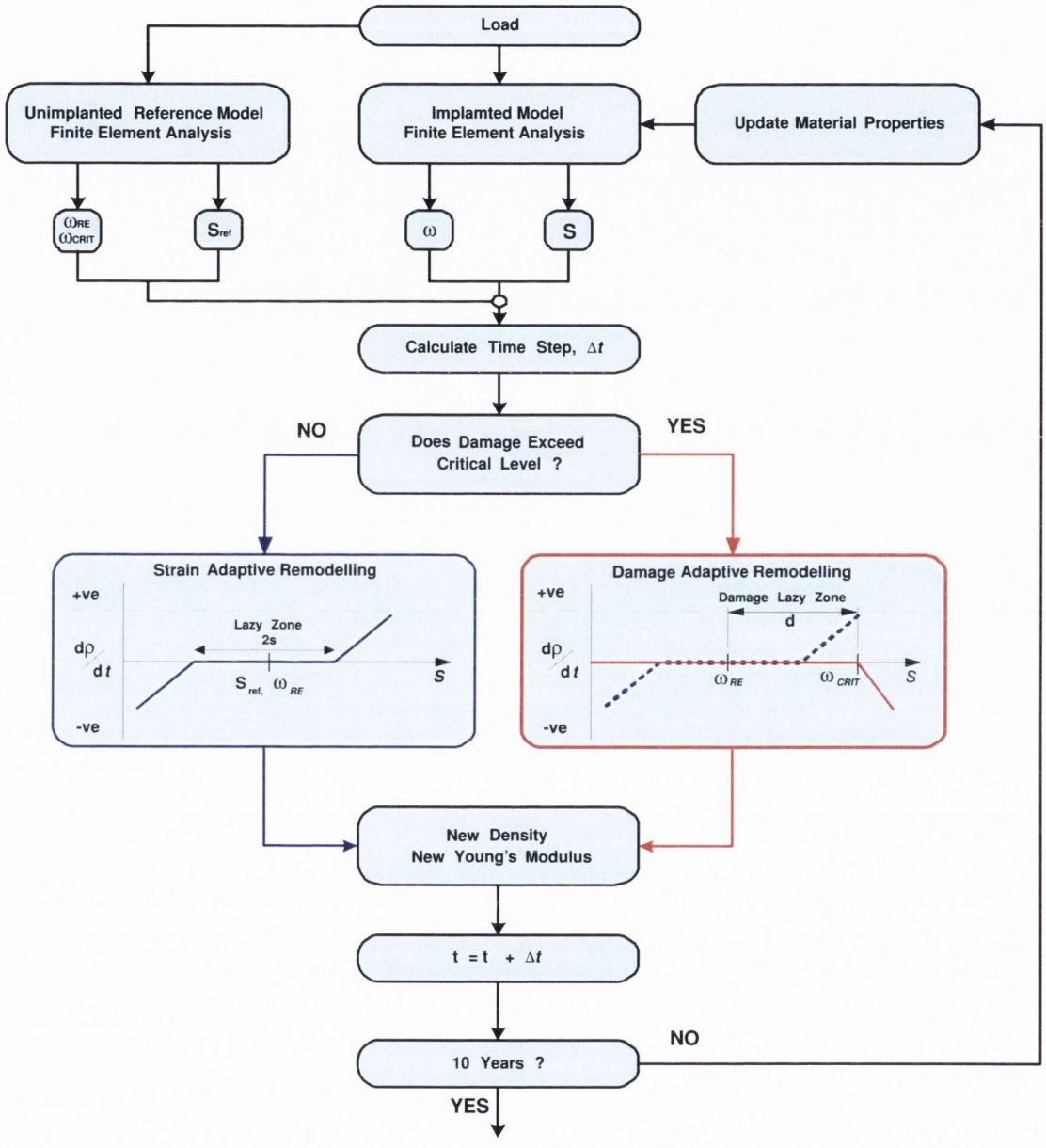

Figure 3.15. Schematic of combined strain-damage bone remodelling algorithm. If the accumulated damage exceeds the critical amount, calculated in the reference model, damage-based resorption is initiated.

3.4.1.4.1 Stem stiffness parametric study

The influence of stem stiffness on both interfacial bone adaptations and bulk bone remodelling was studied by applying the remodelling algorithm to three stem material models: a fictitious iso-elastic stem with an elastic modulus similar to that of bone, a titanium alloy (Ti6Al4V), and a cobalt-chrome alloy (CoCrMo), see Table 3.3 (Weinans et al., 1992).

Table 3.3. Stem material properties.

Material	Elastic modulus E [GPa]	Poisson's ratio υ
Iso-elastic	20	0.3
Titanium alloy	110	0.3
Cobalt-Chrome alloy	210	0.3

3.4.2 Combined bone remodelling and tissue differentiation algorithm

3.4.2.1 Remodelling stimuli

The remodelling stimuli, strain and damage, are calculated in the same manner as those calculated in the remodelling only algorithm.

3.4.2.2 Differentiation stimulus

Once the density of bone reaches its minimum of 0.01 g/cm^3, complete bone resorption is assumed. The resorbed bone is subsequently replaced by granulation tissue, which is assumed to be filled by mesenchymal stem cells in a homogeneous distribution. These cells can differentiate into different phenotypes based on a local biophysical stimulus regulating tissue differentiation as defined by Prendergast et al. (1997), see Fig. 3.16.

The biophysical stimulus is based on two mechanical stimuli: octahedral shear strain, γ, and fluid velocity, ν, where the octahedral shear strain is calculated from

the principal stresses σ_1, σ_2, and σ_3

$$\gamma = \frac{1}{3}\sqrt{(\sigma_1 - \sigma_2)^2 + (\sigma_2 - \sigma_3)^2 + (\sigma_3 - \sigma_1)^2} \tag{3.18}$$

and the maximum resultant fluid velocity is calculated as

$$\nu = \sqrt{\nu_x^2 + \nu_y^2 + \nu_z^2} \tag{3.19}$$

The stimulus for differentiation, S_d, can now be calculated as

$$S_d = \frac{\gamma}{a} + \frac{\nu}{b} \tag{3.20}$$

where $a = 3.75\%$ and $b = 3\mu m s^{-1}$ (Huiskes et al., 1997).

Following Lacroix and Prendergast (2002a), the value of S_d, cells can synthesise new tissue by differentiating into the following cell phenotypes:

$$\begin{aligned} n_{resorption} < \quad S_d \quad < n_{mature} &\quad \text{osteoblasts : mature woven bone} \\ n_{mature} < \quad S_d \quad < 1 &\quad \text{osteoblasts : immature woven bone} \\ 1 < \quad S_d \quad < m &\quad \text{chondrocyte : cartilage} \\ S_d \quad > m &\quad \text{fibroblast : fibrous connective tissue} \end{aligned} \tag{3.21}$$

where $n_{resorption} = 0.01$, $n_{mature} = 0.53$, and $m = 3$, determined by the previous work of Huiskes et al. (1997), represent the boundary conditions of the mechanoregualtion diagram shown in Fig. 3.16. The material properties of each tissue type are listed in Table 3.4 (Kelly and Prendergast, 2005).

Table 3.4. Tissue material properties.

	Granulation tissue	Fibrous tissue	Cartilage	Immature bone	Mature bone	Cortical bone
Young's modulus [MPa]	0.2	2	10	1000	6000	17,000
Permeability [$m^4/Ns \times 10^{-14}$]	1	1	0.5	0.1	0.37	0.001
Poisson's ratio	0.167	0.167	0.167	0.3	0.3	0.3

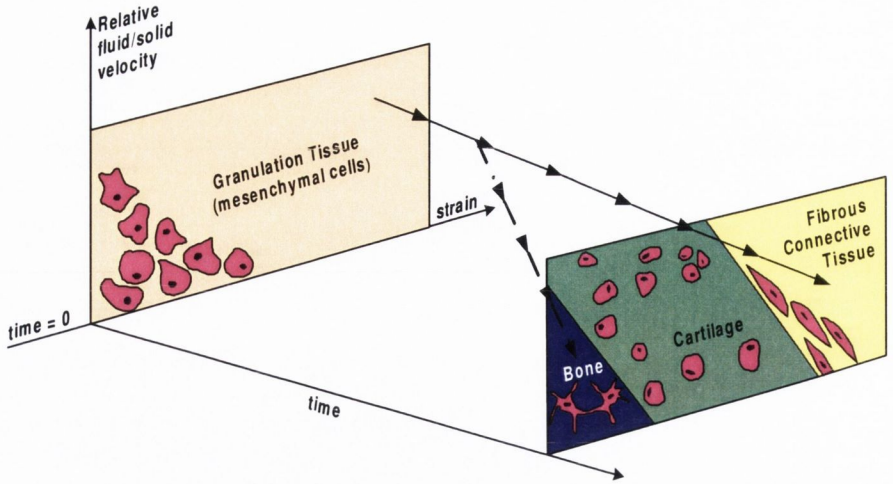

Figure 3.16. Mechanoregulation regulating cell differentiation based on two biophysical stimuli: octahedral shear strain and fluid velocity. Adapted from Prendergast et al. (1997).

3.4.2.2.1 Updating tissue material properties

Both the Young's modulus and permeability are assumed to change from an initial values of 0.2 MPa and 1 $m^4/Ns \times 10^{-14}$, typical of granulation tissue, to the maximum values for each of the predicted tissue types shown in Table 3.4 over a period of 75 days (2.5 months). This time period is based on the observation that fracture callus density equals or exceeds that of the cortex after 10 weeks or more after injury (Islam et al., 2000).

Once complete bone resorption has occurred, granulation tissue takes its place and is capable of differentiating. The differentiation time, t_{diff}, accumulates from this point forward and is calculated as

$$t_{diff_i} = t_{diff_{i-1}} + \Delta t \tag{3.22}$$

where Δt is the time step in the remodelling process.

The Young's modulus and permeability can be calculated using the equation of a straight line

$$y = mx + c \tag{3.23}$$

where y is the permeability or Young's modulus, m is the slope of the line, x is the time t_{diff}, and c is the y intercept. The changes in Young's modulus and perme-

ability over time are shown in Figs. 3.17 and 3.18 respectively and can be calculated using Equations 3.24 and 3.25. The permeability and stiffness of the tissue type predicted reaches a maximum value after 2.5 months, after which mechanoregulation "switch off" occurs and both differentiation and remodelling ceases for the concerned integration point.

$$\begin{aligned} E &= 0.7440 \times (time) + 0.2 \quad \text{granulation tissue to fibrous tissue} \\ &= 4.0507 \times (time) + 0.2 \quad \text{granulation tissue to cartilage} \\ &= 413.25 \times (time) + 0.2 \quad \text{granulation tissue to immature bone} \\ &= 2479.9 \times (time) + 0.2 \quad \text{granulation tissue to mature bone} \end{aligned} \tag{3.24}$$

$$\begin{aligned} k &= -2 \times 10^{-15} \times (time) + 1 \times 10^{-14} \quad \text{granulation tissue to cartilage} \\ &= -4 \times 10^{-15} \times (time) + 1 \times 10^{-14} \quad \text{granulation tissue to immature bone} \\ &= -3 \times 10^{-15} \times (time) + 1 \times 10^{-14} \quad \text{granulation tissue to mature bone} \end{aligned} \tag{3.25}$$

Both the elastic modulus and permeability are considered to be isotropic. Hence $E_1 = E_2 = E_3$ and $k_1 = k_2 = k_3$.

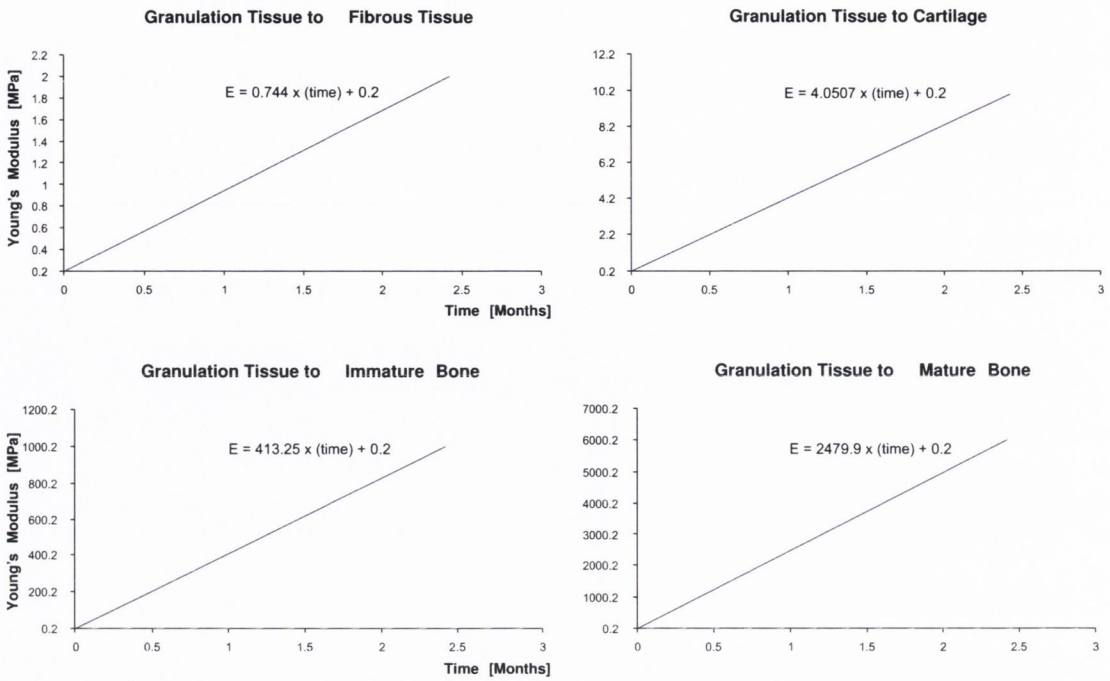

Figure 3.17. Development of tissue Young's modulus over 75 days.

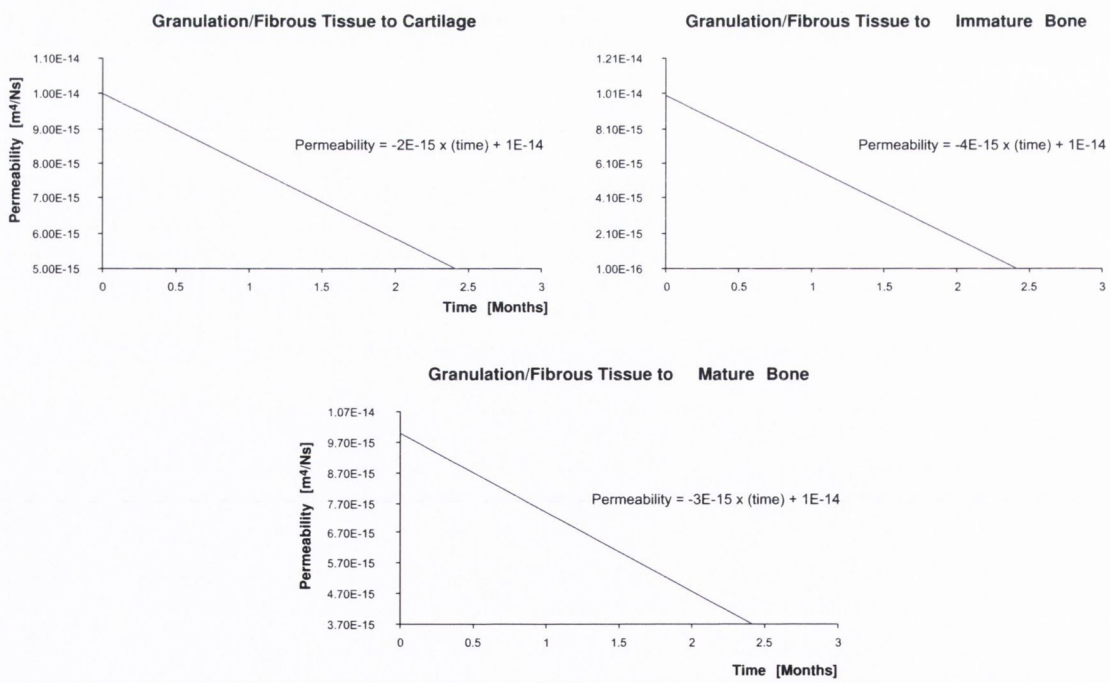

Figure 3.18. Development of tissue permeability over 75 days.

3.4.2.1 Application to finite element model

The combined remodelling and tissue differentiation algorithm is shown in Fig. 3.19. The twenty-node hexahedral biphasic element models of the intact and implanted femur were used in the simulation. The algorithm is carried out in the much the same way as that for the bone remodelling algorithm shown in Fig. 3.15 with the exception that a check is performed on each integration point at the stem-bone interface to determine if the density has reached it's minimum value. If it has been reached, granulation tissue forms, and tissue differentiation is initiated. The fluid velocity and octahedral shear stress are calculated using the PLOTV and ELEVAR user subroutines respectively. Based on these values the tissue phenotype is determined and the Young's modulus and permeability calculated using Equations 3.24 and 3.25 and updated in the model using the HYPELA and UPERM user subroutines. If tissue differentiation is not initiated bone remodelling persists as described in chapter 3.4.1.4.

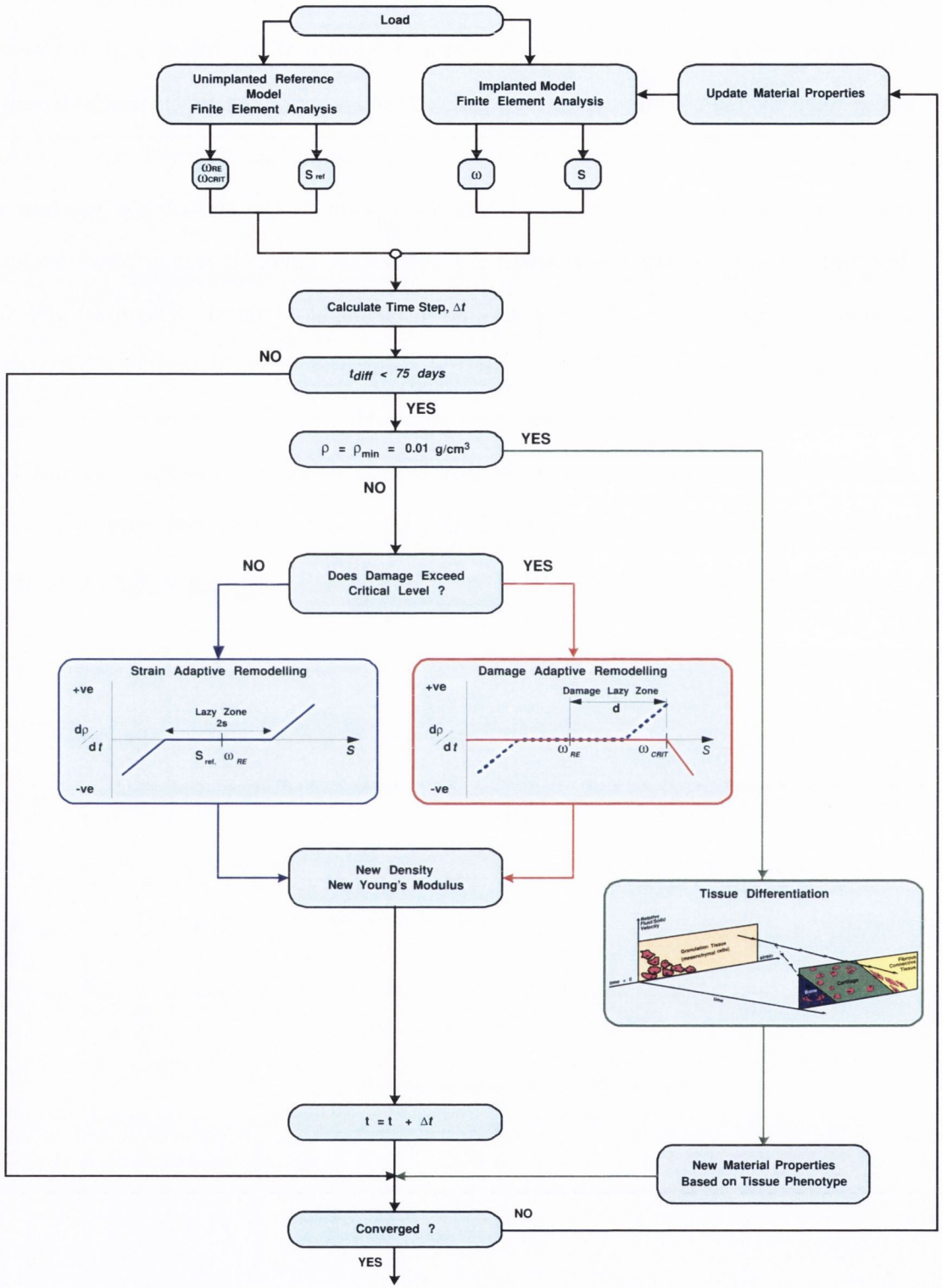

Figure 3.19. Schematic of combined strain-damage bone remodelling and tissue differentiation algorithm.

3.4.2.1.1 Stem stiffness parametric study

The same stem material properties were used as in the study using the bone remodelling algorithm only i.e. iso-elastic, titanium, and cobalt-chrome alloy .

3.5 Summary

To investigate the hypothesis that high interfacial stresses promote damage accumulation at the stem-bone, leading to bone resorption and interfacial fibrous tissue formation, a combined strain-damage remodelling algorithm was developed and applied to three-dimensional finite element models of an uncemented femoral prostheses. The effect of varying the prosthesis stiffness on both interfacial and bulk bone adaptations was investigated. In addition, a combined remodelling-tissue differentiation algorithm is proposed and applied to the finite element models and the formation of interfacial tissues is analysed. The results of these analyses are presented in chapter 4.

Chapter 4

Results

Contents

4.1 Introduction

The predicted peri-prosthetic bone adaptations surrounding the three stem materials, using both the remodelling and the combined remodelling-tissue differentiation algorithms, are presented in this chapter.

All remodelling results are presented per Gruen zone to allow for better comparison between each stem model. Furthermore, each Gruen zone has been divided into

an anterior and posterior aspect. Both the *bulk* and *interfacial* bone adaptations are reported, where *bulk* refers to the entire bone mass in the Gruen zone considered, while *interfacial* refers to the nodes on the bone surface adjacent to the stem-bone interface. The percentage volume of bulk bone experiencing stress shielding, and interfacial bone undergoing damage stimulated remodelling is presented along with the percentage change in bone mass over time. Interfacial and bulk bone contour plots show the predicted density and strain energy density per unit mass distribution.

Contour plots of the predicted tissue type following bone resorption are presented for each stem model. The magnitude of the stimulus regulating differentiation over a period of five years is also shown.

4.2 Bone remodelling

This section presents the results obtained for the bone remodelling simulations performed. Comparisons between each stem model are made on the load transfer and resulting bulk and interfacial bone adaptations.

4.2.1 Bulk bone remodelling

4.2.1.1 Bulk load transfer

Load transfer begins proximally in the iso-elastic stem, midway down zone 2 and at the start of zone 6, see Fig. 4.1a. As the stem stiffness increases, load transfer moves distally to zone 3 and mid zone 6 for the titanium stem (Fig. 4.1b), and mid zone 3 and zone 5 for the CoCrMo stem (Fig. 4.1c). As of a result of this, varying degrees of stress shielding are experienced depending on the stem material, see Fig. 4.2. Proximal stress shielding in zones 1 and 7 is most severe for the CoCrMo stem at 21% and 57% volume respectively. This reduces to 17% and 34%, and 9% and 16% for the titanium and iso-elastic stems. Stress shielding around the mid-stem position, zones 2 and 6, reduces in all cases except that of zone 2 in the CoCrMo stem model, which peaks at 54% (see Appendix C). Distally, the amount of bone experiencing stress shielding reduces with no stress shielding experienced in zone 5

with all three stems, and 0%, 2% and 6% in zone 3 in the iso-elastic, titanium and CoCrMo stems.

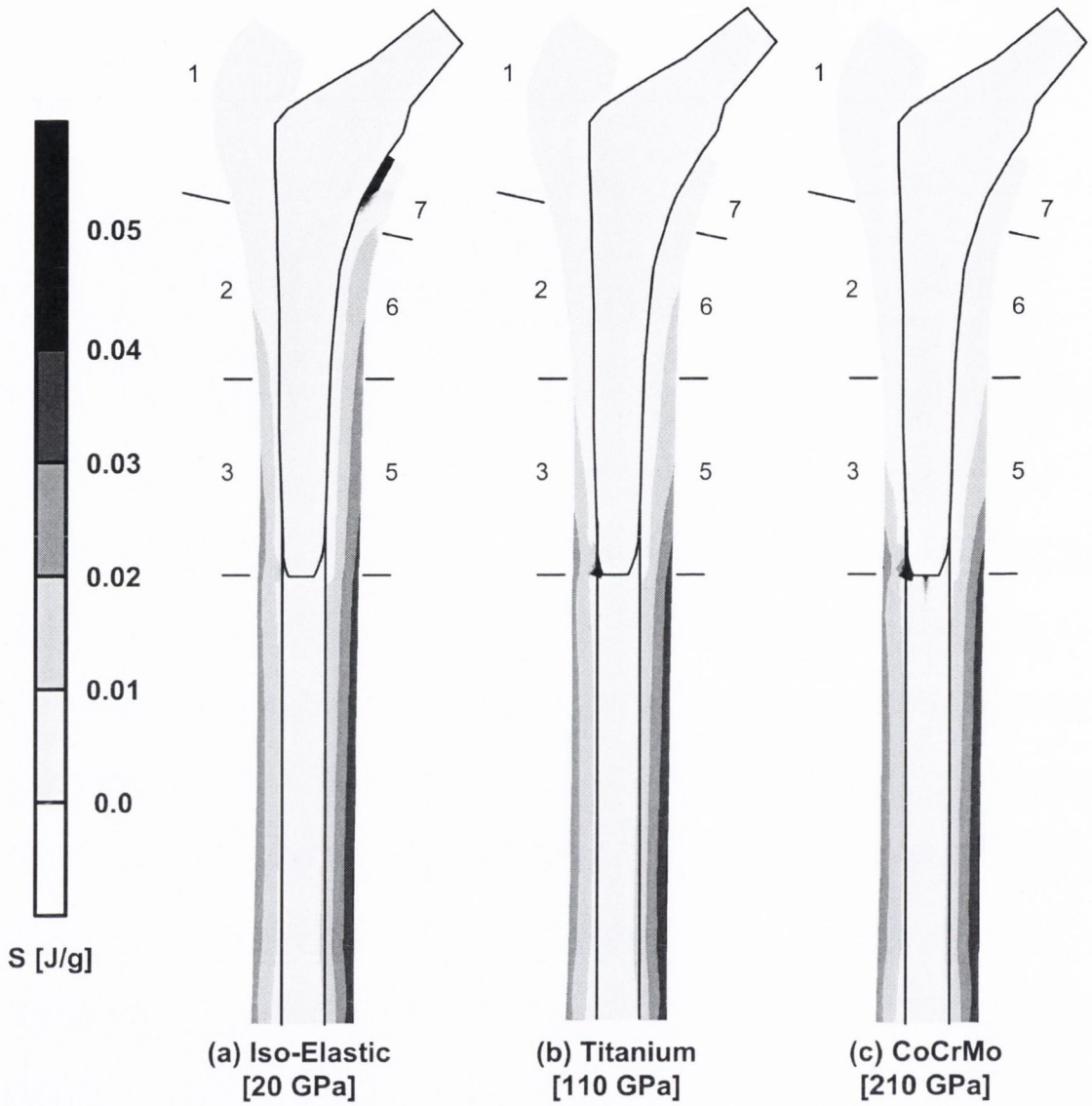

Figure 4.1. Mid-plane cross section showing distribution of the strain energy density per unit mass in the (a) iso-elastic, (b) titanium, and (c) CoCrMo stems.

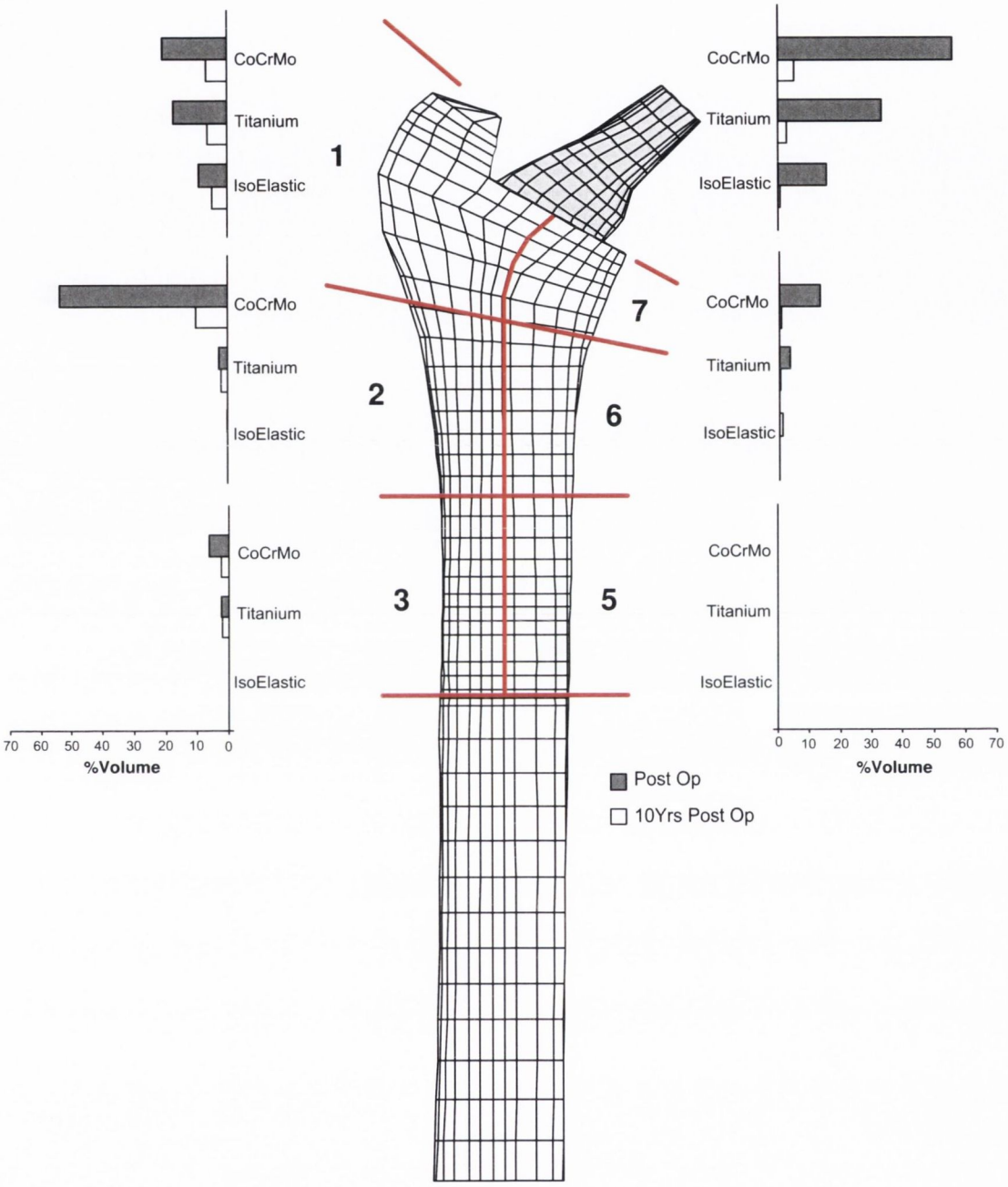

Figure 4.2. Percentage volume of bone experiencing stress shielding immediately post-op, and after 10 years in all three stem models.

4.2.1.2 Predicted bulk density distribution

The change in bulk-bone density in the anterior and posterior of all Gruen zones in all three modulus stems was calculated. For the majority of Gruen zones there is a high rate of bulk bone loss over the first six months. After the sixth month the rate of bone loss slows, and from year two no more significant bone loss is observed, see Fig. 4.3. The predicted bulk density distribution, ten years post-operatively, is plotted for all three stems in Fig. 4.4.

Proximal bone loss (zones 1 and 7), as a result of stress shielding, is most severe for the CoCrMo stem and peaks at 77.4% in the anterior section of zone 7, see Fig. 4.5. This compares to 63.8% and 24.4% for the titanium and iso-elastic stems in the same region. At the mid-stem position (zones 2 and 6) loss of bone mass is again most severe for the CoCrMo stem in the medial anterior aspect at 14.8% with the remaining regions reducing by between 2.6 and 13.7%. A 10.5% reduction in bone mass is observed in the medial anterior region of the titanium stem, with little change occurring elsewhere. Negligible bulk bone adaptations are observed mid-stem with the iso-elastic stem model, between 1.1% loss and 0.37% gain in density. Bulk bone adaptations at the distal tip (zones 3 and 5) peak at a 8.9% loss in the anterior region of zone 5 for the CoCrMo stem. This is reflected in the minimal amount of bone experiencing stress shielding in these zones, a maximum of 6% in zone 3 of the CoCrMo stem and 0% for all 3 stems in zone 5 (Fig. 4.2).

It is shown in Fig. 4.2 that after ten years the percentage volume of bone experiencing stress shielding has been reduced considerably while the amount of bone within the lazy zone has increased, shown in Fig. 4.6. At least 90% of the volume in each Gruen zone lies within the lazy zone after ten years. This corresponds to the leveling off of the rate of bone resorption/formation in Fig. 4.3.

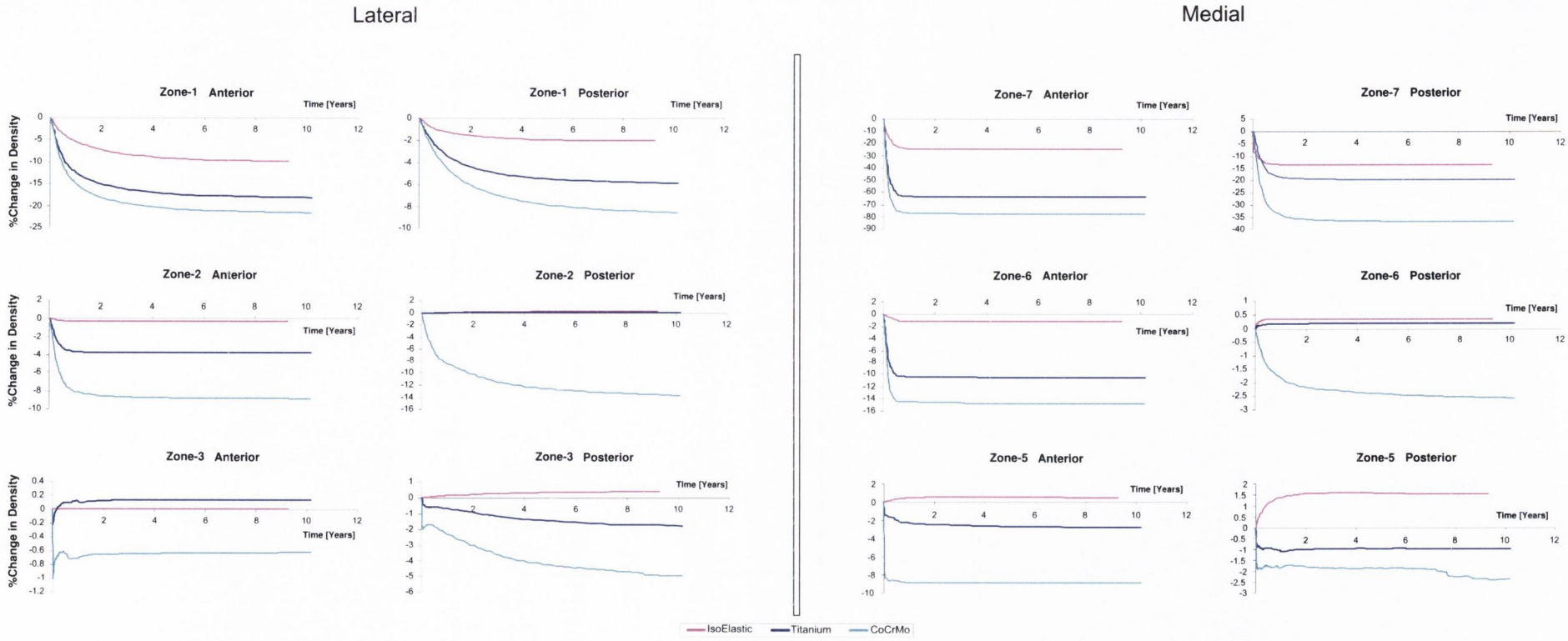

Figure 4.3. Percentage change in bulk density per Gruen zone over time.

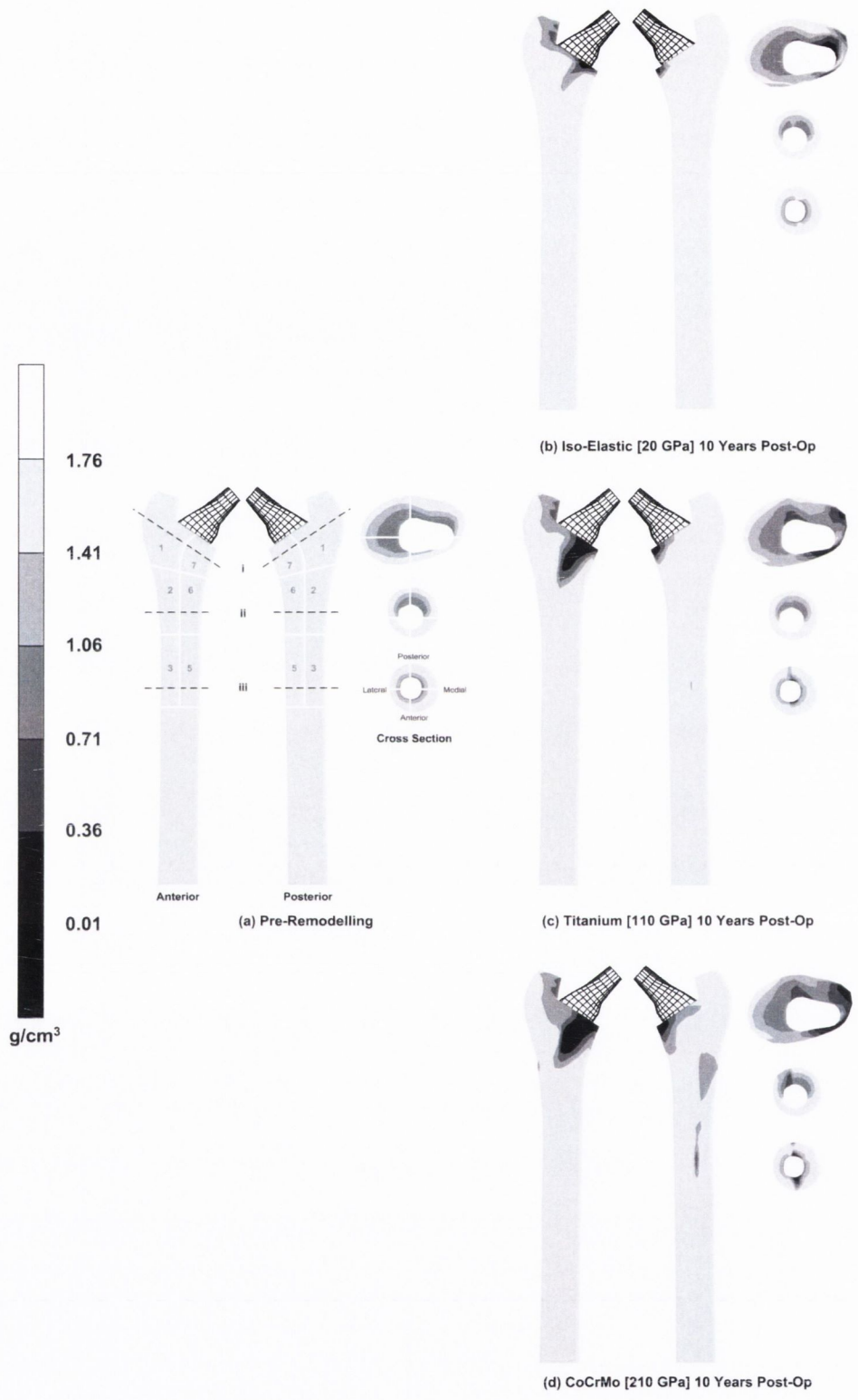

Figure 4.4. Anterior, posterior, and cross-sectional bulk density distribution (a) pre-remodelling, and 10 years post-op for the (b) iso-elastic, (c) titanium, and (d) CoCrMo stems. (White lines outline Gruen zones).

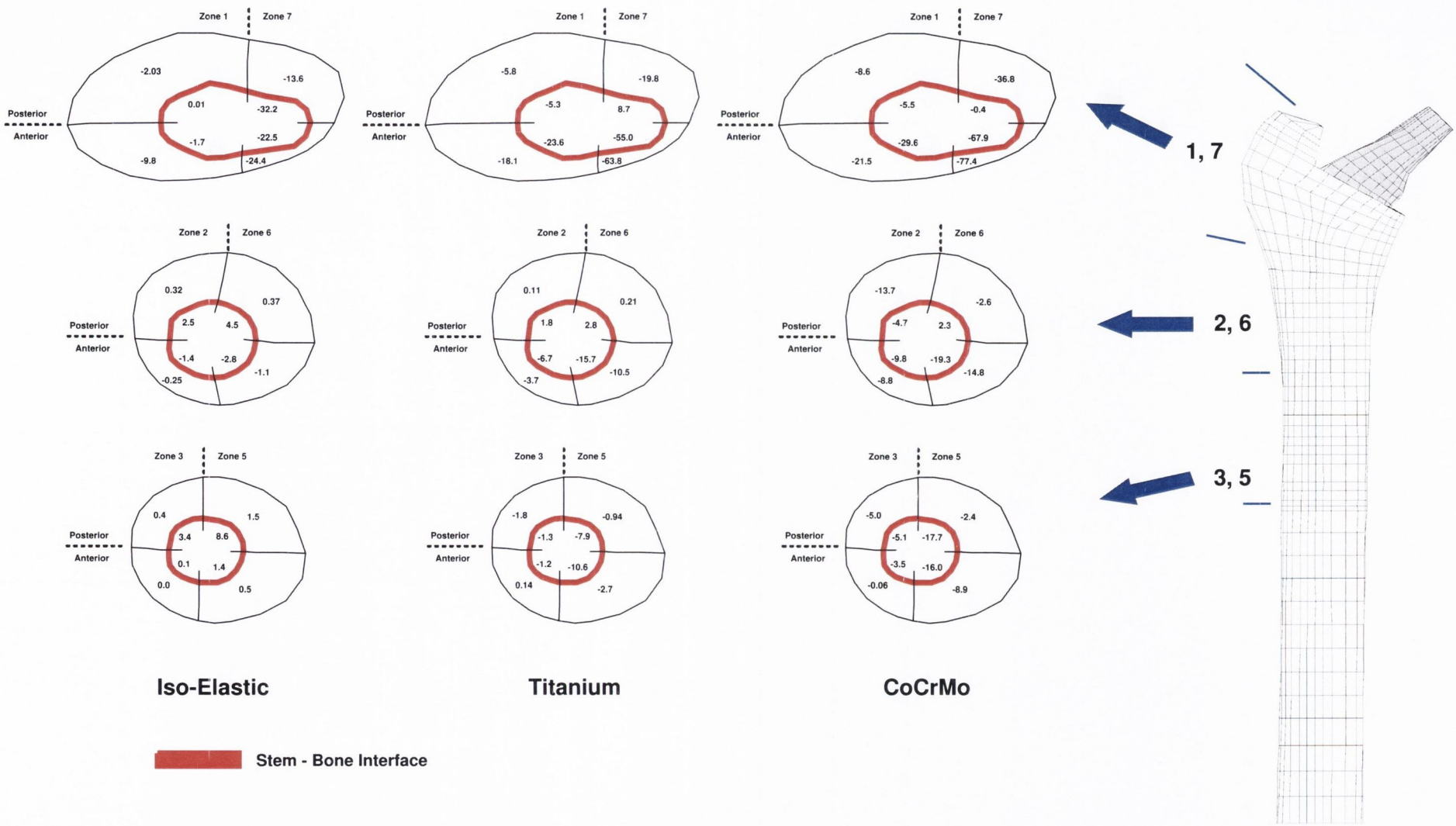

Figure 4.5. Percentage change in bulk and interfacial density per Gruen zone (anterior and posterior) after 10 years.

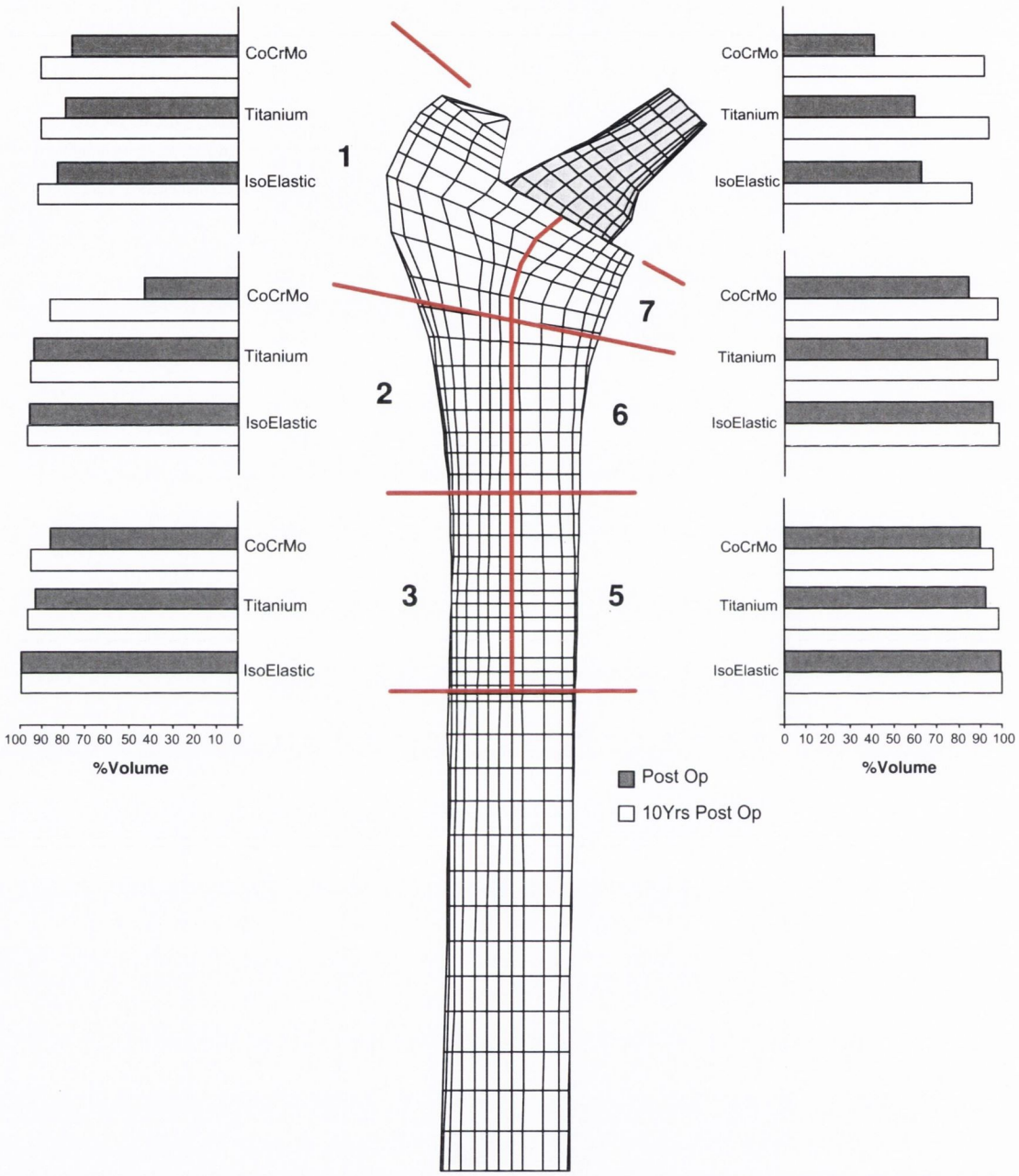

Figure 4.6. Percentage volume of bone within the lazy-zone immediately post-op, and after 10 years in all three stem models.

4.2.2 Interfacial bone remodelling

4.2.2.1 Interfacial load transfer

Peak load transfer for both the titanium and CoCrMo stems occurs distally in zones 3 and 5, both anteriorly and posteriorly, with the CoCrMo stem experiencing the highest degree of load transfer in these zones. Peak load transfer for the iso-elastic stem occurs proximally in posterior aspect of zone 7 and anterior aspect of zone 1. This pattern of load transfer from the prosthesis to the interfacial bone is shown in the distribution of the strain energy density per unit mass at the interface in Fig. 4.7 for all three stem materials. The areas of peak load transfer correspond to the areas of bone undergoing damage stimulated bone resorption shown in Fig. 4.8. Damage exceeds the critical amount, and undergoes damage stimulated resorption, in 9% of the volume in both zones 3 and 5 of the CoCrMo stem. Zones 3 and 5 of the titanium stem experience 6% and 7% of damage initiated bone resorption. This reduces considerably in the same zones for the flexible iso-elastic stem to 0.5% and 0.6%. In the proximal zones 1 and 7, both the titanium and CoCrMo stem experience no damage initiated bone resorption, while 11% of zone 7 and 1% of zone 1 of the iso-elastic stem experience damage stimulated resorption.

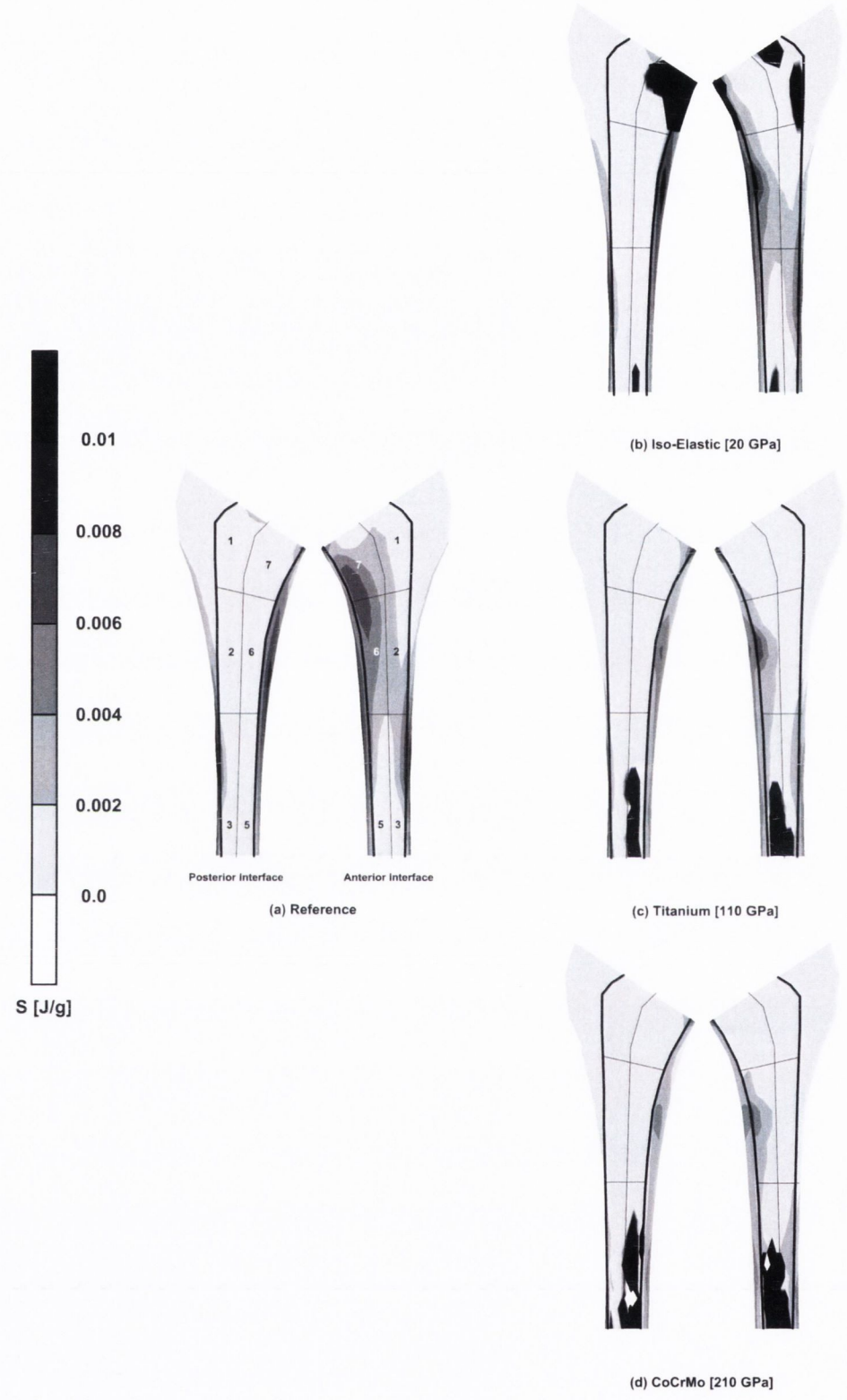

Figure 4.7. Posterior and anterior interface strain energy density per unit mass distribution for the (a) reference model, (b) iso-elastic, (c) titanium, and (d) CoCrMo stems. (Black line outlines stem position and Gruen zones).

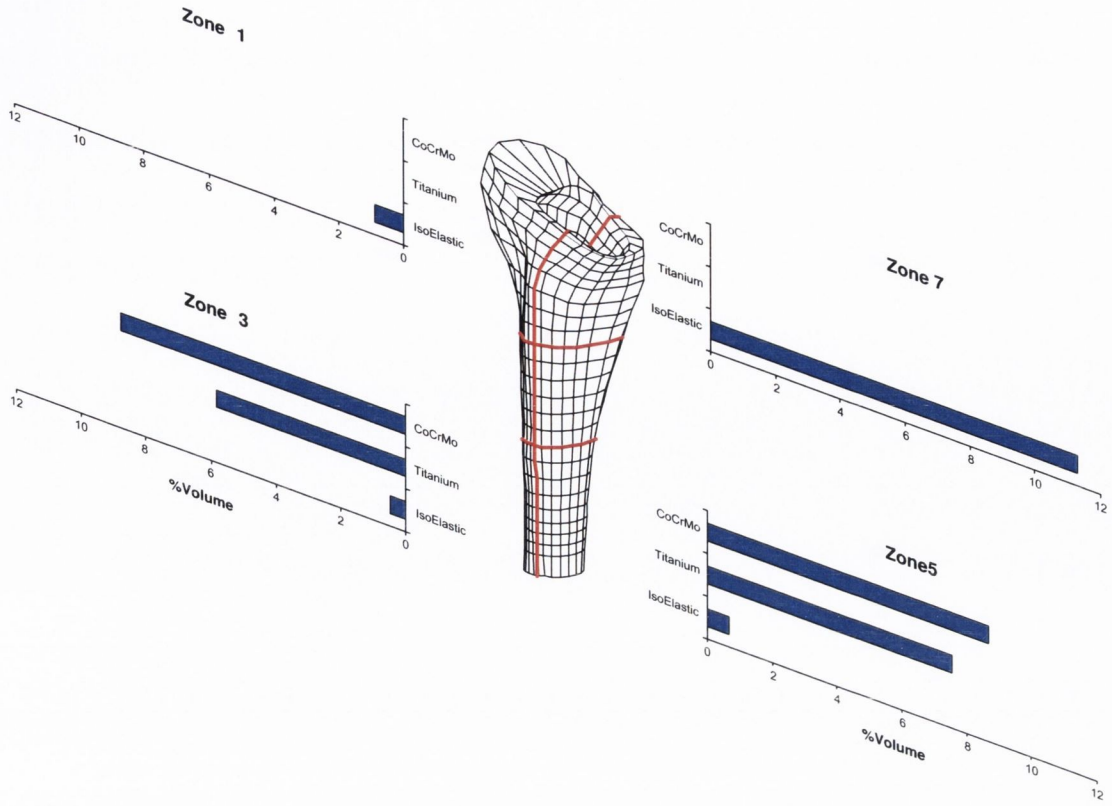

Figure 4.8. Percentage volume of interfacial bone experiencing damage stimulated remodelling in all three stem models.

4.2.2.2 Predicted interface density distribution

As with bulk remodelling the majority of bone adaptation occurs within the first six months, slowing thereafter, and from year two no appreciable density change is observed in the majority of Gruen zones. However, the posterior aspect of zones 3 and 5 of the CoCrMo stem continues to loose bone mass even after two years, see Fig. 4.9.

Proximal interfacial bone loss occurs in the posterior aspect of zone 7 for the iso-elastic stem (see Fig. 4.10) with a drop in density of 32.2% (stem-bone interface values, Fig. 4.5). In the same zone of the titanium and CoCrMo stem an 8.7% gain and 0.4% loss in density is experienced respectively. The proximal anterior interface of zone 7 shows a distinct drop in bone density for both the titanium (55%) and CoCrMo (67.9%) stems. By comparing this resorption pattern to the the distribution of strain energy density per unit mass in Fig. 4.7 it is clear that this bone loss is as a result of bulk-bone remodelling, due to stress shielding, encroaching

on the interface and therefore is not a response to interfacial damage accumulation.

Distal interfacial bone resorption increases as the stem stiffness increases, see Fig. 4.10. No interfacial bone resorption is predicted with the iso-elastic model, in fact bone formation of between 0.1 and 8.6% is found, shown in Fig. 4.5. A reduction of between 1.2% and 10.6% in bone mass occurs with the titanium stem increasing to between 3.5% and 17.7% with the CoCrMo stem. These areas of high interfacial bone loss correspond to the areas of high load transfer shown in Fig. 4.7.

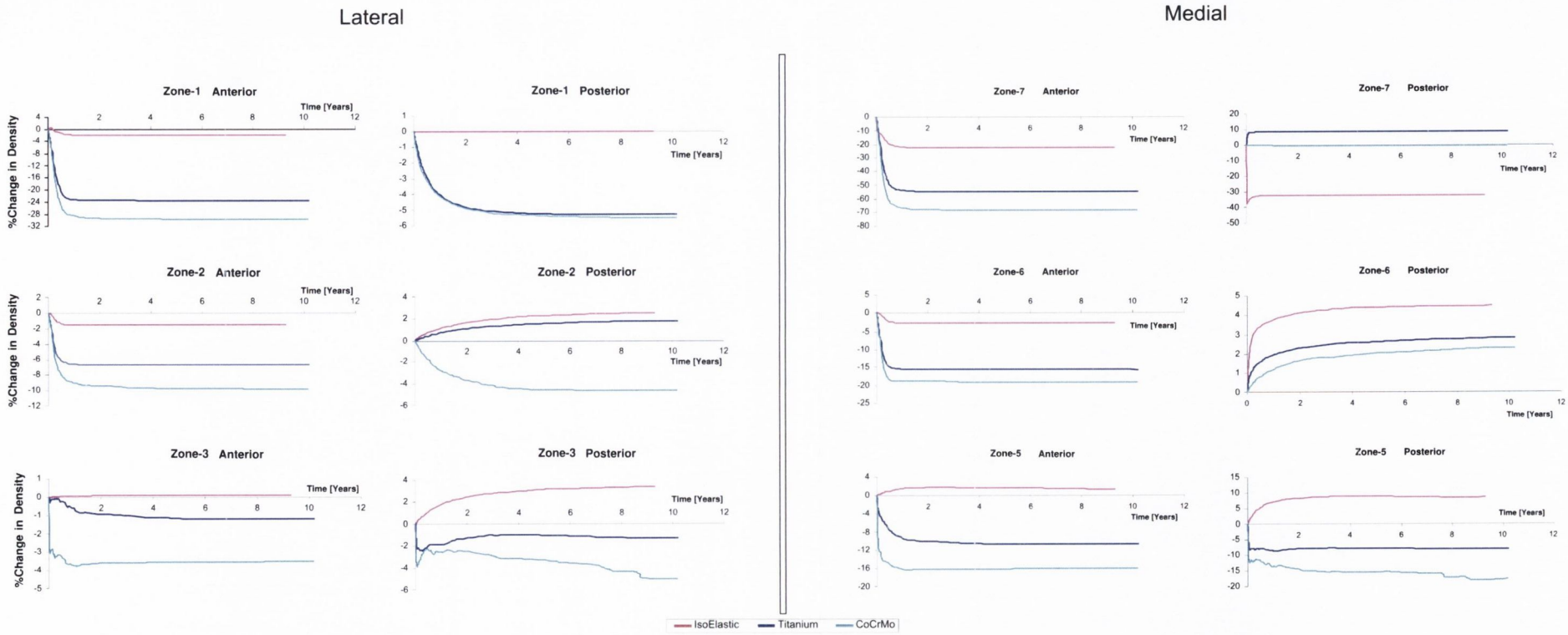

Figure 4.9. Percentage change in interfacial density per Gruen zone over time.

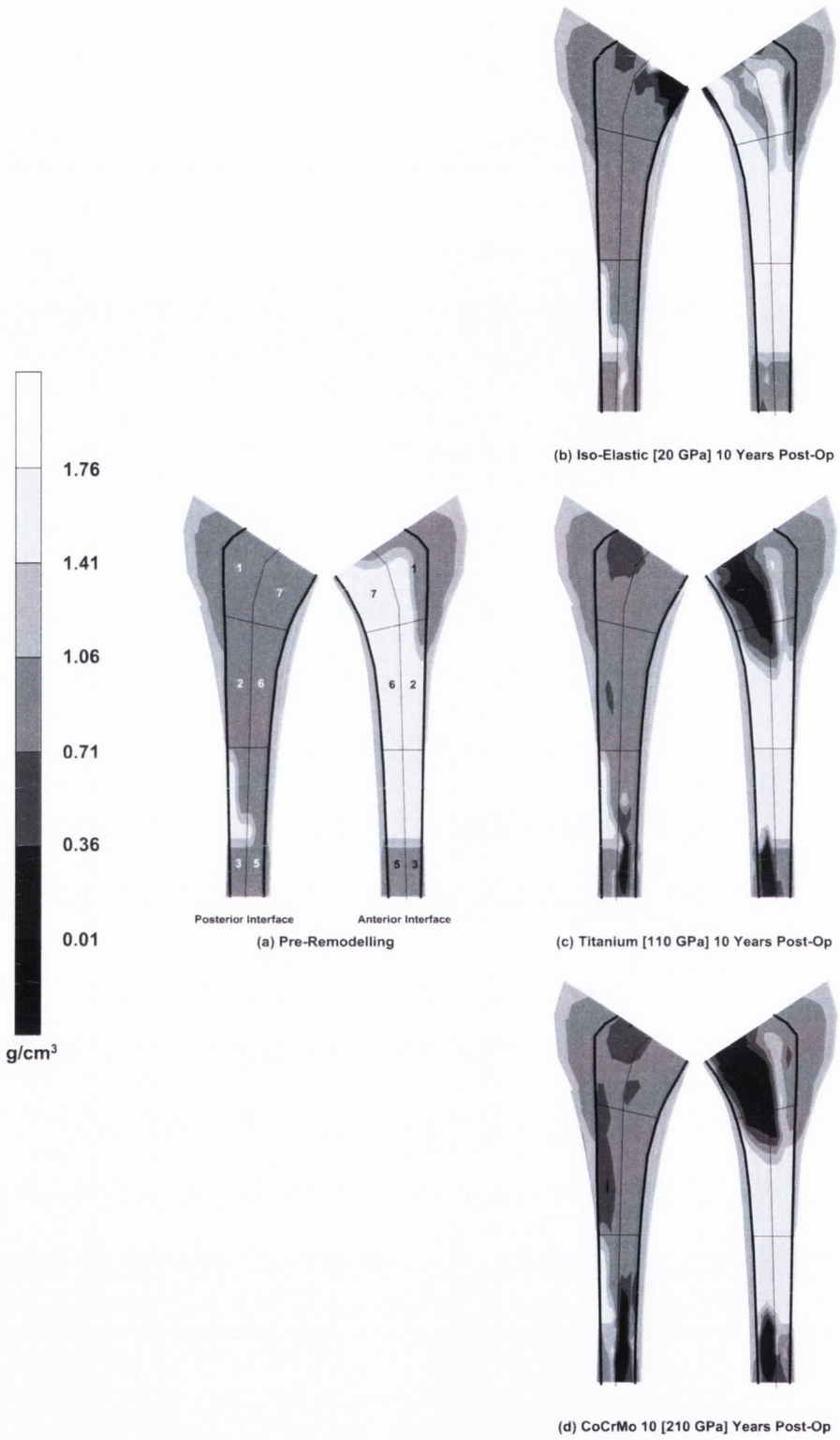

Figure 4.10. Posterior and anterior interface density distribution (a) pre-remodelling, and 10 years post-op for the (b) iso-elastic, (c) titanium, and (d) CoCrMo stems. (Black line outlines stem position and Gruen zones).

4.3 Bone remodelling and tissue differentiation

This section presents the results obtained for the combined bone remodelling and tissue differentiation simulations performed for each stem material. Contour plots of the predicted tissue phenotype over a period of five years at the stem-bone interface[1], and the change in the regulating stimulus for tissue differentiation over the same time period, are presented.

4.3.1 Iso-elastic stem

At 0.5 months a differentiation stimulus of $S \simeq 0.25$ at point 1 predicts mature bone formation through intramembranous ossification, see Fig. 4.11. The magnitude of the stimulus drops to a homeostatic value of $S \simeq 0.15$ at three months, which lies within the boundaries of $0.01 < S < 0.53$ maintaining mature bone formation throughout the five years, see Fig. 4.12.

Fibrous tissue formation is predicted at point 2 up to a period of 6 months post-operatively with an initial differentiation stimulus of $S \simeq 9$ predicted at 0.5 months, see Fig. 4.11. This reduces to a homeostatic value of $S \simeq 1$, which lies within the limits of cartilage formation $1 < S < 3$, by year 1 and cartilaginous tissue persists, see Fig. 4.12.

Endochondral ossification is predicted at point 3 with cartilage formation predicted up to month 3 ($1 < S < 3$), see Fig. 4.11. After month 3 the stimulus level drops to a magnitude conducive to immature bone formation ($0.53 < S < 1$) up to the first year, and mature bone formation ($0.01 < S < 0.53$) thereafter, see Fig. 4.12.

[1]Note that the contour plots show the tissue phenotype predicted only for bone which has been completely resorbed i.e. $\rho = 0.01$ g/cm^3. Surrounding tissue, shown in blue, is bone tissue with densities greater than 0.01 g/cm^3 which is still subject to bone remodelling.

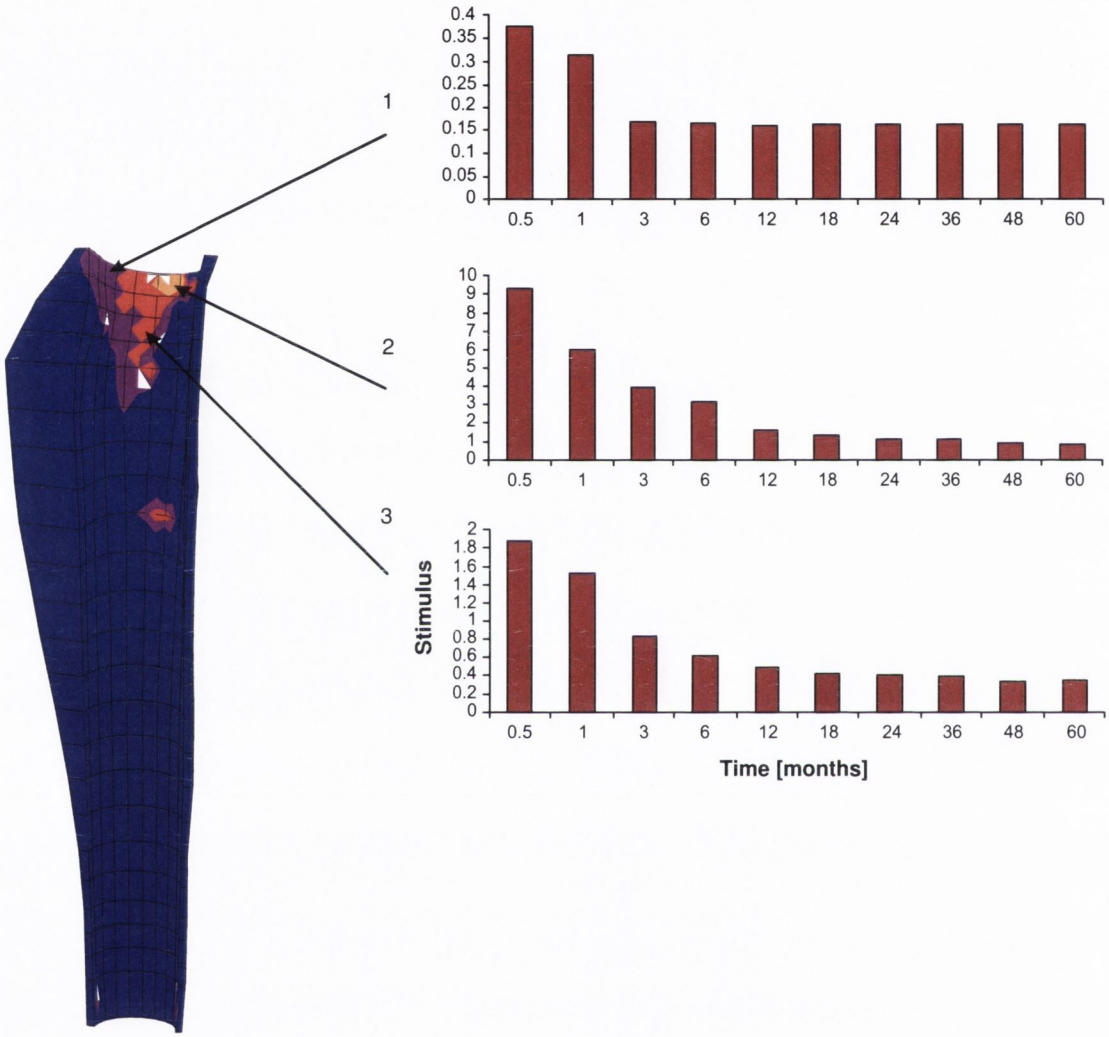

Figure 4.11. Change in tissue differentiation stimulus over at three points at the medial interface of the iso-elastic stem.

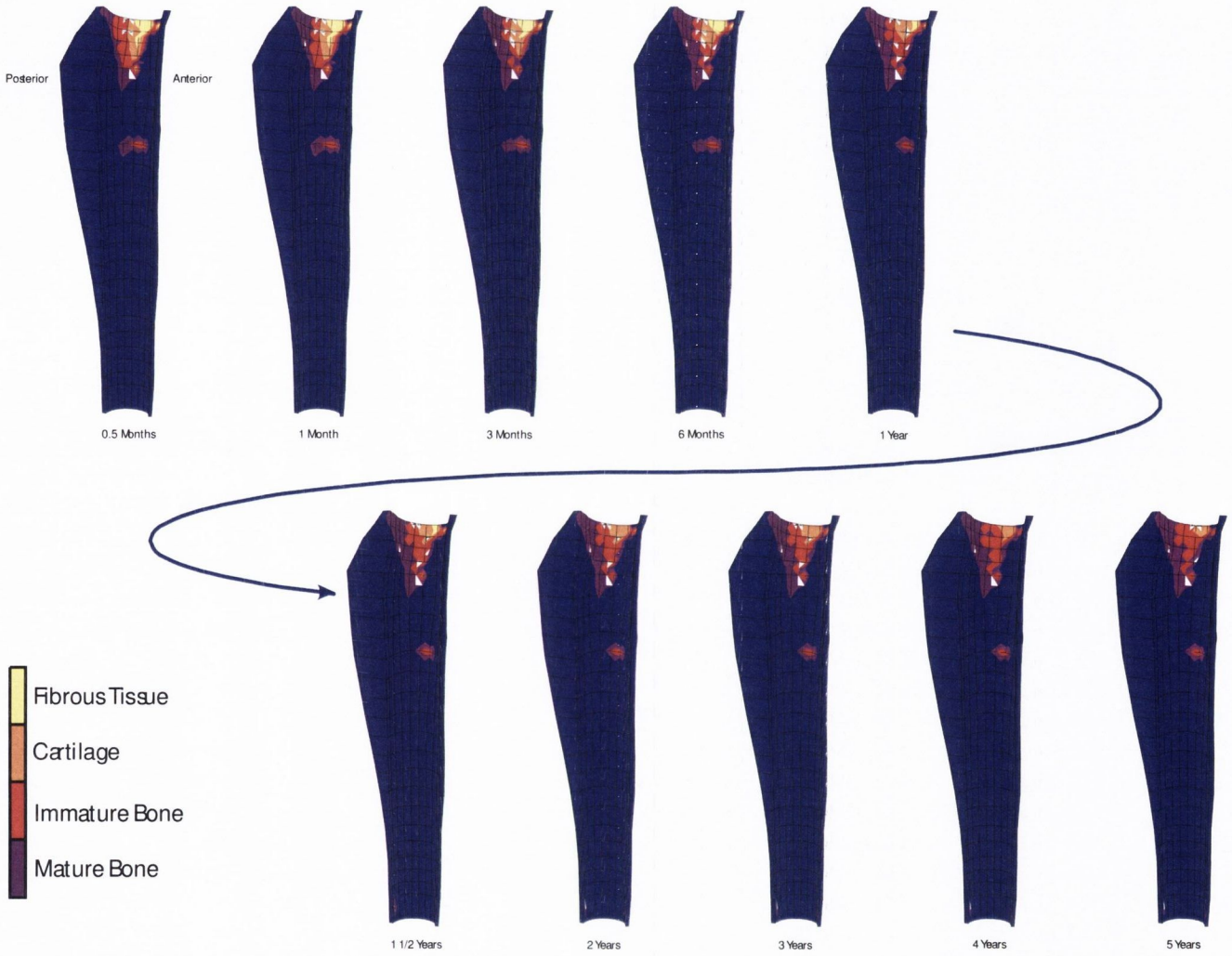

Figure 4.12. Change in tissue phenotype over time at the medial interface of the iso-elastic stem. Fibrous tissue (yellow) disappears by year 1 but small amounts of cartilage and immature bone is predicted to persist.

4.3.2 Titanium stem

At the posterior interface both intramembranous ossification and endochondral ossification are predicted. A stimulus of $S \simeq 1.3$ is predicted at point 1 promoting cartilage formation at 0.5 months, see Fig. 4.13a. As the stimulus drops, immature bone and eventually mature bone formation is predicted through endochondral ossification by month 3, see Fig. 4.14.

Initially a low stimulus is predicted at point 2, $S \simeq 0.05$, increasing to a maximum value of $S \simeq 0.2$ by three months, see Fig. 4.13a. This can be attributed to the gradual resorption of the element over the three months increasing the differentiation stimulus, and subsequent refilling of resorbed bone with mature bone after the third month through intramembranous ossification. There is little change in the stimulus after the third month with S varying between 0.1 and 0.17, and mature bone persists, see Fig. 4.14.

Similar trends are observed at the anterior interface to those described described above for the posterior interface. The anterior interface experiences both endochondral ossification (point 3 and 4) and intramembranous ossification (point 5), see Fig. 4.13b. Slightly higher initial stimulus values are predicted than those at the posterior interface. However, these values still lie within the stimulus boundaries for promoting cartilage formation and mature bone formation. More tissue differentiation activity is observed as bone resorption at the anterior interface is more extensive than that at the posterior interface.

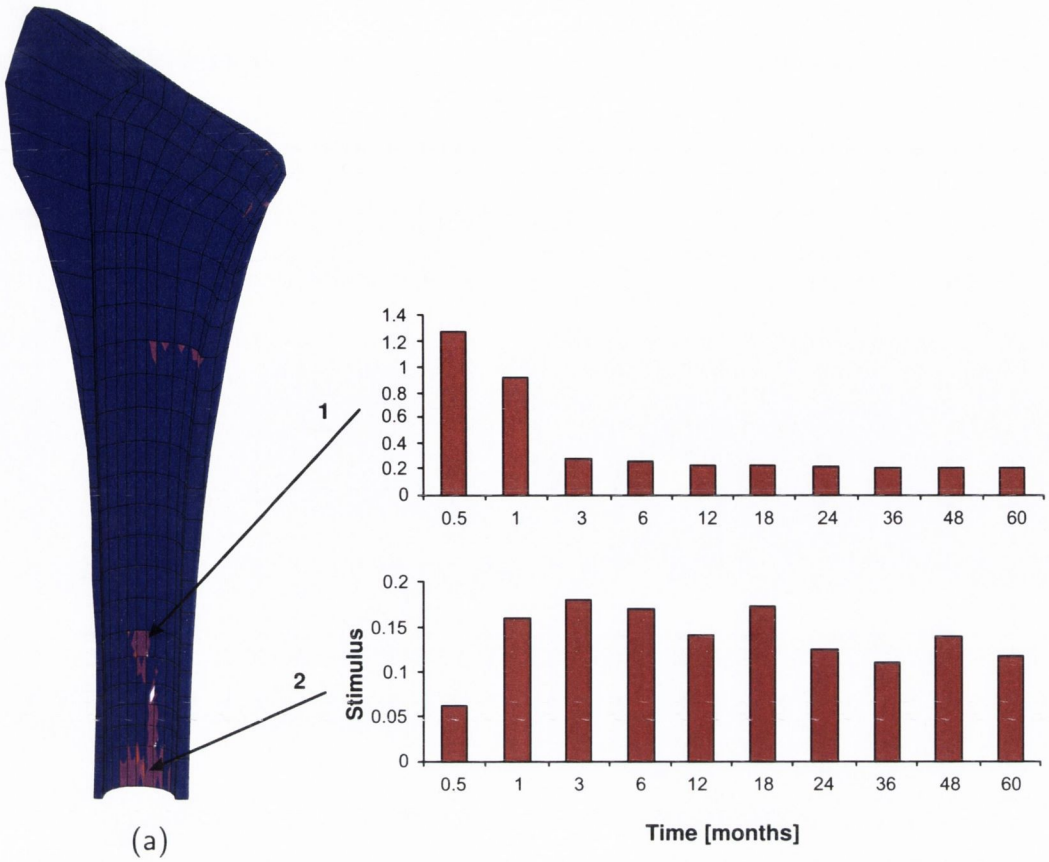

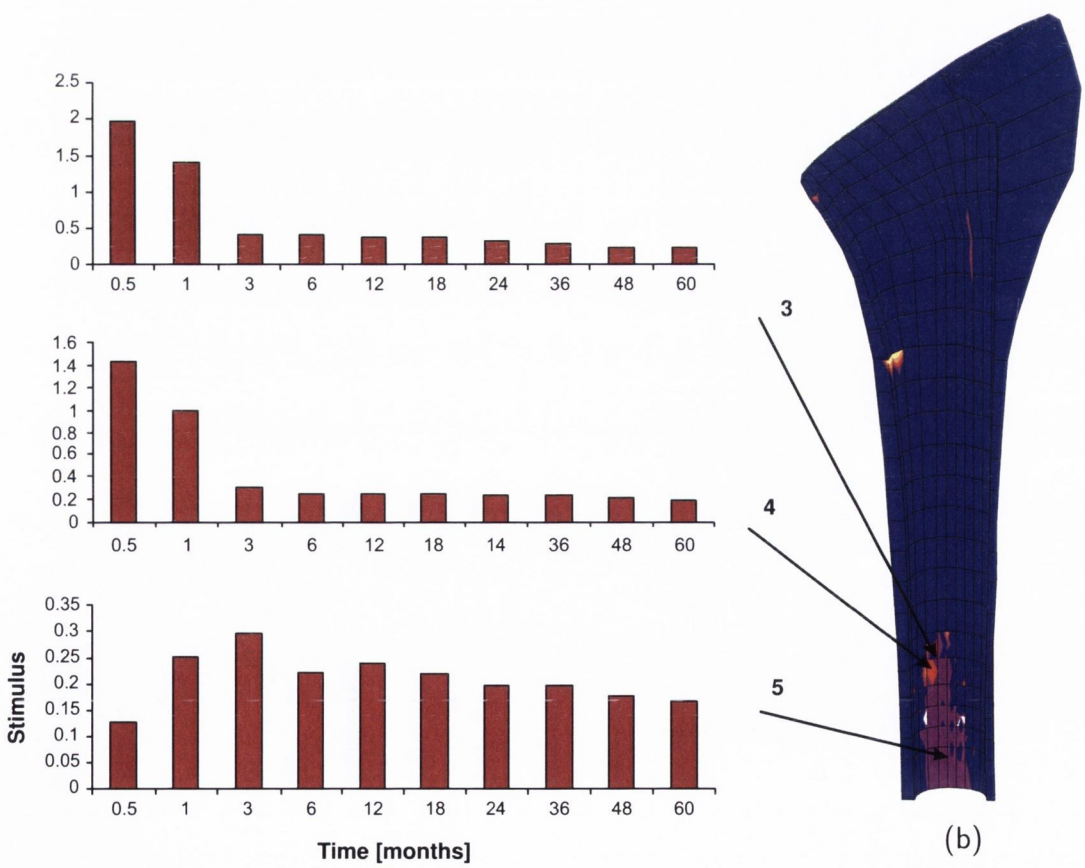

Figure 4.13. Change in tissue differentiation stimulus at two points at the (a) posterior and three points at the (b) anterior interface over time of the titanium stem.

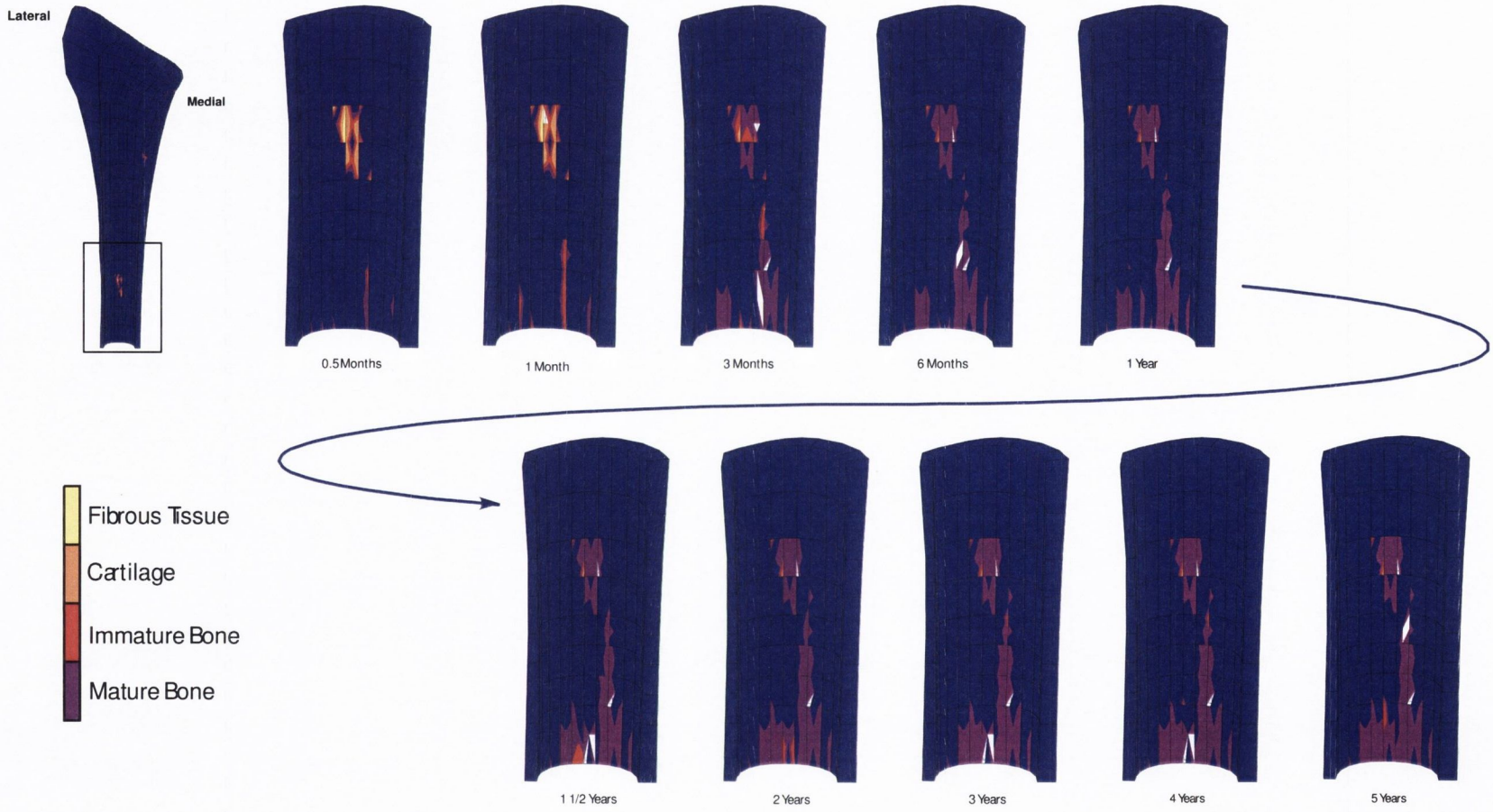

Figure 4.14. Change in tissue phenotype over time at the posterior interface of the titanium stem. Fibrous tissue appears at the distal tip and disappears completely (bone ingrowth) by the third month.

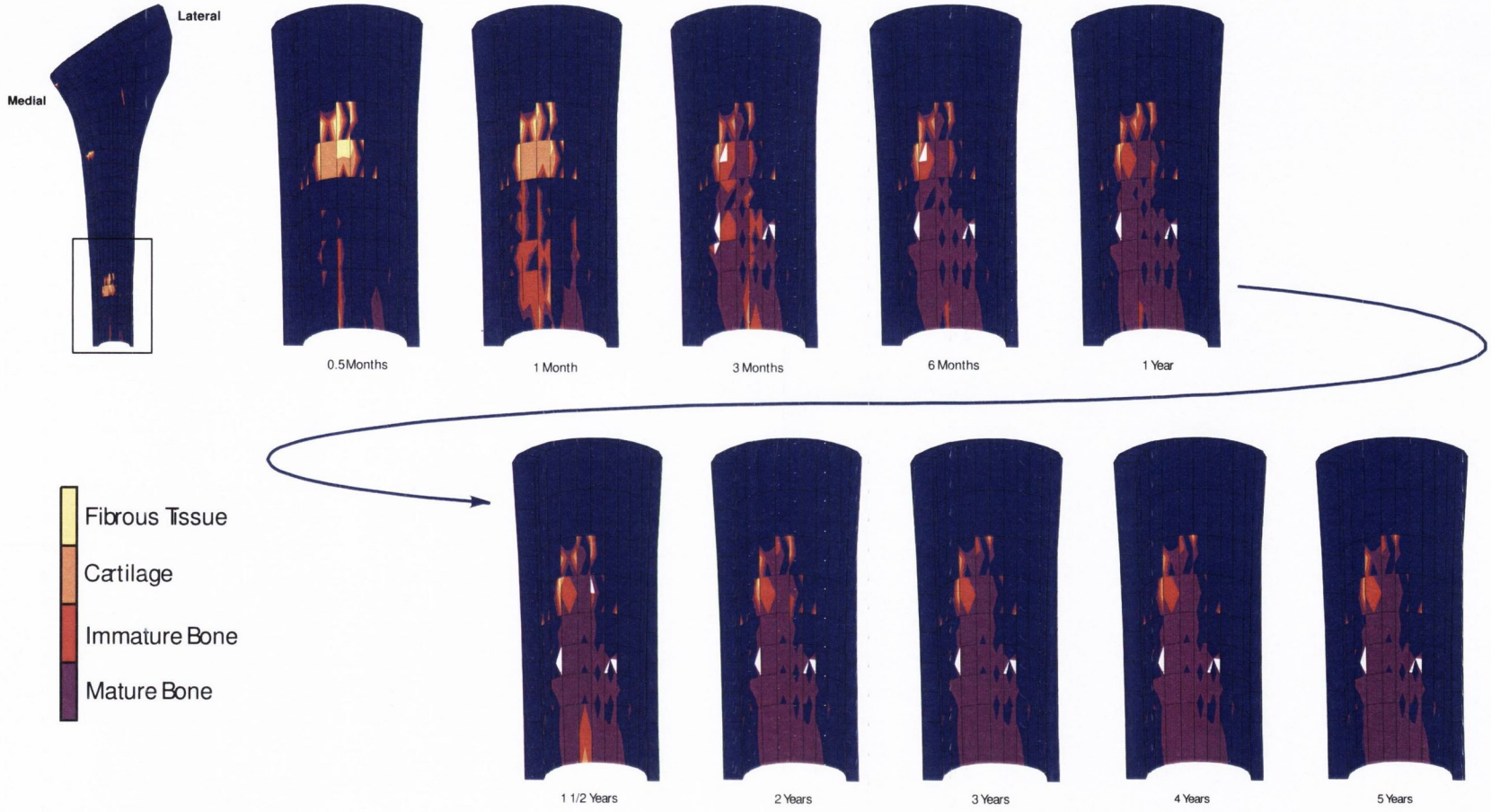

Figure 4.15. Change in tissue phenotype over time at the anterior interface of the titanium stem. Fibrous tissue and cartilage formation predicted at the distal tip almost completely converted to mature bone by month six.

4.3.3 CoCrMo stem

Stimulus values at point 1 over the first 2 weeks of differentiation are conducive to cartilage formation with $S \simeq 1.2$, see Fig. 4.16a. After the first month this value drops to $S \simeq 0.7$ promoting immature bone formation through endochondral ossification. From month three on the stimulus level drops further to a homeostatic value less than 0.53, and mature bone formation persists, see Fig. 4.17.

As with the titanium stem intramembranous ossification is predicted at point 2 with an initial stimulus of $S \simeq 0.2$ increasing to $S \simeq 0.25$ by the fist month, see Fig. 4.16a. This reduces to a homeostatic value of $S \simeq 0.15$ by the sixth month. Mature bone formation is predicted throughout the five years, see Fig. 4.17.

At the anterior interface stimulus levels of: $S \simeq 3$ predict fibrous tissue formation (point 3), $S \simeq 1.6$ predict cartilage formation (point 4), and $S \simeq 0.2$ predict mature bone formation (point 5) during the first 2 weeks of differentiation, see Fig. 4.16b. Over time the stimulus levels at points 3 and 4 drop to a homeostatic level of $S \simeq 0.5$ and $S \simeq 0.2$ predicting both mature and immature bone formation by endochondral ossification, see Fig. 4.18. The stimulus magnitude at point 5 increases to $S \simeq 0.5$ by month one, reducing to $S \simeq 0.2$ by month six. Mature bone formation is predicted throughout the five years through intramembranous ossification, see Fig. 4.18.

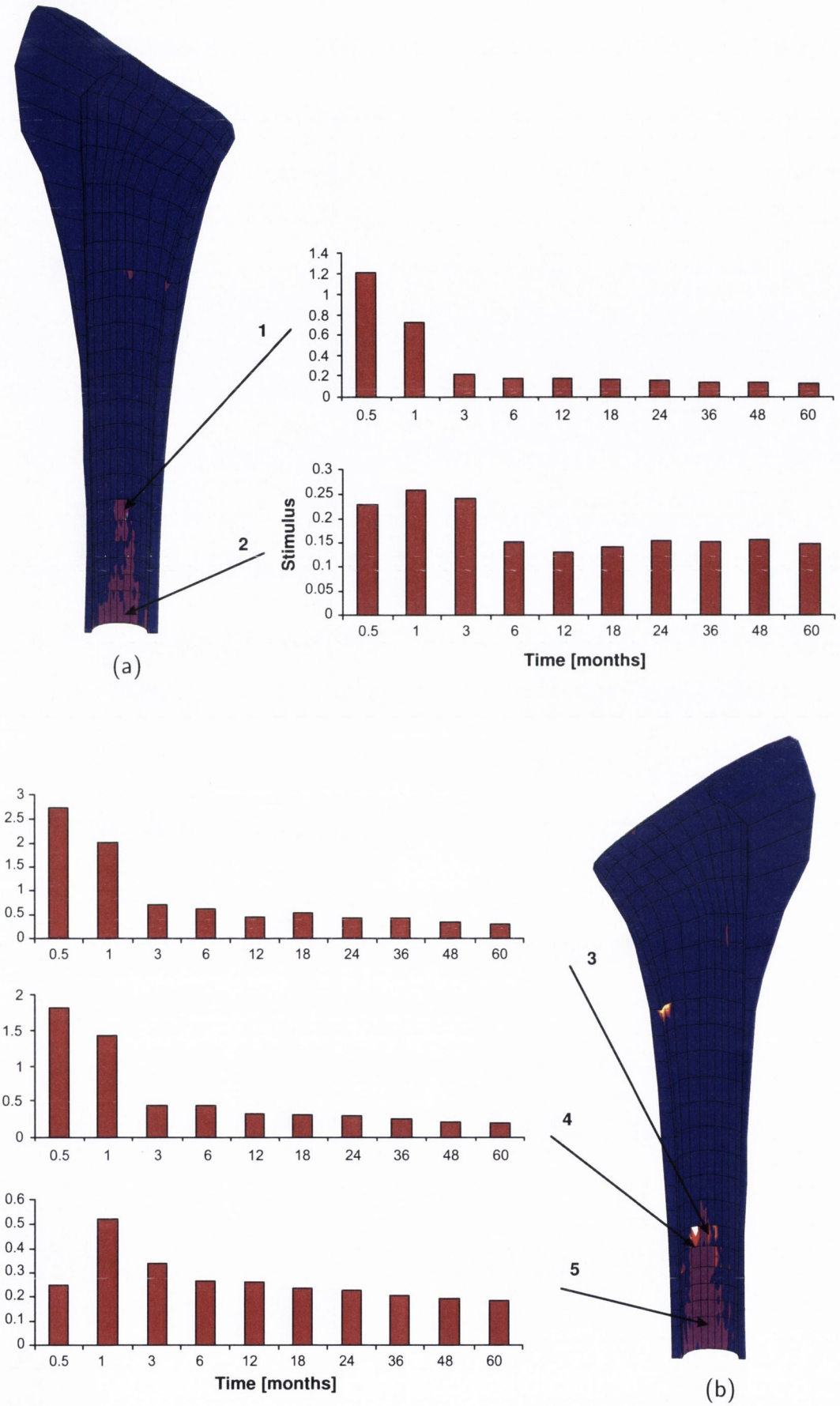

Figure 4.16. Change in tissue differentiation stimulus at two points at the (a) posterior and three points at the (b) anterior interface over time of the CoCrMo stem.

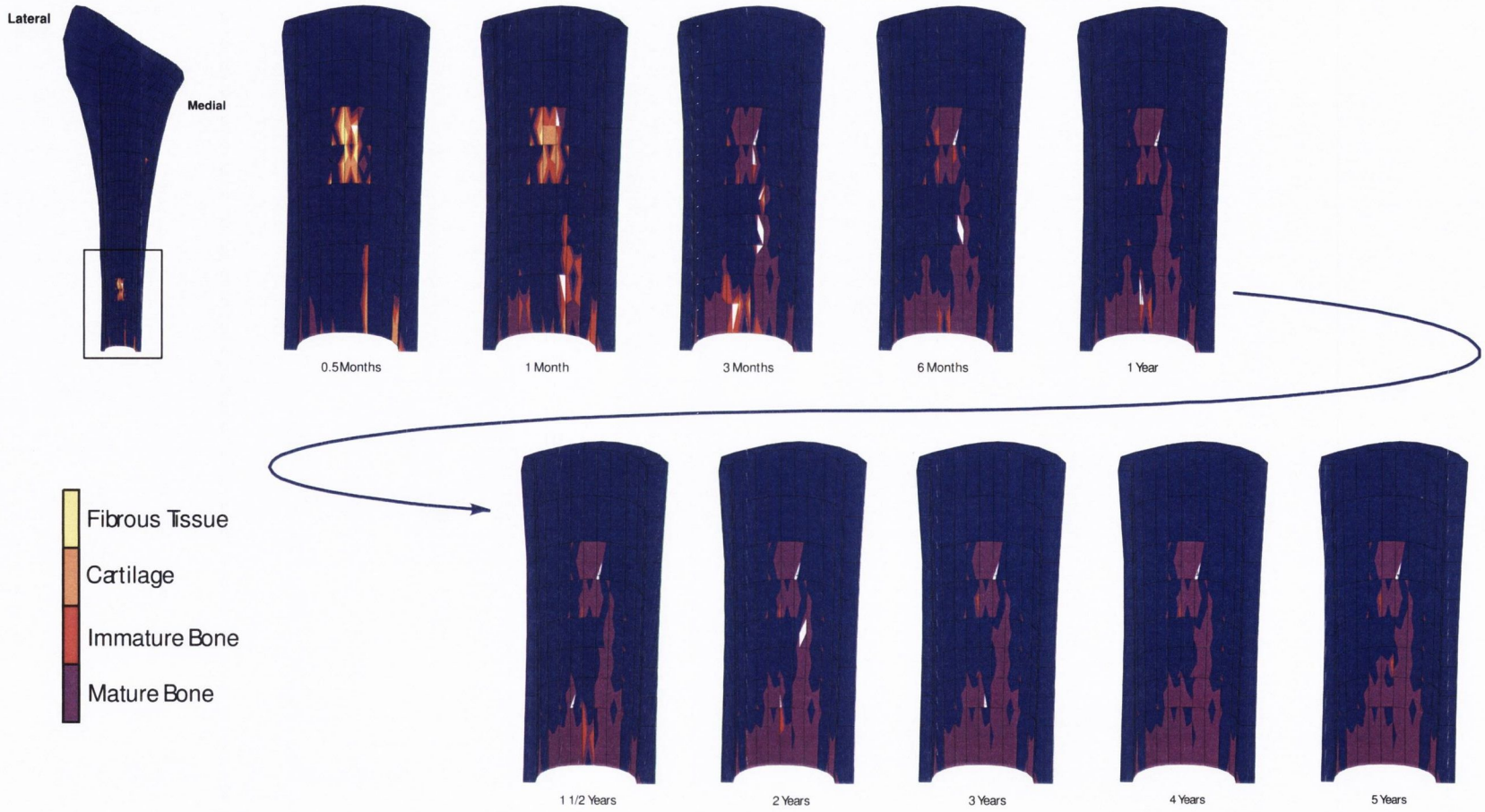

Figure 4.17. Change in tissue phenotype over time at the posterior interface of the CoCrMo stem. Fibrous tissue appears at the distal tip and disappears completely (bone ingrowth) by the third month.

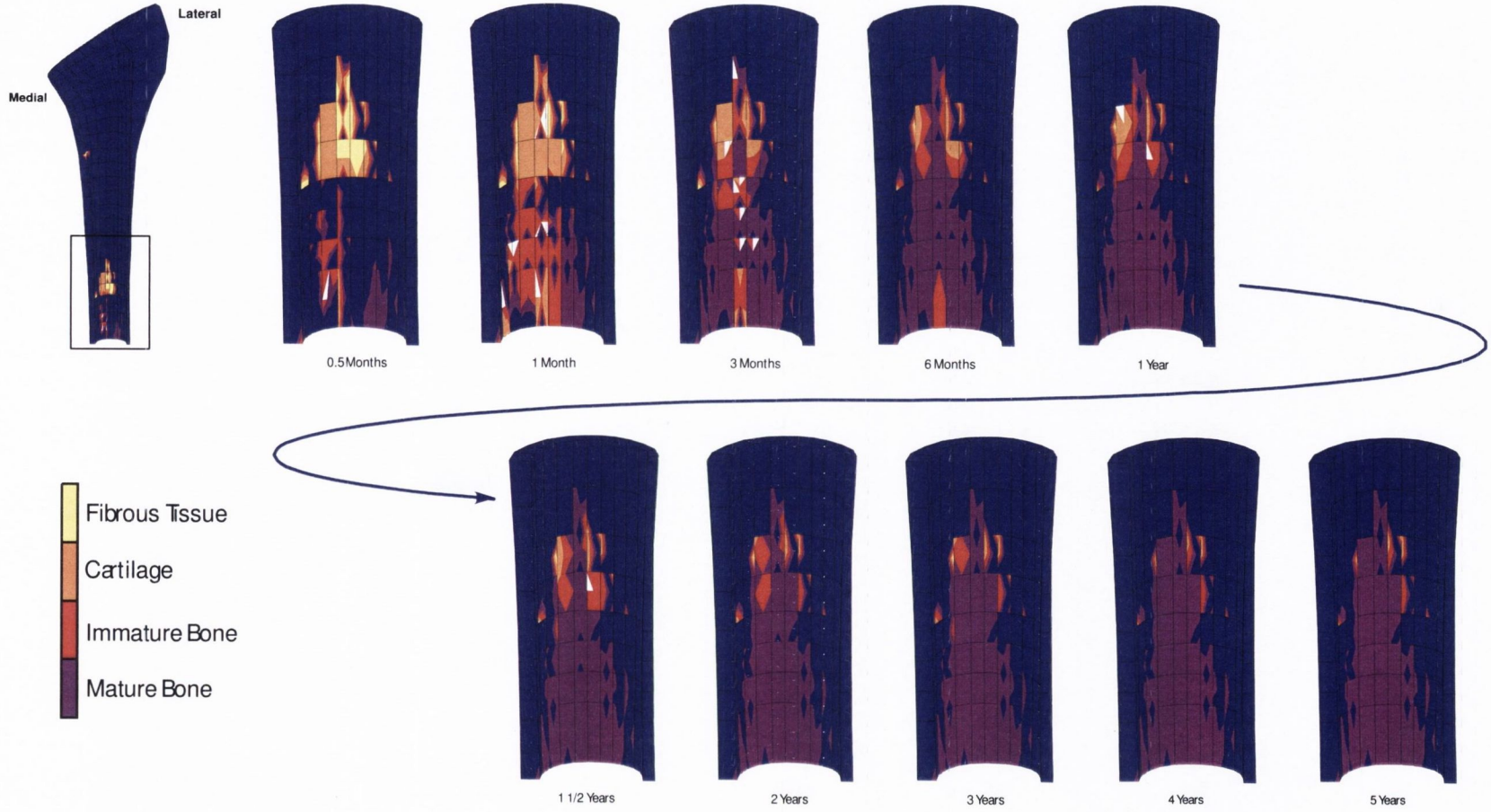

Figure 4.18. Change in tissue phenotype over time at the anterior interface of the CoCrMo stem. Fibrous tissue and cartilage formation predicted at the distal tip almost completely converted to mature bone by one and a half years.

4.4 Summary of results

This section summarises the main results of obtained from the bone remodelling and combined remodelling-tissue differentiation simulations of a realistic three-dimensional geometry of a noncemented femoral prosthesis.

4.4.1 Bone remodelling

It was predicted that although flexible stems reduce bulk-bone loss due to stress shielding, they induce high proximal interface stresses causing damage accumulation leading to interfacial bone resorption. Conversely, stiff stems increase both stress shielding and distal load transfer promoting proximal bone resorption and distal damage induced resorption respectively.

4.4.2 Combined remodelling and tissue differentiation

Both intramembranous and endochondral ossification was predicted in all three stem models. The flexible iso-elastic stem promotes proximal medial fibrous tissue formation which is subsequently replaced by cartilage. Refilling of resorbed bone with mature bone, through both intramembranous and endochondral ossification, at the distal tip of both the titanium and CoCrMo stems is predicted.

Chapter 5

Discussion

Contents

5.1 Introduction

In this thesis, the hypothesis that computational algorithms can predict both bulk *and* interfacial peri-prosthetic bone adaptations is proposed. An algorithm incor-

porating both strain and damage as remodelling stimuli was developed to test this hypothesis. Furthermore, a tissue differentiation algorithm was incorporated to predict tissue regeneration following interfacial bone resorption, thus further enhancing the predictive power of the mechanobiological model. To the author's knowledge, this thesis represents the first attempt to simulate bulk and interfacial adaptation together with interfacial tissue differentiation algorithms in realistic three dimensional geometries.

The justification of this thesis stands on the predictive power of the computational model. Comparison to what has been previously observed experimentally and computationally shall be made to support the author's results.

5.2 Limitations

The models and algorithms used to predict peri-prosthetic bone adaptations are based on a number of assumptions. This section considers these assumptions and limitations.

5.2.1 Finite element model

A number of assumptions were made in the development of the finite element model described in chapter 3.3.

The initial material properties of the cancellous and cortical bone were considered as homogeneous and were assumed to be linear elastic and isotropic. However, in reality cancellous and cortical bone material properties are known to be heterogeneous and anisotropic. Furthermore, only the elements at the stem/bone interface were considered as biphasic, or poroelastic, in the tissue differentiation model, with the surrounding cortical bone cortex modeled as impermeable. An improvement in the model would be to model the entire bone cortex as poroelastic with the external surface modeled as impermeable.

The loading consisted of only one load case, that at the instance of maximum in vivo hip joint loading during walking. Given that walking accounts for 80% of the dynamic load (Bergmann and Duda, 1998) and 10.2% of daily activity (Mor-

lock et al., 2001), it was considered sufficient to realistically influence remodelling. Furthermore it is assumed that the pre and post-operative loads are equal. The femoral head of the intact model was not explicitly modeled. Hence, the hip contact load in the intact femur was applied to the model through the use of beam elements connecting the point of hip loading to the face of the resected bone. It would be of interest to model the head of the femur of the intact model when determining the reference stimulus and damage values.

A perfect fit between the stem and bone is assumed with the coated portion of the stem considered fully bonded. However this is only an approximation; in reality, some gaps between the stem and bone are certain to occur, and the osseointegration between the bone and hydroxyapatite coating on the stem occurs over a period of time and is determined by numerous factors such as the relative micromotions between the stem and bone (Søballe et al., 1992a). However, if the algorithm presented in this thesis were to be run without a bonded hydroxyapatite/bone interface (i.e. loose) the stem would subside provoking large micromotions between the stem and bone resulting in either high compressive interface stresses (without friction) or shear interface stresses (with friction) (Weinans et al., 1994; Huiskes and van Rietbergen, 1995) leading to interfacial bone resorption and persistent fibrous tissue formation. To allow for such realistic interface conditions a further improvement in the model would be to model bone ingrowth as a function of relative interface micromotions (Andreykiv et al., 2005).

Considering these assumptions, the results presented must be considered as trends in an idealised situation for one particular stem geometry. Furthermore, these limitations are constant for each stem material model and therefore comparisons can be made between each prosthesis material.

5.2.2 Bone remodelling algorithm

The remodelling algorithm itself is subject to a number of assumptions. First and foremost it is assumed that the remodelling is stimulated by two mechanical signals, namely strain and damage. Following successful predictions of trabecular architec-

ture (Mullender et al., 1994; Mullender and Huiskes, 1995) and bone adaptations around noncemented femoral prostheses (Weinans et al., 1992; Huiskes et al., 1992; van Rietbergen et al., 1993), the strain component of the remodelling stimulus S was chosen as the strain energy density per unit mass. While the damage stimulus is based on the relationship of Carter et al. (1976), as used by McNamara and Prendergast (2006) in the prediction of remodelling on the surface of a trabecula.

The rate of remodelling due to strain was based on that proposed by Weinans et al. (1993) as a first approximation, while the rate of damage-stimulated remodelling was determined from a parametric study. This parametric study was carried out on the titanium stem only as this allowed for comparison of the predicted results to clinical findings (Sluimer et al., 2006). Clinically, radiolucent lines, indicative of fibrous tissue formation, is seen predominately around the distal tip of the stem (Gruen zones 3 and 5) and occurs predominately during the first two post-operative years stabilizing thereafter (D'Antonio et al., 1996; Sluimer et al., 2006). In our model we assume that radiolucent lines, and hence fibrous tissue formation, are represented by interfacial bone resorption following excessive damage accumulation. The damage rate constant was varied until the amount and rate of distal bone resorption closely matched those reported by Sluimer et al. (2006).

Another important aspect of the remodelling algorithm is the influence of the width of the lazy zone. A parametric study of three widths was performed: s=$\pm$0.35,$\pm$0.5, and $\pm$0.75. The use of a small lazy zone resulted in extensive proximal bone loss, which was deemed unrealistic. The larger lazy zone width (s=$\pm$0.75) resulted in more realistic amount of bone resorption, and this agrees with the findings of Huiskes et al. (1992) and Huiskes and van Rietbergen (1995). However, it has been suggested by Huiskes et al. (1992) that the width of the lazy zone may be patient-specific, and this would account for individual variations in bone resorption patterns. Furthermore, large amounts of bone remodelling may be predicted for very small changes in stimulus, particularly for locations within the bone which normally experience very low magnitudes of load, and hence a low reference stimulus. This observation lends itself to suggest that not only is the width of the lazy zone patient-

specific, but may also be site-specific. Hence, the amount of bone resorption may be over predicted in these locations in this model. Additionally, the idea of a damage lazy zone is also proposed, whereby bone mass is maintained between a remodelling equilibrium amount of damage, ω_{RE}, and an upper limit of critical damage, ω_{CRIT}. This assumes that an amount of microdamage exists at remodelling equilibrium; this hypothesis was proposed by Prendergast and Taylor (1994) and was substantiated by Lee et al. (2002) who found microcracks present in the control group of normal sheep. The proposed damage lazy zone is analogous to the explanation for the lazy zone by Taylor (1997) who states "it is the zone within which normal maintenance processes are able to work."

5.2.3 Combined remodelling-tissue differentiation algorithm

The limitations previously mentioned for the remodelling algorithm are also applicable to the combined remodelling-differentiation algorithm. In additions several other limitations for the combined algorithm should be noted.

The diffusion of mesenchymal stem cells into areas of resorbed bone to simulate migration and proliferation (Lacroix et al., 2002) was not included in this model. It was assumed that mesenchymal stems cells (MSCs) would spread homogeneously throughout the resorbed bone. However, this is not the case in reality as MSC's will take some time to migrate and proliferate in the tissue (Iwaki et al., 1997). Furthermore, the effect of mechanical stimuli on cell mitosis and apoptosis (Kelly and Prendergast, 2005) was not included. The incorporation of these processes could prevent the prediction of mature bone formation where one would expect persistence of a fibrous tissue interface, namely the distal tip and proximal medial interface of the CoCrMo and iso-elastic stem respectively.

The limits of the mechano-regulation rule were determined from a two dimensional axisymmetric FE model of the piston micro-motion experiment of Søballe (1993). While this model has been successfully applied to several types of models: tissue differentiation at implant interfaces (Prendergast et al., 1997; Huiskes

et al., 1997; Geris et al., 2003), fracture healing (Lacroix and Prendergast, 2002a,b; Lacroix et al., 2002; Isaksson et al., 2006), and osteochondral defect repair (Kelly and Prendergast, 2005, 2006), it remains untested on realistic three dimensional implant geometries.

The time period over which tissue differentiation was assumed to occur was based, as a first approximation, on the observation that fracture callus density equals or exceeds that of the cortex after 10 weeks or more after injury (Islam et al., 2000). The choice of this time frame can be justified as it has been shown that there is no increase in the bonding strength of HA coated intramedullary implants after 12 weeks (Ducheyne et al., 1980).

5.2.4 Computer simulations of mechanobiological processes

The implementation of biological processes, such as bone remodelling and tissue differentiation, in computational models is reliant on a number of empirical assumptions due to the difficulty of obtaining accurate parameters of the cellular response to mechanical stimuli. This problem has been overcome with the use of parametric variation studies to match predicted outcomes to those observed clinically. Varying these parameters has been considered as 'tuning' such that it is near impossible not to obtain predictions which match those observed clinically (Prendergast, 2001). However, these parameters are dependant on the patients genetic makeup, and may be subject to a certain degree of 'tuning' by parametric variation on a patient specific basis.

5.3 Assessment of the algorithms

In this section the predictions for each stem material, based on both the remodelling and combined remodelling-tissue differentiation simulations, are contrasted to illustrate the influence of material choice on peri-prosthetic bone adaptations. The predicted adaptations are compared to those of similar computational studies as well as clinical observations.

5.3.1 Influence of stem stiffness on bone remodelling

Convergence was assumed when the change in density became negligible, less than 1%, and the percentage volume of bone within the lazy zone was 90% or above. One would expect 100% to represent complete convergence, however, Maloney et al. (1989) have shown that some degree of stress shielding persists as long as 17 years post-operatively, justifying our choice of 90% volume within lazy zone in conjunction with negligible density change.

Considering bulk-bone remodelling first, it is clear that stiffer stems, particularly the CoCrMo stem, provoke more stress shielding (Fig. 4.2) and proximal bone resorption (Fig. 4.4). By increasing the stiffness of the prosthesis the tendency of the prosthesis to carry more of the load increases, thus shielding the proximal bone from the load as shown in Fig. 4.1. Therefore it would seem a logical design choice to reduce the stem stiffness in an attempt to reduce proximal bone loss as of a result of stress shielding. However, to better understand the relationship between peri-prosthetic bone adaptations and prosthesis material, the interfacial stresses and resulting adaptations must also be considered. The location and amount of interfacial bone adaptations vary for each stem material. The peak interfacial stimulus, and hence load transfer, occurs at the distal tip for the titanium and CoCrMo stems, with the area of bone experiencing maximum load transfer for the CoCrMo stem exceeding that of the titanium stem (see Fig. 4.7). As the stiffness is reduced to that of the iso-elastic stem, peak load transfer moves proximally. The locations and areas of the peak stimulus corresponds to the areas of highest interfacial bone loss, shown in Fig. 4.10. The flexible stem produces proximal interface bone resorption at high stresses surrounding the coated portion of the stem. However, it must be noted that it is assumed that the hydroxyapatite coating is fully osseointegrated, when in reality this is not the case, at least initially, and the high interface stresses would probably inhibit bony ingrowth in the first place. With regard to this point it should be noted that bone loss in the posterior medial proximal interface of zone 7, see Fig. 4.9, occurs almost instantaneously, which may interpreted as immediate failed ingrowth. The stiff CoCrMo stem produces extensive proximal bone loss due

to stress shielding and excessive resorption around the distal tip due to damage accumulation. This could lead to a failure similar to that described by Gruen et al. (1979), mode II: medial stem pivot, where migration of both the proximal stem and distal stem tip occurs, caused by a weak proximal medial, or calcar, support combined with a lack of distal acrylic support, which in the cementless model could be interpreted as extensive resorption around the distal tip.

Considering both the bulk and interfacial bone adaptations a more informed decision on prosthesis material choice can be made. It is the author's opinion that the titanium stem would be the preferred material choice. This is based on the prediction that the titanium stem reduces both the unfavourable proximal bone loss and distal interface resorption caused by the CoCrMo stem, and proximal interfacial resorption caused by the iso-elastic stem. The choice of titanium as the preferred material choice can be validated by comparing the predicted adaptations to previous numerical and clinical investigations in the following sections.

5.3.2 Influence of stem stiffness on combined remodelling-differentiation

The influence of stem stiffness on tissue differentiation is not apparent if we consider only the converged homeostatic state (i.e. from the third month on) as bone formation is predicted at all points, except point 2 of the iso-elastic stem which is predicted as forming cartilage (Fig. 4.11). If we consider the time leading up to month three, subtle differences can be distinguished: fibrous tissue is predicted at point 3 in the CoCrMo (Fig. 4.16b) stem while at the same point in the titanium model cartilage is predicted (Fig. 4.13b). However, the influence of stem material on the magnitude of the differentiation stimulus can be established for the titanium and CoCrMo[2]. At all points, except point 1, the magnitude of the differentiation stimulus is higher for the CoCrMo stem over the initial 3 months. Thereafter, the homeostatic levels reached at each point for both stems are of similar magnitudes, see Fig. 5.1. This is an important observation if we were to consider cell death in the

[2]These stems were chosen as the location of the differentiating tissue is similar.

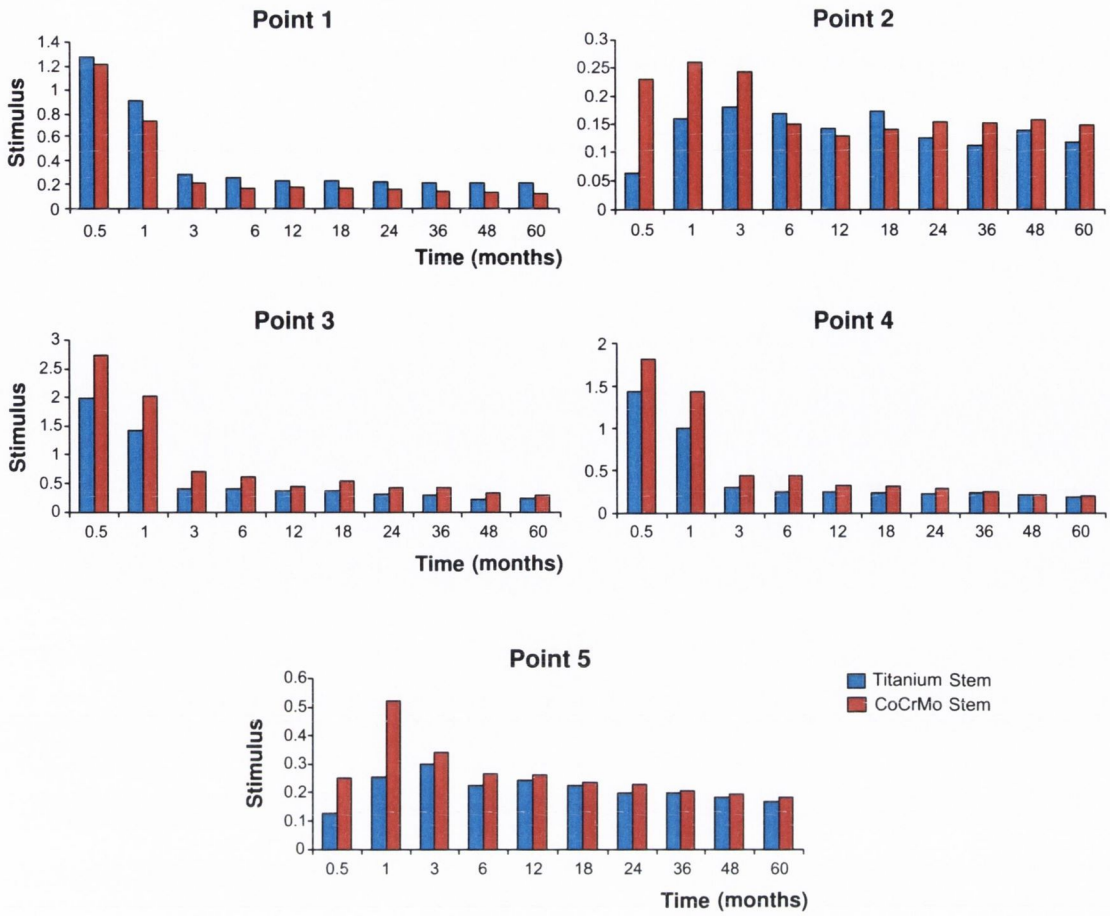

Figure 5.1. Comparison of differentiation stimulus between the titanium and CoCrMo stems for points 1-5 (see Figs. 4.13 and 4.16 for location of points). Note stimulus, $S = \frac{\gamma}{a} + \frac{\nu}{b}$.

model as elevated stimulus (strain) levels promote cell death leading to degradation of the tissue. This could be achieved using the method developed by Kelly and Prendergast (2005) where cell mitosis and apoptosis is modeled as a function of the stimulus

$$\frac{\mathrm{d}n^i}{\mathrm{d}t} = D^i \nabla^2 n^i + P^i(S) n^i - K(S) n^i \tag{5.1}$$

where the number of cells of phenotype i is denoted as n^i, D^i is the diffusion coefficient for phenotype i, and $P^i(S)$ and $K^i(S)$ is the cell proliferation and death rate respectively as a function of the stimulus. The inclusion of cell mitosis and apoptosis may lead to persistence of fibrous tissue formation surrounding the distal tip of the CoCrMo stem and the proximal medial interface of the iso-elastic stem.

Furthermore, similar amounts and locations of interfacial bone resorption in both the 8 node remodelling only (linear elastic) and 20 node combined remodelling-

differentiation (poroelastic) models are observed, see Fig. 5.2. There is a possibility that the stimulus levels for bone tissue immediately adjacent to areas of complete bone resorption (remodelling only model) and corresponding areas of differentiating tissue (combined remodelling-differentiation model) differ slightly due to the relative differences in tissue stiffness i.e. stiffness predicted at $\rho = \rho_{min}$ versus the stiffness predicted for each tissue type. However, no quantitative comparison was performed. Following resorption at the stem-bone interface, it is assumed that a homogeneous distribution of mesenchymal cells is fills the 'gap'[3].

[3]Gap not physically modeled, but assumed by a minimum density of 0.01 g/cm^3.

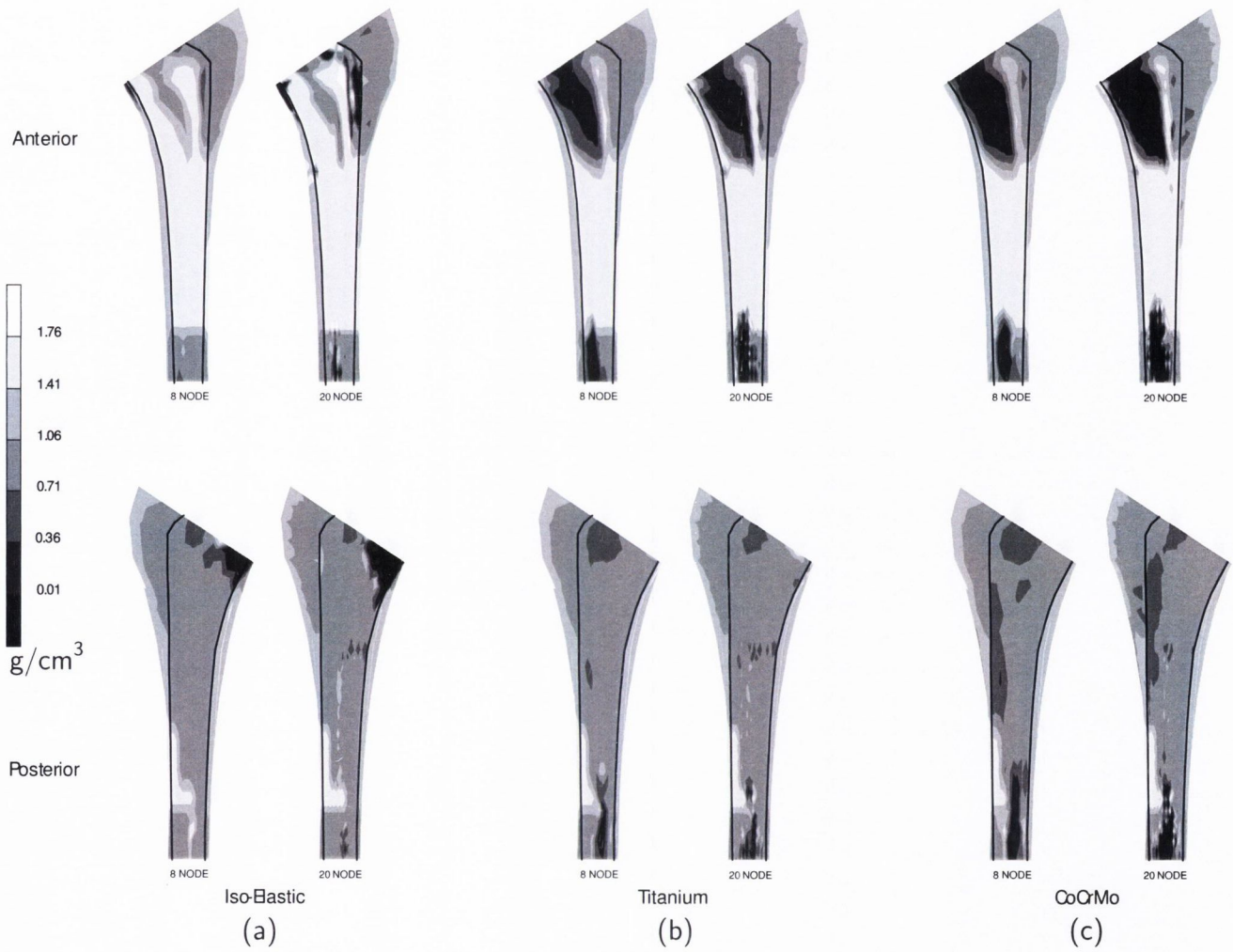

Figure 5.2. Comparison of predicted interfacial density changes for the 8 node linear elastic model against the 20 node biphasic model for the (a) iso-elastic, (b) titanium, and (c) CoCrMo stems.

5.3.3 Comparison of results with other numerical simulations

A plethora of simulations of adaptive bone remodelling following the introduction of a prosthesis have been performed with the influence of numerous variables investigated: stem material properties (Huiskes et al., 1989; Weinans et al., 1992; Huiskes et al., 1992), placing of the hydroxyapatite coating (Huiskes and van Rietbergen, 1995), fit and bonding characteristics (Weinans et al., 1994). Comparisons of the bone remodelling results obtained in this study can be compared to a number of other studies of bone remodelling surrounding cementless femoral components, namely those by Weinans et al. (1992) and Huiskes et al. (1992).

Weinans et al. (1992) applied a similar remodelling algorithm to a two dimensional finite element model of both cemented and uncemented femoral prostheses. The material properties used for the uncemented models were the same as those used in this thesis. The CoCrMo and titanium stems predicted a 76% and 54% reduction in proximal bone density respectively, while little bone loss (7%) was predicted for the iso-elastic stem, see Fig. 2.19. This corresponds to the values predicted in this study of a 59%, 43%, and 19% drop in density for the CoCrMo, titanium, and iso-elastic stem, where the percentages are calculated for combined posterior and anterior Gruen zones. While the values do not match those predicted by Weinans et al. (1992), they do follow the same trend i.e. proximal bone loss increases as the stem stiffness increases. Furthermore, an analysis on the interfacial stresses by Weinans et al. (1992) revealed an increase in proximal interface stresses for the iso-elastic stem relative to the stiffer stems, while interface stresses peak distally for the titanium and CoCrMo stems. This corresponds to the location of the predicted interfacial bone loss for the iso-elastic stem reported in this thesis, see Fig. 4.10.

Huiskes et al. (1992), again using similar theory, studied the effects of stem material on bone remodelling around a uncemented stem. However, this time a realistic three dimensional model of the human femur was used. The effects of bone stiffness and bone reactivity were also investigated. The distribution of the initial stimulus ($S - S_{\text{ref}}$) showed that stress shielding was more prominent in the stiffer

titanium stem, and a positive stimulus (indicating a possible increase in density) was found near the distal tip of the titanium stem and at the proximal medial interface of the iso-elastic stem. This was also found in the predictions of the bulk strain energy density per unit mass presented in chapter 4.2.1.1, see Fig.4.1a,b. Net bone loss of 68%, 35%, 3% and a gain of 4% was predicted medially from proximal to distal, with 35% bone loss found in the greater trochanter, see Fig. 5.3a. This compares to bone loss, in similar zones, of 43%, 5%, and 2% medially proximal to distal, with a 10% drop in bone mass found in the greater trochanter, see Fig. 5.3b. As with the comparison to Weinans et al. (1992), the trend in the predicted percentage changes in bone mass are similar, rather than the actual values. One difference should be noted; while an increase in density is predicted in zone 4 due to high stresses by Huiskes et al. (1992), a loss in medial distal density is predicted due to damage accumulation in the model presented in this thesis. The influence of reducing the stem stiffness is the same in both approaches; a reduction in the amount of bone loss, see Fig. 5.3. Furthermore the influence of reducing the lazy zone to s=0.35 is corroborated. In both approaches the amount of bone loss increases if s is decreased from 0.75 to 0.35, see Fig. 5.3. Using a value of $s = 0.75$ has been used by several other researchers and found to give realistic predictions (Weinans, 1991; Huiskes et al., 1992; Huiskes and van Rietbergen, 1995; Kerner et al., 1999; Gupta et al., 2006). The influence of stem stiffness on interface stresses was also investigated by Huiskes et al. (1992) for four models of stem elastic moduli: 20, 50, 80, and 110 GPa. It was predicted that as stem stiffness reduces, proximal interface stresses increases (see Fig. 2.20) which further corroborates our results of interfacial bone resorption. Huiskes et al. (1992) performed an additional simulation of the effect of the initial bone material properties on remodelling, see Fig. 5.3a. It was found that increasing the bone stiffness reduced the amount of bone resorption, suggesting that the implant stiffness relative to the bone stiffness, rather than implant stiffness alone, is an important causative factor for bone remodelling.

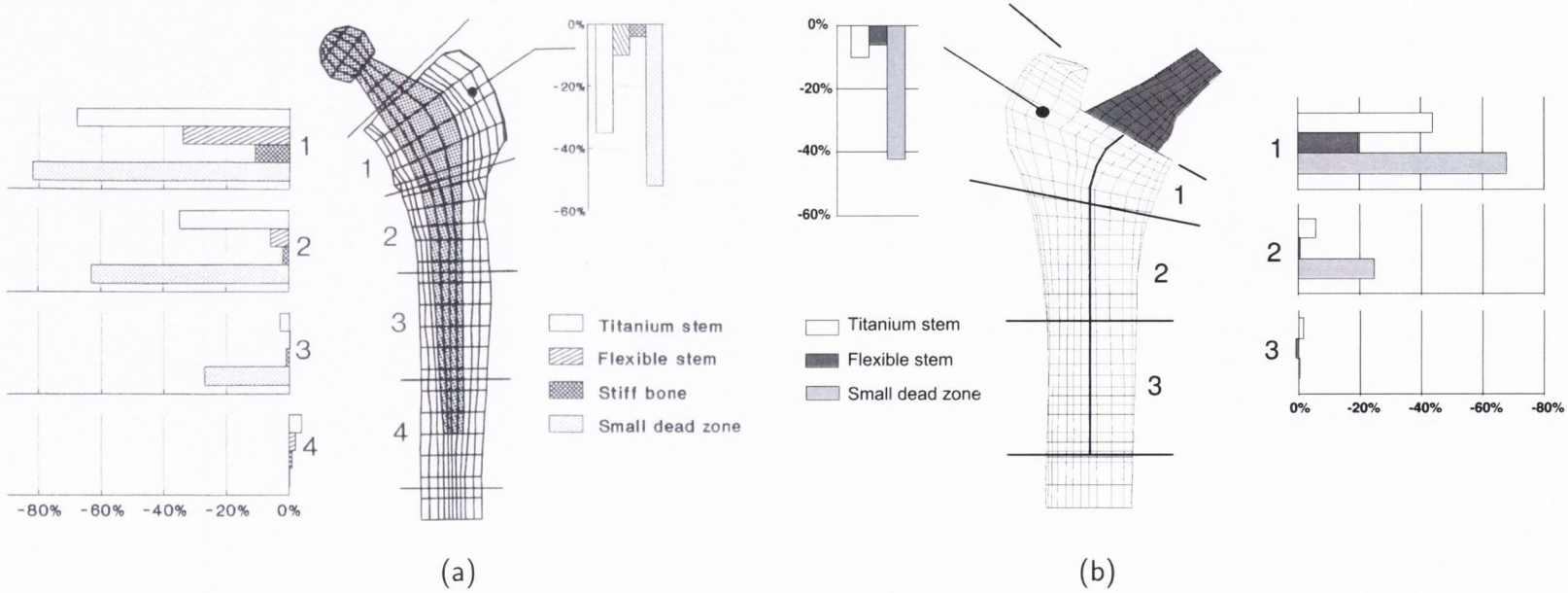

Figure 5.3. Comparison of simulated density loss for a titanium stem, flexible stem, and a small lazy zone (i.e. $s = 0.35$) as predicted in (a) Huiskes et al. (1992) and (b) this thesis. It is predicted, in both models, that reducing the stem stiffness reduces the amount of bone resorption, while reducing the width of the lazy zone increases the amount of bone resorption.

The importance of bone material properties on the performance of hip prostheses has been previously investigated by Taylor et al. (1995) and Wong et al. (2005). Taylor et al. (1995) showed that a reduction in cancellous bone modulus increases the principal interface strains by approximately 200%. Following this Wong et al. (2005) have shown that reductions in the cortical bone modulus also affect the interface strains. They showed that reducing the Young's modulius of the cortical and cancellous bone causes micromotions and interfacial strains to increase reducing the area of potential bone ingrowth. Clinically, the influence of bone mineral content on bone remodelling has been shown to have a strong correlation (Sychterz and Engh, 1996). It was shown that femurs with a relatively low bone mineral content experienced greater bone loss than those with high bone mineral content.

To the author's knowledge no peri-prosthetic tissue differentiation simulations in realistic three dimensional models of uncemented hip prostheses have been carried out previously. Hence, direct comparisons cannot be made to other models. However, a comparison against the simplified model used by Huiskes et al. (1997) reveals a similar trend in the evolution of interfacial fibrous tissue differentiation. As an effect of the tissue increasing in stiffness and reducing in permeability the tissue strains and fluid velocity reduce, and hence so does the stimulus. As the stimulus progressively reduces all elements eventually turn to bone, with fibrocartilage as an intermediate stage. This can be seen in Fig. 2.21c where the phase diagram shows all elements have turned to bone after the 15^{th} iteration (Huiskes et al., 1997), and in Figs. 4.11, 4.13, and 4.16 where the predicted stimulus level, for all three stems, falls to a level conducive to bone formation $0.01 < S < 1$ by the third month.

5.3.4 Comparison of results with clinical findings

The influence of stem stiffness on bone remodelling have been studied in human (Engh et al., 1987; Engh and Bobyn, 1988; Engh et al., 1999), dog (Bobyn et al., 1992; Harvey et al., 1999), and goat (Buma et al., 1997) models, all of which have shown that greater bone loss occurs with stiffer stems compared to more flexible stems. Engh et al. (1999) performed a postmortem comparison of bilateral femoral

implants of different stiffness in two patients. The femur implanted with the stiffer stem had between 65% (case 1) and 78% (case 2) less bone mass around the proximal third of the stem than the femur implanted with the more flexible stem, see Fig. 5.4a. Furthermore, it was shown that the flexible stem demonstrated radiographic signs (a radiolucent gap) of failed ingrowth proximally, see Fig. 5.4b.

Similar results were found in dogs (Harvey et al., 1999) and goats (Buma et al., 1997) implanted with prostheses of varying stiffness. Namely, the use of more flexible stems resulted in a reduction of stress shielding and an increase in radiopaque line formation. Histological analysis revealed these lines to be indicative of fibrous tissue formation. Furthermore, a finite element analysis of the animal model (Buma et al., 1997) revealed that the location of fibrous tissue formation coincided with the locations of the highest interface stresses. It has also been shown that differentiation of the peri-prosthetic gap tissue, in the femoral condyles of dogs, is a functions of the magnitude of micrmotion at the stem-bone interface (Søballe et al., 1992a,b), where excessive micromotions inhibit bone formation and lead to maintenance of a fibrous tissue.

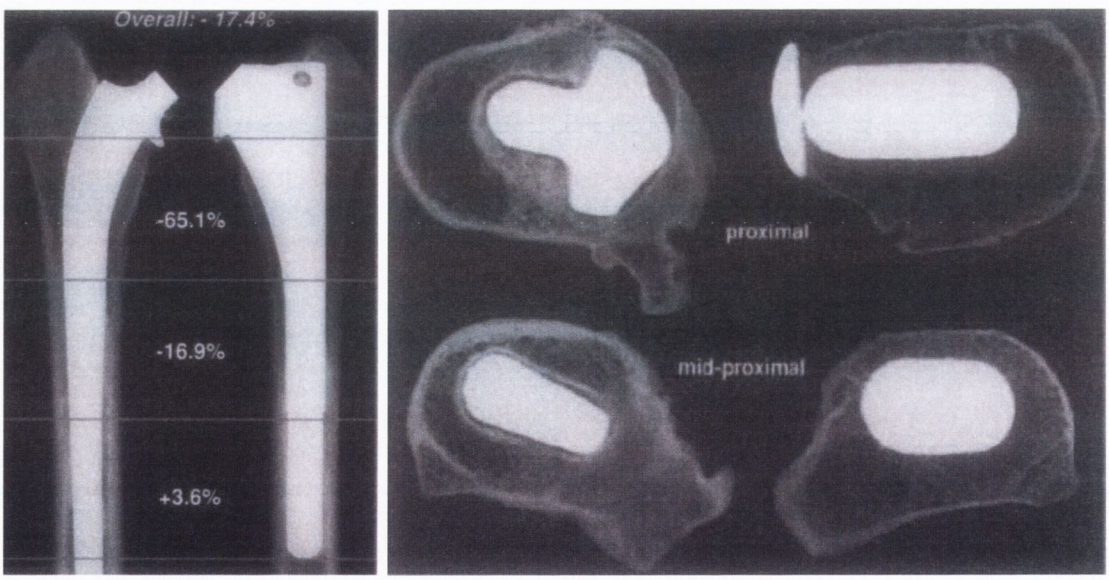

(a) (b)

Figure 5.4. Radiographs of (a) the percentage difference in bone mineral content between the femur implanted with the stiffer stem (right) and more flexible stem (left), and (b) proximal cross sections of the femur implanted with the stiffer stem (right) and more flexible stem showing radiolucent gaps(left). Taken from Engh et al. (1999).

The predicted changes in bone mass over time shown in Figs. 4.3 and 4.9 is corroborated by the observations of D'Antonio et al. (1992), Jaffe and Scott (1996), and Sluimer et al. (2006); these three groups of researchers found that most of the changes seen in the bone radiographically occur over the first post-operative year with little to no changes observed after the second year. With regard to tissue differentiation at the bone-implant interface a similar trend is predicted (see Figs. 4.11 to 4.18) to that observed by de Waal Malefijt (1988) in the histological analysis of the bone-implant interface of cementless prostheses implanted in goats. The cell rich hematoma which filled the gaps between the stem and implant was found to promote fibrous tissue formation after two weeks. Over a course of five weeks woven bone was progressively deposited at the bone side, and by the sixth week the gap was almost completely filled with new woven bone with a thin fibrous tissue layer persisting between the implant and bone.

The aforementioned clinical findings of the influence of stem stiffness on periprosthetic bone adaptations substantiate the predicted results presented in chapter 4. Namely that the use flexible stem materials reduce the degree of stress shielding, while also increasing the likelihood of failed ingrowth into the proximal stem coating as a result of increased interfacial stresses inducing fibrous tissue formation. Furthermore, the predicted evolution of tissue differentiation, subsequent to interfacial resorption, follows similar trends to those observed clinically; i.e. fibrous tissue, to cartilage, to bone.

5.4 Potential use as a pre-clinical testing tool

The long-term survival of a femoral prosthesis can, in part, be determined by the design of the prosthesis, as it is the influence of these design characteristics which determine the adaptations of the surrounding tissues, particulary in the case of uncemented stems. By incorporating mechanoregualtion algorithms of *both* bone remodelling and tissue differentiation a significant improvement in potential for the pre-clinical testing of hip prostheses has been achieved. These algorithms could be used to design an optimal stem stiffness from the point of view of minimizing adverse

peri-prosthetic tissue reactions. Furthermore, these algorithms could be applied on a patient-specific basis whereby each model is tailored to individual patients to account for bone quality and size, activity level, weight and age. Validations of such models may be achieved through retrospective studies, as shown by Lennon et al. (2006), where the predictions of cement creep and fatigue in 16 patient specific finite element models correctly ranked 5 out of the 6 clinically observed.

5.5 Summary and perspectives

The motivation for this thesis was to develop further mechanoregulation algorithms capable of simulating both bulk *and* interfacial peri-prosthetic bone adaptations to better predict the long-term performance of femoral hip prostheses. Furthermore, such simulations could be used in pre-clinical testing as part of the design process.

In a comparative simulation of three stem materials it was shown that the degree and location of interfacial damage accumulation and subsequent bone resorption is dependent on the stem stiffness. Flexible stems increase proximal interfacial bone resorption and the likelihood of failed ingrowth, while stiffer stems suffer from interfacial resorption at the distal tip of the prosthesis. Furthermore, the influence of stem stiffness on proximal stress shielding was successfully predicted. Hence, considering both the predicted bulk and interfacial adaptations the titanium stem is considered to be the optimal stem material as it reduces both the proximal interfacial resorption and stress shielding predicted to occur for the iso-elastic and CoCrMo stems respectively.

The integration of a simplified tissue differentiation algorithm further enhances the predictive power of the simulation. Refilling of the resorbed bone with new bone through both endochondral and intramembranous ossification is predicted to occur in all three stems, with the exception of the iso-elastic stem where some cartilaginous tissue is predicted to persist. Clinically, a fibrous tissue interface has been found to persist where flexible stem materials have been used. The model will have to be further developed to include cell proliferation and apoptosis to better simulate the biological process of tissue differentiation.

Chapter 6

Conclusions

Contents

6.1 Main conclusion

1. A mechanoregulation algorithm based on both strain and damage stimulated remodelling can realistically predict both bulk and interfacial peri-prosthetic bone adaptations under idealized bonding conditions.

2. It is possible to simulate both bone remodelling and tissue differentiation simultaneously. The combined algorithm has potential in a patient-specific pre-clinical testing tool; however difficulty exists because parameters such as cell mitosis and apoptosis may be genetically determined.

6.1.1 Conclusions relating to bone remodelling

- Stiff stems invoke higher amounts of proximal bulk bone loss as of a result of stress shielding.
- A possible failed ingrowth scenario is predicted for the flexible iso-elastic stem where high proximal interfacial stresses cause damage accumulation leading to interfacial bone resorption which is not fully repaired but persists as fibrous tissue.
- The high distal load transfer of stiff implants can lead to interfacial resorption of the bone surrounding the distal tip which, in conjunction with proximal bone loss due to stress shielding, may lead to implant loosening and a failure scenario analogous to failure mode II: medial stem pivot Gruen et al. (1979).

6.1.2 Conclusions relating to combined remodelling-tissue differentiation

- Interfacial fibrous tissue and cartilage formation predicted at the interface of all three stems eventually forms bone through endochondral ossification.
- Intramembranous ossification forming mature bone is predicted at the distal tip of both the titanium and CoCrMo stems following bone resorption due to damage accumulation.

6.2 Future work

The following recommendations are suggested as possible future improvements on the mechanoregulation models presented in this thesis:

- Experimental verification by applying the algorithm to patient specific models. This may also yield more characteristic strain and damage remodelling rates.
- Incorporating external remodelling whereby the geometry as well as the density can change as a function of the applied load.

- Realistically simulating the process of osseointegration by modeling the initial stem/bone interface as press-fit, after which the degree of bonding, through osseointegration, is a function of the relative stem/bone micromotion.

- Inclusion of the effect of mechanical stimuli on cell mitosis and apoptosis. This may yield more realistic tissue phenotype formation at highly stressed interfaces.

Bibliography

Altman, G., Horan, R., Martin, I., Farhadi, J., Stark, P., Volloch, V., Vunjak-Novakovic, G., Richmond, J., and Kaplan, D. L., 2002. Cell differentiation by mechanical stress. *FASEB J*, **16**:270–272.

Ando, M., Imura, S., Omori, H., Okumura, Y., Bo, A., and Baba, H., 1999. Nonlinear three-dimensional finite element analysis of newly designed cementless total hip stems. *Artificial Organs*, **23**(4):339–346.

Andreykiv, A., Prendergast, P. J., van Keulen, F., Swieszkowski, W., and Rozing, P. M., 2005. Bone ingrowth simulation for a concept glenoid component design. *Journal of Biomechanics*, **38**:1023–1033.

Angele, P., Yoo, J. U., Mansour, J., Jepsen, K. J., Nerlich, M., and Johnstone, B., 2003. Cyclic hydrostatic pressure enhances the chondrogenic phenotype of human mesenchymal progenitor cells differentiated in vitro. *Journal of Orthopaedic Research*, **21**(3):451–457.

Barry, F. P., 2003. Biology and clinical applications of mesenchymal stem cells. *Birth Defects Research*, **69**:250–256.

Beaupré, G. S., Orr, T. E., and Carter, D. R., 1990a. An approach for time-dependent bone modeling and remodeling - application: A preliminary remodeling simulation. *Journal of Orthopaedic Research*, **8**(5):662–670.

Beaupré, G. S., Orr, T. E., and Carter, D. R., 1990b. An approach for time-dependent bone modeling and remodeling - theoretical development. *Journal of Orthopaedic Research*, **8**(5):651–661.

Bentolila, V., Boyce, T. M., Fyhrie, D. P., Drumb, R., Skerry, T. M., and Schaffler, M. B., 1998. Intracortical remodeling in adult rat long bones after fatigue loading. *Bone*, **23**(3):275–281.

Bergmann, G. and Duda, G., 1998. Development of the loading configuration: report for contract SMT4-CT96-2076 preclinical testing of cemented hip replacement implants: pre-normative research for a european standard. Technical report, Nigmegen, the Netherlands.

Bergmann, G., Graichen, F., and Rohlmann, A., 1993. Hip joint loading during walking and running measured in two patients. *Journal of Biomechanics*, **26**(8):969–990.

Blenman, P. R., Carter, D., and Beaupré, G. S., 1989. Role of mechanical loading in the progressive ossification of a fracture callus. *Journal of Orthopaedic Research*, **7**:398–407.

Bobyn, J. D., Mortimer, E. S., Glassman, A. H., Engh, C. A., Miller, J. E., and Brooks, C. E., 1992. Producing and avoiding stress shielding. laboratory and clinical observations of noncemented total hip arthroplasty. *Clinical Orthopaedics and Related Research*, **274**:79–96.

Buma, P., van Loon, P. J. M., Versleyen, H., Weinans, H., Slooff, T. J. J. H., de Groot, K., and Huiskes, R., 1997. Histological and biomechanical analysis of bone and interface reactions around hydroxyapatite-coated intramedullary implants of different stiffness: a pilot study. *Biomaterials*, **18**:1251–1260.

Burger, E. H., 2001. Experiments on cell mechanosensitivity: Bone cells as engineers. In S. C. Cowin, ed., *Bone Mechanics Handbook.*, chapter 28, pages 1–16. CRC Press, Boca Raton, FL.

Burger, E. H. and Klein-Neulend, 1999. Mechanotransduction in bone - role of the lacuno-canalicular network. *FASEB J*, **13**:S101–S112.

Burr, D. B., 1993. Remodeling and the repair of fatigue damage. *Calcified Tissue International*, **53**:S75–S80.

Burr, D. B., Martin, R. B., Schaffler, M. B., and Radin, E. L., 1985. Bone remodelling in response to in vivo fatigie microdamage. *Journal of Biomechanics*, **18**(3):189–200.

Capello, W. N., D'Antonio, J. A., Feinberg, J. R., and Manley, M. T., 1997. Hydroxyapatite-coated total hip femoral components in patients less than fifty years old. *The Journal of Bone and Joint Surgery*, **79**(A7):1023–1029.

Caplan, A. I. and Bruder, S. P., 2001. Mesenchymal stem cells: building blocks for molecular medicine in the 21st century. *Trends in Molecular Medicine*, **7**(6):259–264.

Carter, D. R., 1984. Mechanical loading histories and cortical bone remodeling. *Calcified Tissue International*, **36**:S19–24.

Carter, D. R., Blenman, P. R., and Beaupré, G. S., 1988. Correlations between mechanical stress history and tissue differentiation in initial fracture healing. *Journal of Orthopaedic Research*, **6**(5):736–748.

Carter, D. R., Bouxsein, M. L., and Marcus, R., 1992. New approaches for interpreting projected bone densitometry data. *Journal of Bone and Mineral Research*, **7**(2):137–145.

Carter, D. R., Fyhrie, D. P., and Whelan, R. T., 1987. Trabecular bone density and loading history: regulation of connective tissue biology by mechanical energy. *Journal of Biomechanics*, **20**:785–794.

Carter, D. R. and Hayes, W., 1977. The compressive behaviour of bone as a two-phase porous structure. *The Journal of Bone and Joint Surgery*, **59**(A7):954–962.

Carter, D. R., Hayes, W., and Schurman, D. J., 1976. Fatigue life of compact bone-ii: Effects of microstructure and density. *Journal of Biomechanics*, **9**(4):211–218.

Carter, D. R., Orr, T. E., and Fyhrie, D. P., 1989. Relationships between loading history and femoral cancellous bone architecture. *Journal of Biomechanics*, **22**(3):231–244.

Carter, D. R. and Wong, M., 1988. The role of mechanical loading histories in the development of diarthroidal joints. *Journal of Orthopaedic Research*, **6**:804–816.

Charnely, J., 1960. Anchorage of the femoral head prosthesis to the shaft of the femur. *The Journal of Bone and Joint Surgery*, **42**(B):28–30.

Claes, L. E. and Heigele, C. A., 1999. Magnitudes of stress and strain along bony surfaces predict the course and type of fracture healing. *Journal of Biomechanics*, **32**:255–266.

Cowin, S. C., 1991. Candidates for the mechanosensory system in bone. *Journal of Biomechanical Engineering*, **113**:191–197.

Cowin, S. C. and Buskirk, W. C. V., 1979. Surface bone remodeling induced by a medullary pin. *Journal of Biomechanics*, **12**(4):269–276.

Cowin, S. C. and Hegedus, D., 1976. Bone remodelling I: Theory of adaptive elasticity. *Journal of Elasticity*, **6**:313–326.

D'Antonio, J. A., Capello, W. N., Crothers, O. D., Jaffe, W. J., and Manley, M. T., 1992. Early clinical experience with hydroxyapatite-coated femoral implants. *The Journal of Bone and Joint Surgery*, **74**(A7):995–1008.

D'Antonio, J. A., Capello, W. N., and Manley, M. T., 1996. Remodeling of bone around hydroxyapatite-coated femoral stems. *The Journal of Bone and Joint Surgery*, **78**(A8):1226–1234.

de Waal Malefijt, J., 1988. *Early features of the bone-implant interface in hip arthroplasty.*. Ph.D. thesis, University of Nijmegen.

Ducheyne, P., Hench, L. L., II, A. K., Martens, M., Bursens, A., and Mulier, J. C., 1980. Effect of hydroxyapatite impregnation on skeletal bonding of porous coated implants. *Journal of Biomedical Materials Research*, **14**:225–237.

Eldridge, J. D. I. and Learmonth, I. D., 1999. Component bone interface in cementless hip arthroplasty. In I. D. Learmonth, ed., *Interfaces in Total Hip Arthroplasty.*, chapter 1, pages 71–80. Springer, London.

Engh, C. A. and Bobyn, J. D., 1988. The influence of stem size and extent of porous coating on femoral bone resorption after primary cementless hip arthroplasty. *Clinical Orthopaedics and Related Research*, **231**:7–28.

Engh, C. A., Bobyn, J. D., and Glassman, A. H., 1987. Porous-coated hip replacement. the factors governing bone ingrowth, stress shielding and clinical results. *The Journal of Bone and Joint Surgery*, **69**(B1):45–55.

Engh, C. A., Sychterz, C., and Engh, C., 1999. Factors affecting femoral bone remodeling after cementless total hip arthroplasty. *The Journal of Arthroplasty*, **14**(5):637–644.

ESRI, 2006. Number of arthroplasty of hip procedures recorded 2000-2005. Technical report, The Economic and Social Research Institute. Personal communication.

Frost, H. M., 1964. *The Laws of Bone Structure*. C. C. Thomas, Springfield, Illinois.

Fyhrie, D. P. and Carter, D. R., 1986. A unifying principle relating stress to trabecular bone morphology. *Journal of Orthopaedic Research*, **4**(3):304–317.

Fyhrie, D. P. and Carter, D. R., 1990. Femoral head apparent density distribution predicted from bone stresses. *Journal of Biomechanics*, **23**(1):1–10.

Gardner, T. N., Mishra, S., and Marks, L., 2004. The role of osteogenic index, octahedral shear stress and dilatational stress in the ossification of a fracture callus. *Medical Engineering and Physics*, **26**:493–501.

Geris, L., van Oosterwyck, H., Sloten, J. V., Duyck, J., and Naert, I., 2003. Assessment of mechanobiological models for the numerical simulation of tissue differentiation around immediately loaded implants. *Computer Methods in Biomechanics and Biomedical Engineering*, **6**(5/6):277–288.

Goldsmith, A. A. J., Dowson, D., Worblewski, B. M., Fleming, A. P., Lane, J. M., Stone, H. M., and Walker, R., 2001. Comparative study of the activity of total hip arthroplasty patients and normal subjects. *Journal of Arthroplasty*, **16**(5):613–619.

Gruen, T. A., McNeice, G. M., and Amstutz, H. C., 1979. "modes of failure" of cemented stem-type femoral components. *Clinical Orthopaedics and Related Research*, **141**:17–27.

Gupta, S., New, A. M. R., and Taylor, M., 2006. Bone remodelling inside a cemented resurfaced femoral head. *Clinical Biomechanics*, **21**:594–602.

Harvey, E. J., Bobyn, J. D., Tanzer, M., Stackpool, G. J., Krygier, J. J., and Hacking, S. A., 1999. Effect of flexibility of the femoral stem on bone-remodeling and fixation of the stem in a canine total hip arthroplasty model without cement. *The Journal of Bone and Joint Surgery*, **81**(A):93–107.

Heller, M. O., Bergmann, G., Kassi, J. P., Claes, L., Haas, N. P., and Duda, G. N., 2005. Determination of muscle loading at the hip joint for use in pre-clinical testing. *Journal of Biomechanics*, **38**:1155–1163.

Huiskes, R., 1993. Failed innovation in total hip replacement. diagnosis and proposals for a cure. *Acta Orthopaedica Scandinavica*, **64**:699–715.

Huiskes, R., van Driel, W. D., Prendergast, P. J., and Søballe, K., 1997. A biomechanical regulatory model for periprosthetic fibrous-tissue differentiation. *Journal of Materials Science: Materials in Medicine*, **8**:785–788.

Huiskes, R. and van Rietbergen, B., 1995. Preclinical testing of total hip stems. the effects of coating placememt. *Clinical Orthopaedics and Related Research*, **319**:64–76.

Huiskes, R., Weinans, H., and Dalstra, M., 1989. Adaptive bone remodeling and biomechanical design considerations for noncemented total hip arthroplasty. *Orthopedics*, **12**(9):1255–1267.

Huiskes, R., Weinans, H., Grootenboer, H. J., Dalstra, M., Fudala, B., and Slooff, T. J., 1987. Adaptive bone-remodeling theory applied to prosthetic design analysis. *Journal of Biomechanics*, **20**:1135–1150.

Huiskes, R., Weinans, H., and van Rietbergen, B., 1992. The relationship between stress shielding and bone resorption around total hip stems and the effects of flexible materials. *Clinical Orthopaedics*, **274**:124–134.

Isaksson, H., Wilson, W., van Donkelaar, C. C., Huiskes, R., and Ito, K., 2006. Comparison of biophysical stimuli for mechano-regulation of tissue differentiation during fracture healing. *Journal of Biomechanics*, **39**:1507–1516.

Islam, O., Soboleski, D., Symons, S., Davidson, L. K., Ashworth, M. A., and Babyn, P., 2000. Development and duration of radiographic signs of bone healing in children. *American Journal of Roentgenology*, **175**(1):75–78.

Iwaki, A., Jingushi, S., Oda, Y., Izumi, T., Shida, J. I., Tsuneyoshi, M., and Sugioka, Y., 1997. Localization and quantification of proliferating cells during rat fracture repair: detection of proliferating cell nuclear antigen by immunohistochemistry. *Journal of Bone and Mineral Research*, **12**(1):96–102.

Jaffe, W. L. and Scott, D. F., 1996. Total hip arthroplasty with hydroxyapatite-coated prostheses. *The Journal of Bone and Joint Surgery*, **78**(A12):1918–1934.

Jakim, I., Barlin, C., and Sweet, M. B., 1998. Rm isoelastic total hip arthroplasty. a review of 34 cases. *Journal of Arthroplasty*, **3**(3):191–199.

Jee, W. S. S., 2001. Integrated bone tissue physiology: Anatomy and physiology. In S. C. Cowin, ed., *Bone Mechanics Handbook.*, chapter 1, pages 1–68. CRC Press, Boca Raton, FL.

Kärrholm, J., Malchau, H., Snorrason, F., and Herberts, P., 1994. Micromotion of femoral stems in total hip arthroplasty. *The Journal of Bone and Joint Surgery*, **76**(A11):1692–1705.

Kelly, D. J. and Prendergast, P. J., 2005. Mechano-regulation of stem cell differentiation and tissue regeneration in osteochondral defects. *Journal of Biomechanics*, **38**:1413–1422.

Kelly, D. J. and Prendergast, P. J., 2006. Prediction of the optimal mechanical properites for a scaffold used in osteochondral defect repair. *Tissue Engineering*, **12**(9):2509–2519.

Kerner, J., Huiskes, R., van Lenthe, G. H., Weinans, H., van Rietbergen, B., Engh, C. A., and Amis, A. A., 1999. Correlations between pre-operative periprosthetic bone density and post-operative bone loss in tha can be explained by strain-adaptive remodelling. *Journal of Biomechanics*, **32**:695–703.

Klein-Nulend, J., der Plas, A. V., Semeins, C. M., Ajubi, N. E., Frangos, J. A., Nijweide, P. J., and Burger, E. H., 1995. Sensitivity of osteocytes to biomechanical stress in vitro. *FASEB J*, **9**:441–445.

Knippenberg, M., Helder, M. N., Doulabi, B. Z., Semeins, C. M., Wuisman, P. I., and Klein-Nulend, J., 2005. Adipose tissue-derived mesenchymal stem cells acquire bone cell-like responsiveness to fluid shear stress on osteogenic stimulation. *Tissue Engineering*, **11**(11/12):1780–1788.

Lacroix, D. and Prendergast, P. J., 2002a. A mechano-regulation model for tissue differentiation during fracture healing: analysis of gap size and loading. *Journal of Biomechanics*, **35**:1163–1171.

Lacroix, D. and Prendergast, P. J., 2002b. Three-dimensional simulation of fracture repair in the human tibia. *Computer Methods in Biomechanics and Biomedical Engineering*, **5**(5):369–376.

Lacroix, D., Prendergast, P. J., and Marsh, D., 2002. Biomechanical model to simulate tissue differentiation and bone regeneration: application to fracture healing. *Medical and Biological Engineering and Computing*, **40**:14–21.

Lanyon, L. E., 1993. Osteocytes, strain detection, bone modeling and remodeling. *Calcified Tissue International*, **53**:S102–S106.

Lanyon, L. E., Goodship, A. E., Pye, C. J., and MacFie, J. H., 1982. Mechanically adaptive bone remodelling. *Journal of Biomechanics*, **15**(3):141–154.

Learmonth, I. D., Grobler, G. P., Dall, D. M., and Jandera, V., 1995. Loss of bone stock with cementless hip arthroplasty. *The Journal of Arthroplasty*, **10**(3):257–263.

Lee, G. Y., Srivastava, A., D'Lima, D. D., Pulido, P. A., and Colwell, C. W., 2005. Hydroxyapatite-coated femoral stem survivorship at 10 years . *The Journal of Arthroplasty*, **20**(7-S3):57–62.

Lee, T. C., Staines, A., and Taylor, D., 2002. Bone adaptation to load: microdamage as a stimulus for bone remodelling. *Journal of Anatomy*, **201**:437–446.

Lennon, A. B., Britton, J. R., MacNiocaill, R. F., Byrne, D. P., Kenny, P. J., and Prendergast, P. J., 2006. Predicting revision risk for aseptic loosening of femoral components in total hip arthroplasty in individual patients - a finite element study. *Journal of Orthopaedic Research*. Accepted.

Lennon, A. B. and Prendergast, P. J., 2001. Evaluation of cement stresses in finite element analyses of cemented orthopaedic implants. *Journal of Biomechanical Engineering*, **123**:623–628.

Maloney, W. J., Jasty, M., Burke, D. W., O'Connor, D. O., Zalenski, E. B., Bragdon, C., and Harris, W. H., 1989. Biomechanical and histological investigation of cemented total hip arthroplasties. a study of autopsy-retrieved femurs after in vivo cycling. *Clinical Orthopaedics and Related Research*, **249**:129–140.

Mann, K. A., Mocarski, R., Damron, L. A., Allen, M. J., and Ayers, D. C., 2001. Mixed-mode failure response of the cemente-bone interfcae. *Journal of Orthopaedic Research*, **19**(6):1153–1161.

Martin, R. B., 1972. The effects of geometric feedback in the development of osteoporosis. *Journal of Biomechanics*, **5**:447–455.

Martin, R. B., 1984. Porosity and specific surface of bone. In *CRC Critical Reviews in Biomedical Engineering.*, volume 10, pages 179–222. CRC Press, Boca Raton, FL.

Martin, R. B., 1992. A theory of fatigue damage accumulation and repair in cortical bone. *Journal of Orthopaedic Research*, **10**:818–825.

Matsuda, N., Morita, N., Matsuda, K., and Watanabe, M., 1998. Proliferation and differentiation of human osteoblastic cells associated with differential activation of map kinases in response to epidermal growth factor, hypoxia, and mechanical stress *in vitro*. *Biochemical and Biophysical Research Communications*, **249**:350–354.

McMahon, L. A., Reid, A. J., Campbell, V. A., and Prendergast, P. J., 2006. The effect of mechanical strain and the involvement of stretch-activated channels on the chondrogenic differentiation of adult rat mesenchymal stem cells. *Stem Cells*. Submitted.

McNamara, B. P., Taylor, D., and Prendergast, P. J., 1997. Computer prediction of adaptive bone remodelling around noncemented femoral prostheses: the relationship between damage-based and strain-based algorithms. *Medical Engineering and Physics*, **19**:454–463.

McNamara, L. M., 2004. *Biomechanical origins of osteoporosis*. Ph.D. thesis, University of Dublin, Trinity College.

McNamara, L. M. and Prendergast, P. J., 2005. Perforation of cancellous bone trabeculae by damage-stimulated remodelling at resorption pits: a computational analysis. *European Journal of Morphology*, **42**:99–109.

McNamara, L. M. and Prendergast, P. J., 2006. Bone remodelling algorithms incorporating both strain and microdamage stimuli. *Journal of Biomechanics*, ***in press***.

Miyanishi, K., Trindade, M. C., Lindsey, D. P., Beaupré, G. S., Carter, D. R., Goodman, S. B., Schurman, D. J., and Smith, R. L., 2006. Effects of hydrostatic pressure and transforming growth factor-beta 3 on adult human mesenchymal stem cell chondrogenesis *in vitro*. *Tissue Engineering*, **12**(6):1419–1428.

Mori, S. and Burr, D. B., 1993. Increased intracortical remodeling following fatigue damage. *Bone*, **14**(2):103–109.

Morlock, M., Schneider, E., Bluhm, A., Vollmer, M., Bergmann, G., Müller, V., and Honl, M., 2001. Duration and frequency of every day activities in total hip patients. *Journal of Biomechanics*, **34**:873–881.

Mosley, J. R. and Lanyon, L. E., 1998. Strain rate as a controlling influence on adaptive modeling in response to dynamic loading of the ulna in growing male rats. *Bone*, **23**(4):313–318.

Mullender, M. G. and Huiskes, R., 1995. Proposal for the regulatory mechanism of wolff's law. *Journal of Orthopaedic Research*, **13**:503–512.

Mullender, M. G. and Huiskes, R., 1997. Osteocytes and bone lining cells: Which are the best candidates for mechano-sensors in cancellous bone? *Bone*, **20**(6):527–532.

Mullender, M. G., Huiskes, R., and Weinans, H., 1994. A physiological approach to the simulation of bone remodeling as a self-organizatioanl control process. *Journal of Biomechanics*, **27**(1):1389–1394.

Noble, B., 2003. Bone microdamage and cell apoptosis. *European Cells and Materials*, **6**:45–56.

Noble, B. S. and Reeve, J., 2000. Osteocyte function, osteocyte death and bone fracture resistance. *Molecular and Cellular Endocrinology*, **159**:7–13.

O'Connor, J. A., Lanyon, L. E., and MacFie, H., 1982. The influence of strain rate on adaptive bone remodelling. *Journal of Biomechanics*, **15**(10):767–781.

Okano, T., Hagino, H., Otsuka, T., Teshima, R., Tamamoto, K., Hirano, Y., and Nakamura, K., 2002. Measurement of periprosthetic bone mineral density by dual-energy x-ray absorptiometry is useful for estimating fixation between the bone and the prosthesis in an early stage. *The Journal of Arthroplasty*, **17**(1):49–55.

Osteonics, 1995. Surgical Protocol for Osteonics® Hydroxylapatite - Coated Femoral Implants. Technical report, Osteonics Corp.

Pauwels, F., 1980. A new theory concerning the influence of mechanical stimuli on the differentiation of the supporting tissues. In *Biomechanics of the Locomotor Appartus.*, pages 375–407. Springer, Berlin. (Translated from the 1965 German edition by P. Manquet and R. Furlong).

Pérez, M. A. and Prendergast, P. J., 2006. Random-walk models of cell dispersal included in mechano-biological simulations of tissue differentiation. *Journal of Biomechanics*. In press.

Perren, S. M., 1979. Physical and biological aspects of fracture healing with special reference to internal fixation. *Clinical Orthopaedics and Related Research*, **138**:175–195.

Prendergast, P. J., 2001. An analysis of theories in biomechanics. *Engineering Transactions*, **49**(2-3):117–133.

Prendergast, P. J., 2002. Mechanics applied to skeletal ontogeny and phylogeny. *Meccanica*, **37**:317–334.

Prendergast, P. J., 2006. Prosthesis fixation for orthopaedics. In J. G. Webster, ed., *Wiley Encyclopaedia of Medical Devices and Instrumentation.*, pages 192–198. John Wiley and Sons, New Jersey.

Prendergast, P. J. and Huiskes, R., 1995. Mathematical modelling of microdamage in bone remodelling and adaptation. In A. Odgaard and H. Weinans, eds., *Bone Structure and Remodelling.*, pages 213–224. World Scientific, Singapore.

Prendergast, P. J. and Huiskes, R., 1996a. Finite element analysis of fibrous tissue morphogensis - a study of osteogenic index using a biphasic approach. *Mechanics of Composite Materials*, **32**(2):209–218.

Prendergast, P. J. and Huiskes, R., 1996b. Microdamage and osteocyte-lacuna strain in bone: A microstructural finite element analysis. *Journal of Biomechanical Engineering*, **118**:240–224.

Prendergast, P. J., Huiskes, R., and Søballe, K., 1997. Biophysical stimuli on cells during tissue differentiation at implant interfaces. *Journal of Biomechanics*, **30**(6):539–548.

Prendergast, P. J., Scannell, P. T., Britton, J. R., and Lennon, A. B., 2006. The role of computation in identifying failure of biomaterials in implant fixation. In *Proceedings of the 16th European Congress on Fracture*. Alexandroupolis, Greece. CD-Rom.

Prendergast, P. J. and Taylor, D., 1992. Design of intramedullary prostheses to prevent bone loss: predictions based on damage-stimulated remodelling. *Journal of Biomedical Engineering*, **14**:499–506.

Prendergast, P. J. and Taylor, D., 1994. Prediction of bone adaptation using damage accumulation. *Journal of Biomechanics*, **27**(8):1067–1076.

Schaffler, M. B., Choi, K., and Milgrom, C., 1995. Aging and matrix microdamage accumulation in human compact bone. *Bone*, **17**(6):521–525.

Scott, D. F. and Jaffe, W. L., 1996. Host-bone response to porous coated cobalt-chrome and hydroxyapatite-coated titanium femoral components in hip arthroplasty. *The Journal of Arthroplasty*, **11**(4):429–437.

Shapiro, F., Koide, S., and Glimcher, M. J., 1993. Cell origin and differentiation in the repair of full-thickness defects of articular cartilage. *The Journal of Bone and Joint Surgery*, **75**(A4):532–553.

Sinha, R. K., Kim, S.-Y., and Rubash, H. E., 2004. Long-stem cemented calcar replacement arthroplasty for proximal femoral bone loss. *The Journal of Arthroplasty*, **19**(2):141–150.

Sluimer, J. C., Hoefnagels, N. H. M., Emans, P. J., Kuijer, R., and Geesink, R. G. T., 2006. Comparison of two hydroxyapatite-coated femoral stems. clinical, functional, and bone densitometry evaluation of patients randomized to a regular or modified hydroxyapatite-coated stem aimed at proximal fixation. *The Journal of Arthroplasty*, **21**(3):344–352.

Søballe, K., 1993. Hydroxyapatote ceramic coating for bone implant fixation. *Acta Orthopaedica Scandinavia*, **64**((S255)):1–48.

Søballe, K., Hansen, E. S., Rasmussen, H. B., and Bünger, C., 1993. Hydroxyapatite coating converts fibrous tissue to bone around loaded implants. *The Journal of Bone and Joint Surgery*, **75**(B):270–278.

Søballe, K., Hansen, E. S., Rasmussen, H. B., Jørgensen, P. H., and Bünger, C., 1992a. Tissue ingrowth into titanium and hydroxyapatite-coated implants during stable and unstable mechanical conditions. *Journal of Orthopaedic Research*, **10**:285–299.

Søballe, K., Rasmussen, H. B., Hansen, E. S., and Bünger, C., 1992b. Hydroxyapatite coating modifies implant memebrane formation. controlled micromotion studied in dogs. *Acta Orthopaedica Scandinavia*, **63**(2):128–140.

Stolk, J., Verdonschot, N., Murphy, B. P., Prendergast, P. J., and Huiskes, R., 2004. Finite element simulation of anisotropic damage accumulation and creep in acrylic bone cement. *Engineering Fracture Mechanics*, **71**:513–528.

Sychterz, C. J., Claus, A. M., and Engh, C. A., 2002. What have we learned about long-term cementless fixation from autopsy retrievals. *Clinical Orthopaedics and Related Research*, **405**:79–91.

Sychterz, C. J. and Engh, C. A., 1996. The influence of clinical factors on periprosthetic bone remodeling. *Clinical Orthopaedics and Related Research*, **322**:285–292.

Taylor, D., 1997. Bone maintenance and remodeling: A control system based on fatigue damage. *Journal of Orthopaedic Research*, **15**:601–606.

Taylor, D., Hazenberg, J. G., and Lee, T. C., 2003. The cellular transducer in damage-stimulated bone remodelling: a theoretical investigation using fracture mechanics. *Journal of Theoretical Biology*, **225**:65–75.

Taylor, M., Tanner, K. E., Freeman, M. A. R., and Yettram, A. L., 1995. Cancellous bone stresses surrounding the femoral component of a hip prosthesis: an elastic-plastic finite element analysis. *Medical Engineering and Physics*, **17**(7):544–550.

Turner, C. H., Akhter, M. P., Raab, D. M., Kimmel, D. B., and Recker, R. R., 1991. A noninvasive, in vivo model for studying strain adaptive bone modeling. *Bone*, **12**(2):73–79.

Turner, C. H., Forwood, M. R., and Otter, M. W., 1994. Mechanotransduction in bone: do bone cells act as sensors of fluid flow? *FASEB J*, **8**:875–878.

Uhthoff, H. K. and Jaworski, Z. F. G., 1978. Bone loss in response to long-term immobilisation. *The Journal of Bone and Joint Surgery*, **60**(B3):420–429.

van Rietbergen, B., Huiskes, R., Weinanas, H., Sumner, D. R., Turner, T. M., and Galante, J. O., 1993. The mechanism of bone remodelling and resorption around press-fitted tha stems. *Journal of Biomechanics*, **26**(4/5):369–382.

Verborgt, O., Gibson, G. J., and Schaffler, M. B., 2000. Loss of osteocyte integrity in association with microdamage and bone remodeling after fatigue in vivo. *Journal of Bone and Mineral Research*, **15**(1):60–67.

Viceconti, M., Ansaloni, M., and Toni, A., 2003. The muscle standardized femur: a step forward in the replication of numerical studies in biomechanics. *Proceedings of the Institution of Mechanical Engineers, Part H: Journal of Engineering in Medicine*, **27**(2):105–110.

Viceconti, M., Casali, M., Massari, B., Cristofolini, L., Bassini, S., and Toni, A., 1996. The 'standardized femur program' proposal for a reference geometry to be used for the creation of finite element models of the femur. *Journal of Biomechanics*, **29**:1241.

Weinans, H., 1991. *Mechanically induced bone adaptations around orthopaedic implants.*. Ph.D. thesis, University of Nijmegen.

Weinans, H., Huiskes, R., and Grootenboer, H. J., 1992. Effect of material properties of femoral hip components on bone remodelling. *Journal of Orthopaedic Research*, **10**:845–853.

Weinans, H., Huiskes, R., and Grootenboer, H. J., 1994. Effects of fit and bonding characteristics of femoral stems on adaptive bone remodelling. *Journal of Biomechanical Engineering*, **116**:393–400.

Weinans, H., Huiskes, R., van Rietbergen, B., Sumner, D. R., Turner, T. M., and Galante, J. O., 1993. Adaptive bone remodeling around bonded

noncemented total hip arthroplasty: a comparison between animal experiments and computer simulations. *Journal of Orthopaedic Research*, **11**:500–513.

Weinans, H. and Prendergast, P. J., 1996. Tissue adaptation as a dynamical process far from equilibrium. *Bone*, **19**(2):143–149.

Willert, H. G. and Buchhorn, G. H., 1999. Osteointegration of cemented and noncemented implants in artificial hip replacement: long-term findings in man. *Journal of Long-Term Effects of Medical Implants*, **9**(1/2):113–130.

Wong, A. S., New, A. M. R., Isaacs, G., and Taylor, M., 2005. Effects of bone material properties on the initial stability of a cementless hip stem: a finite element study. *Proceedings of the Institution of Mechanical Engineers Part H - Journal of Engineering in Medicine*, **219**(H4):265–275.

Appendix A

Parametric variation study 1: lazy zone width

The width of the lazy zone was chosen based on the predicted percentage change in bone mineral density per Gruen zone over two years, compared to the experimental values of Sluimer et al. (2006), and the clinical observations of D'Antonio et al. (1992) over the same time period. The same stem was used in both the computational and experimental analyses, the Osteonics ® Omnifit ® - HA Hip Stem.

Three lazy zone widths were analysed: s = 0.35, 0.5, and 0.75. A value of s=0.75 was found to closely match both the amount, and time course of remodelling observed experimentally in all Gruen zones, see Figure A.1, and also the observation of D'Antonio et al. (1992) who stated that "..most of the changes in the bone that were seen radiographically, occurred within the first postoperative year, with little change during the second year." In Gruen zones 1, 2, and 6 bone loss is over predicted when s is set at 0.35 and 0.5, whilst the amount of bone loss lies within the standard deviation of the experimental data when s has a value of 0.75. Over prediction of bone loss is found with each value of s in zone 7, with s=0.75 resulting in the closest match. In zones 3 and 5 the bone loss observed experimentally over the first six months, and subsequent increase thereafter, is not predicted. Over prediction of bone loss in zone 3 and no changes in zone 5 were found at s=0.35, the closest match was found when s was set at 0.5 and 0.75.

However, it should be noted that the percentage change in bone mineral density

observed by Sluimer et al. (2006) is presented in g/cm^2, while the predicted percentage change is presented in g/cm^3. Dual-energy x-ray absorptiometry (DXA) scans were used by Sluimer et al. (2006) to determine the bone mineral density (BMD) in each Gruen zone. DXA scans determine the BMD as a function of the bone mineral content (BMC), measured in grammes (g), and projected bone scan area (BA), measured in cm^2

$$BMD[\text{g/cm}^2] = \frac{BMC[\text{g}]}{BA[\text{cm}^2]} \tag{A.1}$$

Hence, *areal* BMD is measured which does not account for the bone size. The influence of bone size is such that BMD in larger subjects tend to be overestimated whilst underestimated in smaller subjects, despite having similar volumetric or apparent BMD (Carter et al., 1992), see Figure A.2.

Considering this, the experimental percentage change in density observed by Sluimer et al. (2006) was considered as a good first approximation against which the predicted percentage change in density could be measured, as it was assumed that the standard deviation from the mean, of 40 patients, accounted for the variability in bone size and activity level. Hence, predictions which lay within the standard deviation were assumed to give a close approximation of the clinical observations.

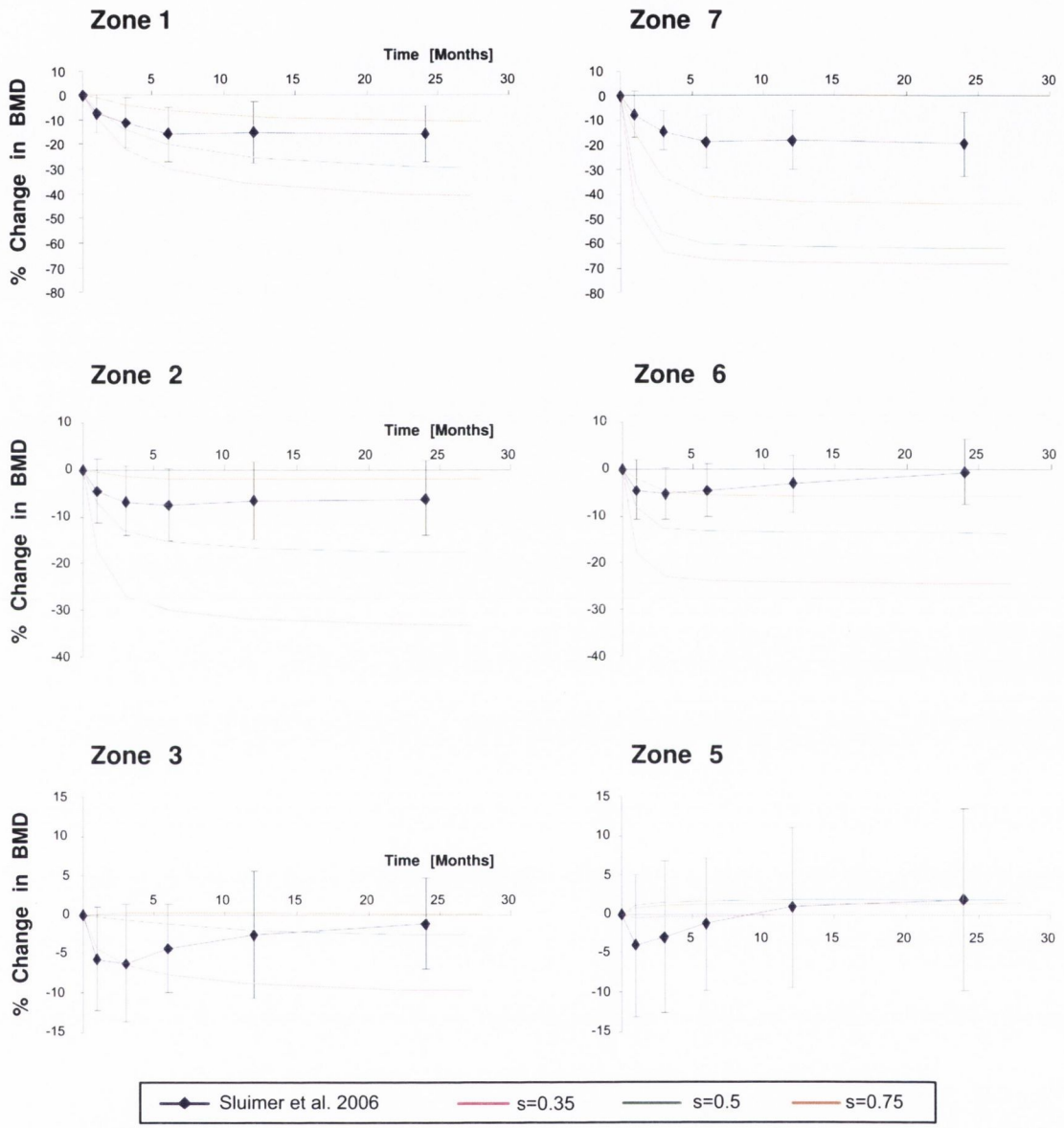

Figure A.1. Comparison of experimental percentage change in BMD over two years (Sluimer et al., 2006) against predicted change for $s = 0.35$, 0.5, and 0.75.

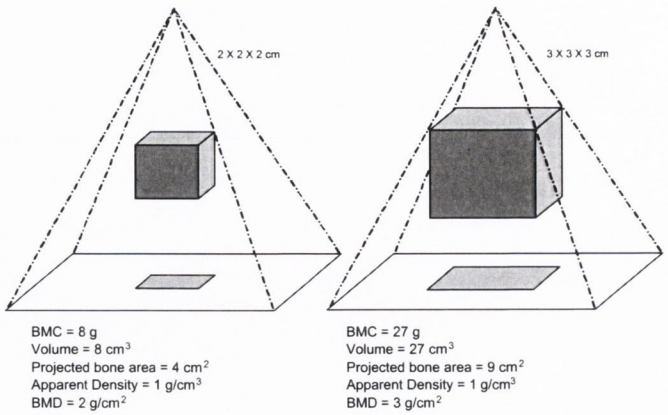

Figure A.2. Relationship between size and BMD. Adapted from Carter et al. (1992).

Table A.1. Predicted percentage change in apparent BMD (g/cm^3) in zones 1-7 over time.

	Zone 1			Zone 2			Zone 3		
Time		s			s			s	
(Months)	0.35	0.5	0.75	0.35	0.5	0.75	0.35	0.5	0.75
0-1	-8.9	-5.5	-1.2	-16.8	-6.9	-0.4	-4.4	-0.2	-0.2
1-3	-21.9	-13.5	-3.6	-27.0	-12.6	-1.2	-6.5	-0.6	-0.3
3-6	-30.3	-20.0	-6.1	-30.1	-15.0	-1.8	-7.7	-1.2	-0.3
6-13	-35.9	-25.6	-8.6	-31.7	-16.4	-1.9	-8.8	-2.0	-0.2
13-28	-40.6	-29.5	-10.5	-33.3	-17.5	-1.9	-9.6	-2.7	-0.1
	Zone 5			Zone 6			Zone 7		
Time		s			s			s	
(Months)	0.35	0.5	0.75	0.35	0.5	0.75	0.35	0.5	0.75
0-1	-0.5	1.0	0.7	-17.7	-8.2	-1.9	-44.4	-35.6	-15.6
1-3	-0.4	1.4	1.0	-22.7	-12.2	-4.5	-63.0	-55.2	-32.5
3-6	-0.2	1.7	1.2	-23.8	-12.9	-5.5	-66.4	-59.8	-40.9
6-13	-0.1	1.8	1.3	-24.2	-13.2	-5.7	-67.5	-61.4	-43.4
13-28	-0.04	1.9	1.4	-24.5	-13.4	-5.7	-67.8	-61.8	-43.8

Table A.2. Mean percentage change in areal BMD (g/cm^2) and standard deviation over time. Adapted from Sluimer et al. (2006).

Time (Months)	Zone 1	(SD)	Zone 2	(SD)	Zone 3	(SD)	Zone 5	(SD)	Zone 6	(SD)	Zone 7	(SD)
1	-7.2	(7.5)	-4.6	(6.8)	-5.7	(6.6)	-4.0	(9.0)	-4.5	(6.3)	-7.6	(9.2)
3	-11.3	(10.1)	-6.7	(7.2)	-6.2	(7.4)	-3.0	(9.7)	-5.1	(5.5)	-14.1	(7.9)
6	-15.7	(10.9)	-7.4	(7.8)	-4.4	(5.6)	-1.3	(8.4)	-4.6	(5.5)	-18.6	(10.9)
12	-14.9	(12.3)	-6.6	(8.1)	-2.6	(8.1)	+0.8	(10.1)	-3.0	(6.0)	-18.0	(11.8)
24	-15.6	(11.5)	-6.1	(7.9)	-1.3	(5.8)	+1.8	(11.6)	-0.5	(6.8)	-19.5	(12.8)

Appendix B

Parametric variation study 2: damage remodelling time constant

The damage time constant, τ_d, was chosen based on the amount of bone remodelling surrounding the distal stem-bone interface of the titanium prosthesis (zones 3 and 5). As peak load transfer occurs distally in the titanium stem, damage accumulation and subsequent damage induced remodelling in Gruen zones 3 and 5 were compared to clinical observations (Okano et al., 2002; Sluimer et al., 2006).

Figure B.1 shows a comparison of the predicted percentage change in density at the anterior and posterior distal stem-bone interface, in zones 3 and 5, over two years for different values of the damage time constant. These plots show that as the value of τ_d increases, the influence of damage on bone resorption increases. Considering the clinical observations of Okano et al. (2002) and Sluimer et al. (2006), that BMD decreases rapidly over the first six months, in zones 3 and 5, and increases there after, low values of τ_d (1E3 - 1E5), which took over five years to converge to a remodelling equilibrium, were considered to underestimate the influence of damage on the rate of resorption. Values of τ_d = 1E6 and 1E7 were found to give the best approximation to the above clinical observation. Figure B.2 shows the combined anterior-posterior predicted percentage change in density for τ_d = 1E6 and 1E7, in zones 3 and 5, against the data of Sluimer et al. (2006). The value of τ_d = 1E7 was found to match the experimental curve the best.

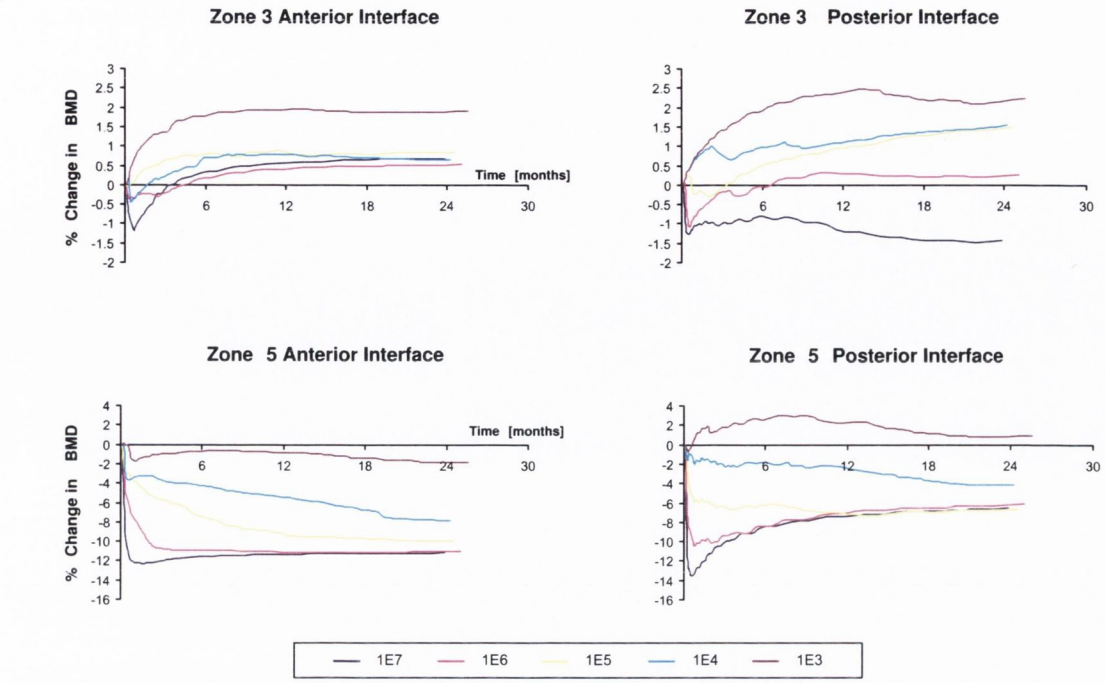

Figure B.1. Comparison of predicted percentage change in BMD surrounding the anterior and posterior distal stem-bone interface (Gruen zones 3 and 5) over two years, with the damage time constant, τ_d, set at: 1E7, 1E6, 1E5, 1E4, and 1E3.

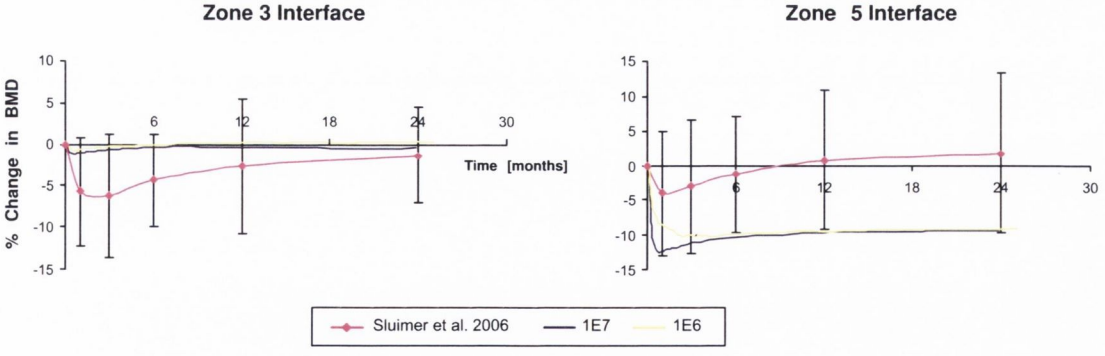

Figure B.2. Comparison of experimental percentage change in BMD (with standard deviations) in zones 3 and 5, over two years (Sluimer et al., 2006) against predicted interfacial change for τ_d = 1E7, and 1E6.

Appendix C

Influence of muscle loads on bulk-bone remodelling

Proximal stress shielding occurs most prominently in the CoCrMo stem. However, the peak percentage volume of stress shielding occurs in zone 2 (54%) and not in zone 1 (21%) as one would expect. This can be explained by the muscle attachments in zone 1 which maintains a degree of load transfer and hence reduces the influence of stress shielding on bone resorption in zone 1. Removing the muscle loading increases the amount of stress shielding in zone 1 to 75% see Fig. C.1. This conversely is not the case for either the titanium or iso-elastic stem as a higher degree of load transfer occurs in zone 2 and is not as susceptible to the effects of stress shielding. Furthermore, without the influence of muscle loading unrealistic bone resorption is predicted with complete resorption of the trochanter, see Fig. C.2

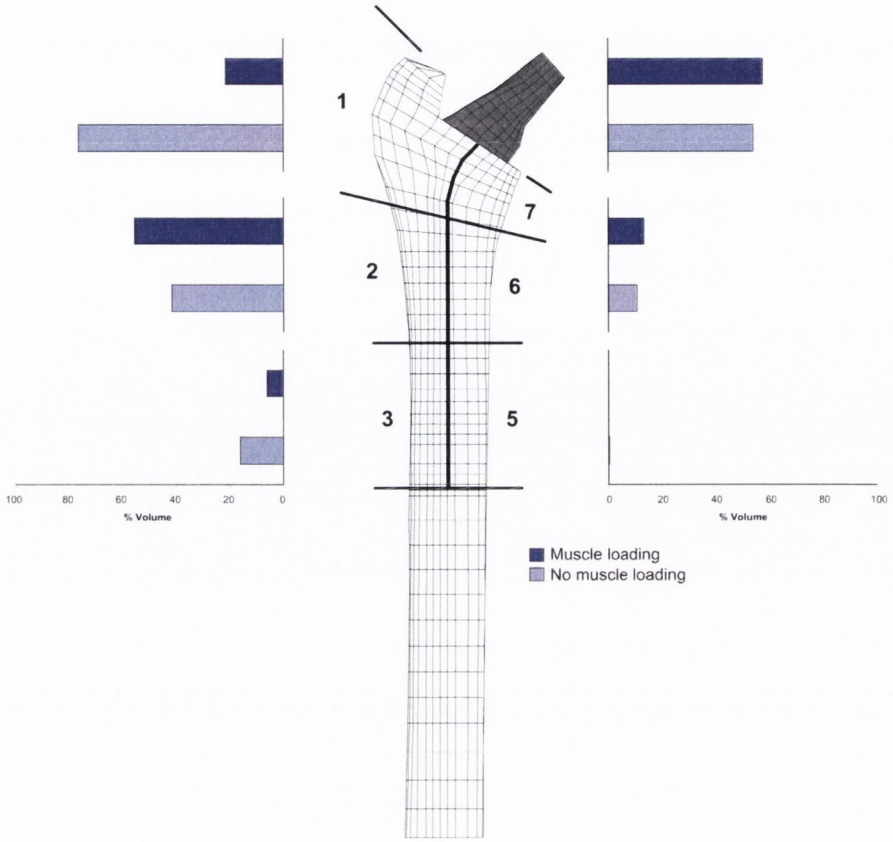

Figure C.1. Percentage volume of bone experiencing stress shielding immediately post-op with and without muscle loading.

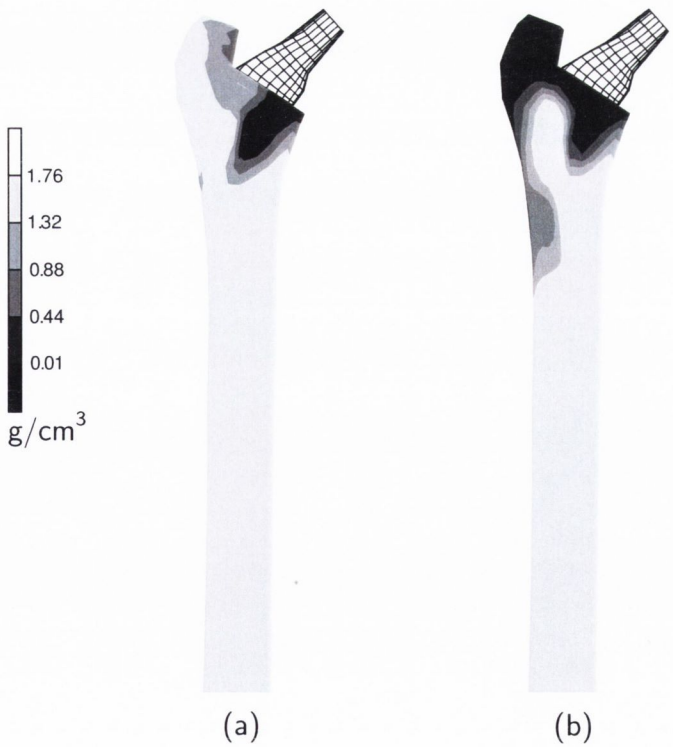

Figure C.2. Predicted change in density (a) with and (b) without muscle loading.